

**AUTOMATIC LOCALIZATION OF EPIDURAL
NEEDLE ENTRY SITE WITH LUMBAR
ULTRASOUND IMAGE PROCESSING**

YU SHUANG

(B.Eng., Huazhong University of Science and Technology)

A THESIS SUBMITTED FOR

THE DEGREE OF DOCTOR OF PHILSOPHY

NUS GRADUATE SCHOOL FOR INTEGRATIVE

SCIENCES AND ENGINEERING

NATIONAL UNIVERSITY OF SINGAPORE

2015

DECLARATION

I hereby declare that this thesis is my original work and it has been written by me in its entirety. I have duly acknowledged all the sources of information which have been used in the thesis.

This thesis has also not been submitted for any degree in any university previously.

Yu, Shuang

Yu Shuang

24 November 2015

Acknowledgements

I would like to express my most sincere gratitude and appreciation to all who helped me during my Ph.D. candidature at National University of Singapore. First of all, I would like to thank my Ph.D. supervisor, Professor Tan Kok Kiong for his insightful instructions, encouragement and support to my study and research work. He provided me with the academic guidance on how to conduct serious research, yet gave me the freedom to work on topics I'm interested in. Without his support, I would not have accomplished this thesis. I would also like to thank the chair of my thesis advisory committee, Professor Lee Tong Heng for his helpful suggestions and advisory for my research.

I am grateful for Prof. Alex Tiong Heng Sia, Dr. Sng Ban Leong, Dr. Li Shengjin and Ms. Teo Agnes from KK Women's and Children's Hospital. They provided invaluable assistance with the clinical data collection and trial, and helped to validate the research presented in this thesis.

I would like to express my appreciation to all of my friends and colleagues from the Mechatronics and Automation Lab. Special thanks must be made to Dr. Liu Lei, Dr. Yuan Jian, Dr. Liang Wenyu and Dr. Nguyen Hoang Tuan Minh, for their kindly help and discussions when I met obstacles both in life and research. Great thanks to Mr. Tan Chee Siong for all the assistance during my experiment. Many thanks to Ms. Er Poi Voon, Mr. Arun Shankar Narayanan, Mr. Kyaw Ko Ko Htet, Mr. Du Xinxin and Mr. Zhu Haiyue, for all the happy memories we shared in the last four years.

I also owe gratitude to NUS Graduate School for Integrative Sciences

and Engineering for providing the NGS scholarship to undertake my Ph.D. Research. The last four years has been a wonderful experience for me and it was made possible by NGS. I would like to thank Prof. Philip Moore Keith, Prof. Tang Bor Luen and Ms. Chuan Irene Christina from NGS office for their warmhearted help during my Ph.D. candidature.

I dedicate this thesis to my family for their unconditional moral support and love throughout the process of my life and research. Finally, I wish to express gratitude to my fiancé, Dr. Baichuan Sun, for being a constant source of mental support and companion in the past 7 years.

Contents

Acknowledgements	i
Table of Contents	iii
Summary	vii
List of Tables	x
List of Figures	xi
1 Introduction	1
1.1 Background	1
1.2 Procedure and Challenges of Epidural Anesthesia	3
1.3 Ultrasound Assisted Epidural Anesthesia	6
1.4 Computer-Aided Lumbar Ultrasound Interpretation	9
1.5 Research Gap and Objectives	11
1.6 Thesis Outline	13
2 Image Preprocessing for Lumbar Ultrasound Images	16
2.1 Introduction	16
2.2 Local Normalization Algorithm	18
2.3 Difference of Gaussian Enhanced Local Normalization Algorithm	20
2.4 Results	23
2.5 Discussions	31
2.6 Conclusion	33
3 Lumbar Level Identification	35

3.1	Introduction	35
3.2	Automatic Sacrum Identification	38
3.2.1	Feature Extraction	38
3.2.2	Support Vector Machine	39
3.3	Panorama Image Stitching	39
3.3.1	Motion Estimation	41
3.3.2	Frame Quality Evaluation	43
3.3.3	Image Stitching	44
3.4	Spinous Level Identification	45
3.5	Image Processing Procedure	46
3.5.1	Materials and Image Acquisition	47
3.6	Results and Discussions	47
3.6.1	Sacrum Identification	47
3.6.2	Result on Frame Quality Evaluation	49
3.6.3	Image Stitching and Spinous Level Identification	50
3.6.4	Computational Speed Tests	51
3.7	Conclusion	51

4 Localization of Precise Needle Insertion Site with Cascading

	Classifier	53
4.1	Introduction	53
4.2	Ultrasound Image Features of Lumbar Spine	54
4.3	Position Correlator	55
4.3.1	Template Matching Algorithm	56
4.3.2	Position Correlator	58
4.3.3	Comparison of Identification Rate and Computation Time	59
4.4	Cascading Classifier	61
4.4.1	Improved Position Correlator	61
4.4.2	Midline Detection	63
4.4.3	Cascading Classifier for Image Classification	65

4.4.4	Identification of Epidural Space	66
4.4.5	Materials and Image Acquisition	68
4.5	Results	70
4.5.1	Precision and Accuracy of Epidural Space Measurement	72
4.6	Discussions	75
4.7	Conclusions	77
5	Image Classification with Machine Learning	79
5.1	Introduction	79
5.2	Materials and Image Acquisition	80
5.3	Feature Extraction	81
5.3.1	Template Matching	82
5.3.2	Midline Detection	84
5.4	Feature Ranking and Feature Selection	86
5.5	Support Vector Machine	88
5.6	Image Identification Procedure	90
5.7	SVM Performance Evaluation Criteria	91
5.8	Results	92
5.8.1	Results of Feature Selection	93
5.8.2	Performance of Support Vector Machine	94
5.8.3	Video Processing	96
5.9	Discussions	100
5.10	Conclusions	103
6	System Integration	105
6.1	Introduction	105
6.2	Image Acquisition System Development	106
6.3	Graphical User Interface Design	107
6.3.1	Longitudinal User Interface	108
6.3.2	Transverse User Interface	111

6.4	Result for Real-time Image Processing	114
6.5	Manual Needle Insertion with Ultrasound Guidance	119
6.6	Mechanical System Design	120
6.6.1	Mechanical Design	121
6.6.2	Control System	122
6.6.3	System Integration	124
6.7	Conclusion	125
7	Conclusions and Future Work	127
7.1	Summary of Contributions	127
7.2	Suggestions for Future Work	130
	Bibliography	133
	List of Publications	144
	Appendices	146
A	Protocol for Real-time Volunteer Study	147
A.1	Computer Software Setup:	147
A.2	Hardware Preparation	147
A.3	Volunteer Preparation	150
A.4	Longitudinal View Scanning	151
A.5	Transverse View Scanning	153
B	IRB Approval for Ultrasound Image Collection	155
C	Informed Consent Form for Ultrasound Data Collection	158
D	IRB Approval for Real-time Volunteer Study	164
E	Informed Consent Form for Real-time Volunteer Study	167

Summary

Epidural anesthesia (EA) is widely used in surgery for pain relief. A properly performed epidural procedure is the ‘gold standard’ of treatment to reduce pain during childbirth. A major technical challenge of EA is the identification of the needle entry site, which is clinically determined by palpating the surface landmarks of the spine. Ultrasonography, as a safe and inexpensive imaging modality, has been proved effective for needle entry site localization for difficult epidural cases.

However, the key limitation of ultrasound in this application is the severe influence of speckle noise that adversely hampers the interpretability of ultrasound images. In order to remove the speckle noise, a pre-processing algorithm named Difference of Gaussian (DoG) enhanced local normalization is proposed. The algorithm is especially suitable for lumbar ultrasound image pre-processing as it not only eliminates the speckle noise, but also effectively overcomes the brightness difference all over the images, thus alleviating the wave attenuation problem encountered in ultrasound images.

The localization of needle entry site can be phased into two stages, the longitudinal view enables the scan for spinal level identification and transverse view allows the scan for precise needle entry point localization. The anatomical features revealed in the ultrasound images are very different in longitudinal and transverse views. Thus, two sets of image processing procedures are developed, corresponding to the two scanning views respectively.

In the longitudinal view, the image processing procedure starts with

automatic sacrum identification with support vector machine (SVM) algorithm. After the sacrum is detected, an automated panorama image stitching procedure is initiated to obtain the overall spinous processes structure. Throughout the image stitching and ultrasound probe movement, an image quality evaluation standard is utilized to select the suitable frames to be stitched onto the panorama image, so as to eliminate the accidental bad-quality frames in case the probe goes out-of-line during the scanning movement. Meanwhile, the spinous levels are identified and divided on the panorama image, which are then projected on the original ultrasound image in real-time, so as to inform anesthetists the location of the L3-L4 level.

After L3-L4 level is identified, the ultrasound probe will be rotated to the transverse view to locate the precise needle entry site. A cascading classifier is first developed as a generalization of the expert knowledge in identifying interspinous images. The cascading classifier contains four layers of weak classifiers and each layers corresponds to a specific selection criterion. If the image cannot be confidently described by a certain classifier then it will be passed to the next classifier, until it is classified with a high confidence level. An accuracy of 94.8% on training set and 93.23% on test set is achieved with the proposed cascading classifier. In addition, the epidural space, i.e., target for EA, can be identified and measured automatically, providing reference to the needle insertion procedure. The automatic epidural space identification versus manual measurement has a standard deviation of 0.0528 cm and mean of 0.0028 cm.

In order to increase the robustness of the interspinous image classification, a machine learning based method, including feature extraction, feature selection and SVM learning procedures, is proposed for the classification of ultrasound images in the transverse plane. The training and test database is established, which contains 1840 images randomly selected from video streams of 46 pregnant subjects. A set of features, including matching values, positions and

appearance of black pixels within predefined windows along the midline, are extracted from the ultrasound images in the database. SVM is then utilized to learn the pattern of interspinous and bone images. The proposed machine learning model is accurate and robust, with 95% accuracy on training set and 93.20% on test set. Further tests on the off-line saved ultrasound videos indicates that the trained SVM model is able to identify the interspinous region and bone region correctly on 45/46 video streams with a computational speed fast enough for real-time processing.

Finally, the proposed algorithms is integrated and packaged with the design of a graphical user interface, along with a real-time image acquisition system. The user interface presents the anesthetists with the ultrasound image processing results and provide guidance for needle entry site localization, with trained SVM model and image processing algorithms working in the background. It is designed in an intuitive approach, therefore requiring least ultrasound knowledge on the part of anesthetists. The developed image acquisition system and user interface has been tested on volunteers in real-time and proved to be able to work accurately and efficiently.

In a nutshell, an intelligent image processing algorithm and procedure based on machine learning for lumbar ultrasound image processing has been proposed and developed in the thesis. The algorithms are able to locate the precise needle entry site as the operator moving the ultrasound probe following a given procedure, thus facilitating the interpretation of ultrasound images and realizing automatic localization of needle entry site.

List of Tables

2.1	Performance Comparison Between Different Filtering Algorithms	30
3.1	Statistics of Training Set and Test Set.	49
3.2	Performance of SVM Classification for Sacrum Identification. . .	49
3.3	Parameters for Frame Quality Evaluation.	51
3.4	Computation Cost of Video Processing with Matlab.	52
4.1	Statistics of Training Set and Test Set.	70
4.2	Classification Result on Training and Test Set.	71
4.3	Computation Cost of Functions with Matlab.	72
5.1	Statistics of Training Set and Test Set.	93
5.2	Best and Worst SVM Performance in the 10 Continuous Training	96
5.3	Computation Cost of Video Processing with Matlab.	100

List of Figures

1.1	Spine Anatomy	2
1.2	Cross-sectional View of Lumbar Spine in the Longitudinal Direction	3
1.3	Tuohy Needle and Catheter Used in EA	4
1.4	Ultrasound Image Feature in the Longitudinal View.	7
1.5	Ultrasound Image Feature of Bone Region in the Transverse View.	7
1.6	Ultrasound Image Feature of Interspinous Region in the Transverse View.	8
2.1	Processing Flow of Local Normalization Algorithm	19
2.2	Processed Image After Local Normalization.	20
2.3	Processing Flow of Local Normalization Algorithm Modified with DoG	22
2.4	Processing Result of DoG Modified Local Normalization with Different Gaussian Kernels	22
2.5	Simulated Test Ultrasound Image with Different Contrast	24
2.6	Comparison of Filtering Result for Test Image with Contrast of 10dB	26
2.7	3D Mesh Plot of Filtering Result for Test Image with Contrast of 10dB	27
2.8	Comparison of Filtering Result for Test Image with Contrast of 5dB	28
2.9	3D Mesh Plot of Filtering Result for Test Image with Contrast of 5dB	29

2.10	Comparison of Filtering Result for Clinical Lumbar Ultrasound Image	32
3.1	Ultrasound Image in the Longitudinal View.	36
3.2	Morphological Feature Extraction for Sacrum.	40
3.3	Phase Correlation Result of Two Similar Ultrasound Image With only Translation Movement.	42
3.4	Panorama Image Stitching	44
3.5	Spinous Level Identification	45
3.6	Spinous Level Identification Result on Original Ultrasound Image	46
3.7	Flow Chart of Ultrasound Image Processing Procedure for Spinous Level Counting	48
3.8	Frame Quality Evaluation for Image Series.	50
4.1	Ultrasound Image of Lumbar Spine	55
4.2	Ultrasound image processing using template matching.	57
4.3	Template Matching Results for Interspinous Image and Bone Image.	58
4.4	Identification Result for Template Matching	60
4.5	Position Correlator	62
4.6	Framework of Cascading Classifier	67
4.7	Search for Epidural Space	69
4.8	Identification Result of Randomly Selected Video Streams	73
4.9	Comparison of Automatic vs. Manual Measured Epidural Depth	74
5.1	Feature Extraction with Template Matching	83
5.2	Feature Extraction with Midline Detection	85
5.3	Ranking of Individual Features	87
5.4	Image Identification Procedure for Lumbar Ultrasound Image	90
5.5	Two Representative Images with Adversarial Labels	92

5.6	Trends of Accuracy, Precision, Recall, F0.5 and AUC along with Feature Dimensions for Training Set	94
5.7	Trends of Accuracy, Precision, Recall, F0.5 and AUC along with Feature Dimensions for Test Set	95
5.8	SVM Performance in 10 Continuous Training	95
5.9	Probability Density Estimation of Decision Function Value for Training Set	97
5.10	Probability Density Estimation of Decision Function Value for Test Set	97
5.11	Histogram of the Decision Function Value for Misclassified Test Data	98
5.12	Classification Result of Selected Video Frames.	99
6.1	Image Acquisition System	107
6.2	Graphical User Interface of Longitudinal View	110
6.3	Working Flow of the Longitudinal User Interface	111
6.4	Graphical User Interface of Transverse View	112
6.5	Working Flow of the Transverse View User Interface	113
6.6	Real-time Image Processing Result of Longitudinal View for Volunteers.	116
6.7	Representative Anechoic Region for the Two Failure Cases at First Scan.	117
6.8	Real-time Image Processing Result of Transverse View for Volunteers.	118
6.9	Simulated Ultrasound Image for the Customized Probe	121
6.10	Mechanical System Design	122
6.11	Control System Design	124
6.12	Proposed System Architecture	124
6.13	Proposed System Working Flow	125

7.1 Framework of Machine Learning Based Ultrasound Image Identification Procedure	132
--	-----

Chapter 1

Introduction

1.1 Background

Epidural anesthesia (EA) is a central neuraxial block technique that is widely performed on women at the point of baby delivery, in order to alleviate the labor pain. Around 60-90% of women in developed countries received EA for pain relief, including both labor and cesarean delivery [1]. EA is also used to provide pain relief after surgery. For some surgeries of the lower limb, such as hip, knee replacement and abdominal surgery, the use of effective EA has been found to reduce blood loss [2, 3].

During EA, analgesic is delivered to the epidural space continuously via a catheter, which provides long-lasting block effect for time-consuming surgery and post operation pain relief. It takes about 10-20 minutes for the medicine to take effect and last for hours. In cases where rapid onset of analgesia is required, e.g. cesarean sections, usually combined spinal and epidural anesthesia (CSE) will be adopted. During CSE, a small dose of local anaesthetic is injected to the subarachnoid space to trigger the immediate anesthetic effect, while the EA provides continuous pain block. Both EA and CSE involve inserting a needle into the lumbar epidural space.

In order to elaborate on the procedure of epidural needle insertion, it is

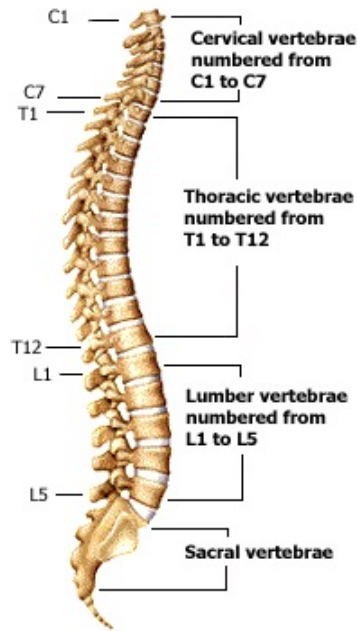


Figure 1.1: Spine Anatomy

necessary to give a brief overview of the spine anatomy. The vertebral column comprises 24 individual vertebrae, including 7 cervical, 12 thoracic and 5 lumbar vertebrae [4]. Extension of the vertebral column consists of the sacrum and coccyx [5]. EA is usually performed at the lumbar spine, which comprises 5 lumbar vertebrae, as shown on Fig 1.1 [6]. The lumbar spine starts from L1 (the upper part) and ends at L5 (the lower part). Each lumbar vertebra contains spinous process, transverse process, articular process and vertebra body. Epidural space lies within the vertebra canal, stretching from foramen magnum of the skull to the sacral hiatus [7]. It is located between ligamentum flavum and dura mater, and contains fat, loose connective tissue and venous plexus. The fat is loose and allows diffusion of injected local anesthetic fluid throughout the epidural space [8]. The width of epidural space ranges from 5-13 mm with 3-8 cm depth below the skin in the lumbar region [7, 9, 10]. It is also reported that a positive correlation exists between the epidural depth and the Body Mass Index (BMI) [10, 11].

Fig 1.2 shows the sagittal section view of the lumbar spine. Adjacent

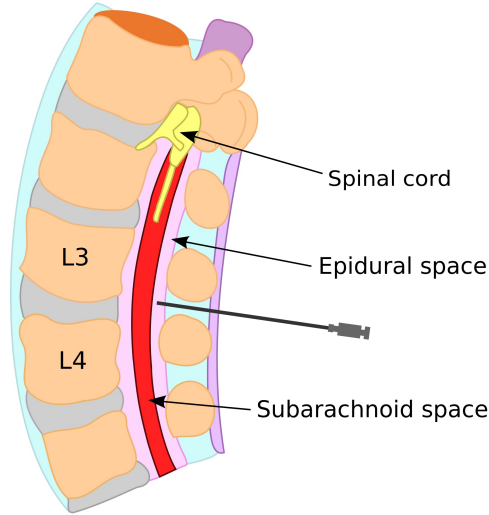


Figure 1.2: Cross-sectional View of Lumbar Spine in the Longitudinal Direction

vertebrae are connected by interspinous ligaments. The interspinous region between L3-L4 is the most common site chosen for epidural needle insertion [12]. The interspinous spaces are the largest at those two levels and this will reduce the difficulty of needle placement compared with the interspaces in thoracic place or other lumbar interspinous levels [5]. Moreover, the width of the epidural space is broader at those two levels, giving the largest safety margin for needle insertion and catheter placement [6, 13]. Interspace above L2-L3 are avoided so as to decrease the risk of dura puncture [12].

1.2 Procedure and Challenges of Epidural Anesthesia

EA is rated as one of the most difficult procedures to perform in anesthesiology [14]. During the EA, an epidural needle, usually a Tuohy needle with hollow in the center, is inserted into the epidural space. After the successful placement of the epidural needle, a catheter will be inserted into the epidural space via the lumen of the needle, which is used for the infusion of medicine. Fig 1.3 shows the comparison of Tuohy needle and catheter. The detailed clinical procedure

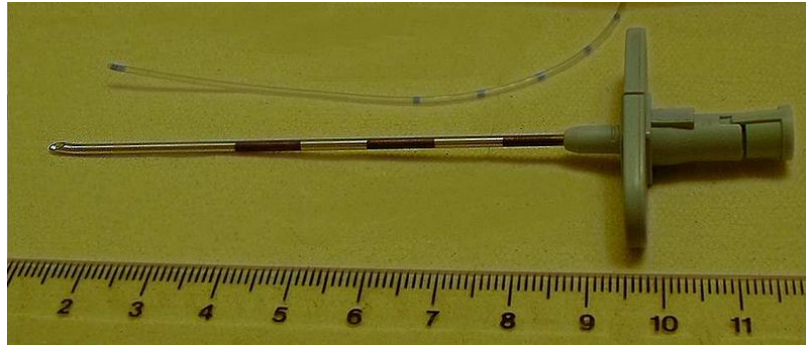


Figure 1.3: Tuohy Needle and Catheter Used in EA

of EA is listed as below:

Step 1. Keep the patient in lateral or sitting position and lean forward, to maximize the ‘opening’ of the vertebra interspaces;

Step 2. Identify anatomical landmarks with palpation, locate midline and L3-L4 interspinous region, to determine the epidural needle insertion site;

Step 3. Sterilize the insertion area and place a local anesthetic to numb the area;

Step 4. Insert epidural needle at the determined site into ligamentum flavum;

Step 5. Loss of resistance technique: if needle is at ligamentum flavum, remove the stylet and attach a syringe, apply steady pressure on the plunger, slowly and steadily advance the needle until loss of resistance is noticed;

Step 6. Once epidural space is reached, insert catheter via the lumen of the epidural needle into the epidural space;

Step 7. Deliver the anesthetic via the catheter and monitor the patients’ blood pressure and oxygen levels in the blood;

The procedure of CSE is different from EA in that: after Step 5 when the epidural needle is placed at epidural space, a long fine spinal needle is then introduced via the epidural needle and through the dura mater into subarachnoid space; the correct position is confirmed when cerebrospinal fluid (CSF) can be seen dripping from the spinal needle; a small dose of local

anaesthetic will be instilled; then the spinal needle will be withdrawn and catheter will be inserted into epidural space as in Step 6. Since the epidural needle insertion procedures are similar for EA and CSE, from now on, only EA will be mentioned.

Although EA has been practised clinically for decades, the failure rate of EA is reported relatively high and in the range of 6-25%, and it is very sensitive to the experience and skills of anesthetists [15, 16]. Caudal epidural trials indicates a failure rate as high as 9-52% of injecting outside epidural space [16, 17]. One of the major reasons leading to the failure and complications of EA is derived from the blind nature of how EA is performed clinically. This technique has remained as skills in the form of mental models, not easily imparted to a trainee, resulting in steep learning curve. The practice of epidural needle insertion relies primarily on the anatomical landmarks to identify the needle insertion site. Anesthetists first identify the insertion spinous level using the Tuffier's line, which is commonly located at the same horizontal level of L3-L4 interspinous region. But this relationship does not always stand true [18]. It has been reported that by using palpation or Tuffier's line method, anaesthetists are correct at 30% of the time in identifying puncture level, compared to the level determined by MRI [19]. After the level is identified, which may not be accurate by palpation or Tuffier's line, the anesthetists then further locate the needle insertion site by palpating the spinous process and interspinous.

However, surface anatomical landmarks, e.g. Tuffier's line, spinous process and interspaces, are not always easily palpable. Moreover, important features, such as the needle entry angle and depth of epidural space, which determines the estimated depth of needle insertion, cannot be obtained by the palpation approach. The final needle insertion procedure can be the result of a trial and error process. When the anesthetist feels that the needle is not inserted along the right path or encounter the bones, they will re-direct the needle or

withdraw the needle and insert it again at another site. This blind technique can result in multiple insertion attempts, thus compounding the discomfort and distress of patients and lowers the efficiency of anesthesia. The difficulty and therefore the failure rate is clearly higher for patients with obesity or previous spinal injuries, since the surface landmark is more difficult to locate with the manual palpation method for this population [20, 21].

1.3 Ultrasound Assisted Epidural Anesthesia

In recent years, the ultrasound imaging technique has been introduced to EA as an imaging method to detect the inner anatomical structure of patients' spine, helping to identify a needle insertion site. Various lines of research in the medical field have confirmed the effectiveness of ultrasound imaging compared to the traditional palpation method [22, 23]. For cases where the palpation based method is difficult or unable to place the needle successfully even after several attempts, ultrasound imaging can help to identify the insertion site [24, 25]. Ultrasound is also reported to significantly improve the epidural needle insertion success than the traditional palpation landmark technique [26]. In addition, with ultrasound imaging, trainee anesthetists are reported to achieve a higher success rate and fewer epidural attempts, compared to those without ultrasound guidance [27, 28]. It has been suggested that ultrasound imaging should become part of continuing professional training for anesthetists and serve as routine clinical practise, to ease the performing of epidurals and add to patients' comfort [9]. Therefore, ultrasound imaging has the potential to bridge the move from a blind technique of needle insertion to a better guided approach, which can help to increase the success rate of EA and reduce the reliance on skills and experience for a successful epidural procedure.

Two acoustic windows are usually employed when using ultrasound for epidural procedure: one is transverse midline approach, the other is the

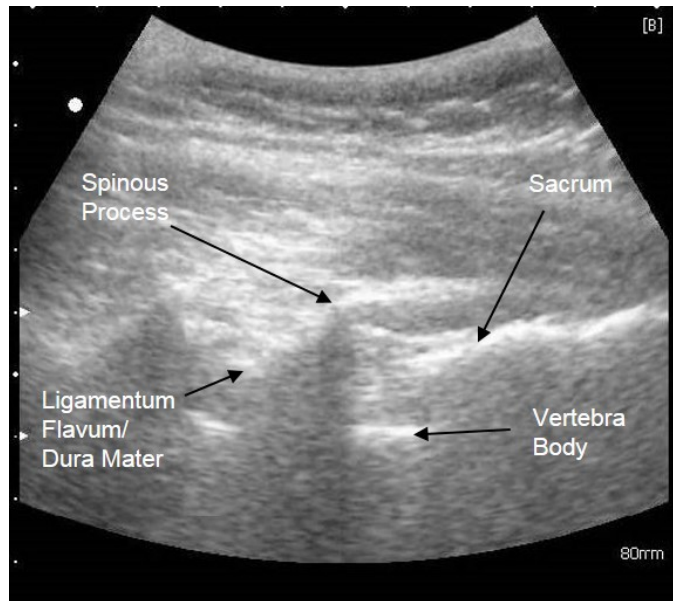


Figure 1.4: Ultrasound Image Feature in the Longitudinal View.

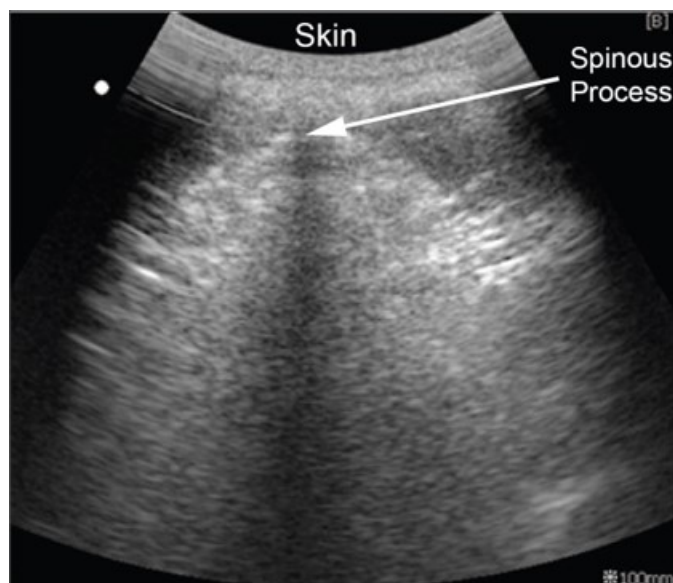


Figure 1.5: Ultrasound Image Feature of Bone Region in the Transverse View.

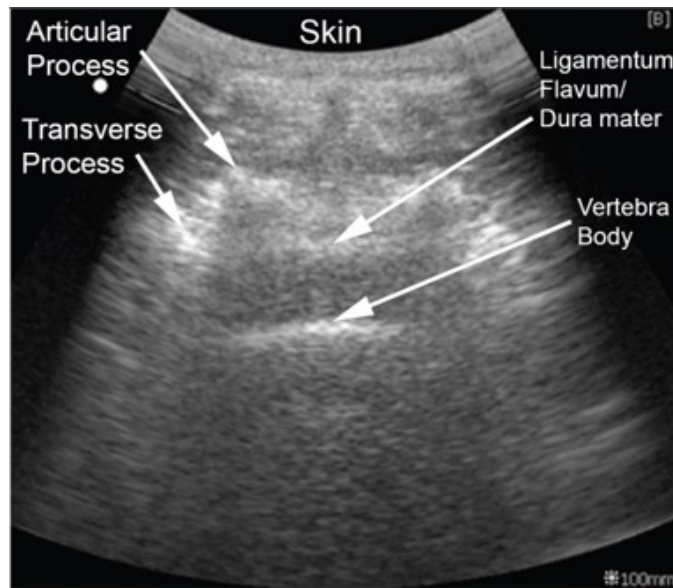


Figure 1.6: Ultrasound Image Feature of Interspinous Region in the Transverse View.

longitudinal paramedian/ median approach. The anatomical features obtained from those two scanning planes complements the other. For the longitudinal plane, the ultrasound probe is positioned vertically, perpendicular to the long axis of the spine. The anatomical elements identifiable includes: sacrum, articular/spinous process, ligamentum flavum, dura mater, and vertebra body, as indicated in Fig 1.4. The probe is initially placed near sacrum area along midline (longitudinal median approach) or 3 cm to the left of the midline (longitudinal paramedian approach). Then the probe is moved upward and the ‘saw-like’ features which represents spinous process will be counted and marked on skin, until L3-L4 interspinous level is reached [19].

After L3-L4 interspace is reached, the probe will be rotated to the transverse approach. In the transverse plane, the probe is positioned horizontally, perpendicular to the long axis of the spine. The identifiable anatomical elements include: spinous process, articular process, transverse process, ligamentum flavum and dura mater (those two usually appears as one single line, given the closeness to each other and the low image resolution) and vertebra body, as illustrated in Fig 1.5 and Fig 1.6. The probe will then be slowly tuned both in angle and position, until the epidural space and vertebra

body is shown clearly in the view, as in Fig 1.6. Then the anesthetist will align the midline to the middle of the probe and mark the level and midline on the patient's back with a sterilized marker pen. The intersection point of the two line is the optimal insertion point [19, 29].

1.4 Computer-Aided Lumbar Ultrasound Interpretation

Ultrasound imaging is different from other medical imaging modalities, e.g. X-ray, CT, MRI, in that it is safe, non-radioactive and low cost, making it an appropriate imaging modality for assisting epidural needle insertion [30]. However, a barrier to reap these benefits lies in the ability to interpret the ultrasound image effectively. For ultrasound guided epidural needle insertion, generally a low frequency (2-5 MHz) curvilinear probe will be adopted, which allows a deeper penetration depth compared with high frequency linear probe. But the deeper penetration depth is achieved at the sacrifice of image quality. The resolution of an ultrasound image is low, usually 1-2 mm along the axial direction and 1-3 mm along the lateral direction, given that the penetration depth of the ultrasound wave is above 10 cm, as required by depth of the spinal anatomical structures. Moreover, the ultrasound images contain severe speckle noises, making the subtle structures indistinguishable from surrounding background [30]. A full interpretation of ultrasound images requires professional training and experiences. In a real-time procedure, the luxury of time to read them carefully or to consult a second opinion is not available. Therefore, while the base technology is viable, using it in an efficient manner, time and accuracy wise, to guide epidural needle insertion has been an open issue, thus explaining the prevalence of conventional approaches still being practised and the reluctance of practicing anesthetists to adopt an ultrasound imaging tool.

There has been some interest in the applicability of computer aided automatic interpretation of ultrasound images, mainly in the longitudinal view. The first research of automatic image interpretation is proposed by Kerby et.al., which focused on the automatic identification of lumbar interspinous level [31]. The ultrasound images were stitched together to generate a panorama image; the obtained panorama image was then filtered with a combination of median filter and linear filter; then least-square parabolic fit was used to describe the edge points of bones, the local parabolic minimum and intersection is identified as a vertebra. By using this algorithm, the author realized the ‘automatic’ identification of spinous levels. 10 panorama images were generated and the automatic level identification has a Root Mean Square (RMS) error of 11.8 mm compared with level identified by sonographer and 4.4 mm compared with expert labeling on the generated panorama image. This thesis is the first of this kind research of automatic level counting. However, two major problems exist or need to be solved. First, the spinous label was identified on the generated panoramas after the scanning process is over, which means that the operator cannot get the real-time level counting information during the scanning and extra landmarks has to be provided to coordinate the level identification on the patients’ back. Secondly, sacrum was assumed as the start point of panorama stitching, but it was not identified by the proposed algorithm. This may result in the misidentification of the L5 spinous level and introduce error to the level counting procedure.

On the basis of Kerby’s et.al research, Ashab et.al further proposed an augmented reality system for the identification of spinous level [32]. Similar level identification approaches were used in this research. Individual frames were collected by the anesthetists and then stitched to a panorama by the computer. Level dividing was performed on the obtained panorama, by extracting the peak and valley of the lower edge of the binarized panorama. The peak followed by a valley was deemed as the spinous process. The level

dividing information was then imposed on the live camera video of the patients' spine. This research has realized the coordination from the level information to the patients back, with mean absolute error ranging from 2.5 mm to 4.2 mm for L1-L5. However, drawbacks still exist for this research, mainly including: 1. it requires the operator to find the proper imaging plane and select the images to be stitched, which still require substantial ultrasound training for the anesthetists; 2. the level dividing using local maximum and minimum may not be accurate for images with local maxima/minimum near each other. In addition, similar as Kerby's method, the identification of sacrum was not considered in this paper, which may introduce errors to the level identification of L5.

Tran et.al. utilized phase symmetry and template matching to extract the lamina and ligamentum flavum in the paramedian images [33]. The algorithm was able to detect the ligamentum flavum in 34 out of 39 paramedian images, with an error of 3.7 mm compared to the one measured by sonographer. However, this method failed on cases where the anatomical feature is not clear or ligamentum flavum is not connected to lamina (i.e. the bone). In addition, it takes 4.3s to process one single image on computer, thus limit its application to off-line processing instead of on-line processing.

1.5 Research Gap and Objectives

As introduced in the last section, related literature mainly focused on the paramedian view. There is a paucity of research reports in relation to automatic image interpretation of US images in the transverse view. The paramedian view is usually employed by practitioners to estimate the L3-L4 spinous level. However, for a more precise localization of the puncture site, the transverse plane, which reveals reliable landmarks, is preferred by some researchers [34, 35]. Furthermore, as the majority of anesthetists adopt a

midline approach for needle insertion, the importance of the transverse view cannot be overemphasized [34]. The major objective of this thesis is to fill the gap of automatic ultrasound image interpretation of lumbar spine in the transverse view for pregnant patients.

On the other hand, although automatic interpretation of longitudinal view has been explored, none of the research has realized real-time online process of the ultrasound image. In addition, sacrum identification is ignored by the researchers, which will potentially bring error to the L5 identification and spinous level counting. In this thesis, the longitudinal view will also be investigated to realize the sacrum identification, accurate level dividing and real-time on-line processing for the ultrasound images acquired from longitudinal view.

The objective of this thesis is to realize the automatic interpretation of lumbar ultrasound images in real-time, include both transverse and longitudinal view. Algorithms have been developed to identify the proper needle insertion level and precise entry point automatically in real-time as the operator moves the probe. Furthermore, important anatomical features will also be extracted automatically, including sacrum, spinous processes in the longitudinal view and vertebra body, epidural space in the transverse view. The information will be fed to the operator in real-time so as to estimate needle insertion depth and the location of epidural space. The final purpose of this research is to enable anesthetists utilizing ultrasound to an extent that the use of ultrasound imaging is as simple as a needle site sensor is available, so that they can enjoy the benefits of ultrasound while relieved from extensive training of ultrasound interpretation. It is expected that the developed image identification algorithms will be helpful to accelerate the pace of ultrasound imaging becoming a routine practise of epidural needle insertion, after the interpretation challenges are solved with the algorithms. The developed algorithms will certainly be helpful for the trainee anesthetists,

to help them better handle the challenges of epidural needle insertion and improve their learning speed to become professionals.

1.6 Thesis Outline

The other six chapters of the thesis are organized as follows.

Chapter 2. Ultrasound Image Preprocessing

Ultrasound image has low spatial resolution and is contaminated with speckle noises, which adversely affect the interpretability. This chapter starts with an general introduction of widely used ultrasound filtering algorithms. Then a preprocessing algorithm of Difference of Gaussian (DoG) enhanced local normalization is proposed, which is able to remove speckle noises and extract the major anatomical features of lumbar ultrasound image. The local normalization algorithm is able to overcome the non-uniform illumination or shading artifact, thus removing potential hazardous elements which may negatively affect the image identification in the following procedures. The filtering result achieved by local normalization algorithm is also compared with generally used filtering algorithms, proving the advantage of the proposed local normalization algorithm on ultrasound preprocessing.

Chapter 3. Spinous Level Identification

In this chapter, the ultrasound image processing in the longitudinal view is presented. An image processing procedure is proposed that is fully automatic to identify the optimal insertion level (L3-L4). The image processing procedure starts with automatic sacrum identification, with feature selection and support vector machine (SVM) classification. After sacrum is detected, a panorama image stitching procedure is initiated to obtain the overall spinous processes structure. Throughout the image stitching and ultrasound probe movement, an image quality evaluation standard is utilized to select the suitable frames to be stitched onto the panorama image, so as to eliminate the accidental bad-quality

frames in case the probe goes out-of-line during the scanning movement. In the meantime, the spinous levels are identified and counted on the panorama image, which are then projected on the original ultrasound image in real time, so as to inform anesthetists where is the level L3-L4 and when to stop scanning. The processing result with off-line collected lumbar ultrasound videos shows a high accuracy on sacrum identification and spinous level identification.

Chapter 4. Cascading Classifier for Image Classification

This chapter focuses on the image classification in the transverse view, so as to locate the proper needle entry point. A simple classifier based on the position relationship of extracted anatomical features is first proposed, for the classification of interspinous and bone images obtained from healthy volunteers. However, this classifier is proved over-simplified and identifies the ultrasound images from pregnant patients with low accuracy. In order to improve the identification accuracy, a cascading classifier comprising four layers and incorporating more parameters is proposed, which is able to classify the ultrasound images from pregnant patients with higher accuracy. Apart from the image classification, this chapter also evaluates the precision of epidural space identification on the frames being identified as interspinous images. The epidural space is calculated automatically by the algorithm, which provides important information for anesthetist to estimate the needle insertion depth.

Chapter 5. Feature Extraction and Machine Learning

On the basis of Chapter 4, this chapter further explores the possibility of improving image classification accuracy and classifier robustness by machine learning method. A feature extraction, selection and machine learning procedure is proposed. A set of features are extracted, including shape features by template matching and black rate near midline by midline detection. The extracted features are then evaluated on their predictability toward the image label with cross correlation. Furthermore, a set of sub-features which yields optimum performance are extracted. For the extracted features, a

classic supervised machine learning method, SVM is employed to classify the interspinous images and bone images, which achieved an accuracy of 95% for training set and 93.20% for test set. The trained SVM model is further tested on obtained off-line ultrasound videos and is able to identify the frame proper for needle insertion.

Chapter 6. System Integration and Real Time User Interface

In order to facilitate anesthetists in using the image processing procedures proposed in the previous chapters, a real-time image processing system with graphical user interface is developed in this chapter. An operation protocol is also designed for the anesthetists to utilize the user interface and locate the needle entry point. Guidance will be provided by the interface on how to move the probe, without the need for anesthetists to interpret the ultrasound images. The whole scanning procedure requires minimal interferences from the anesthetists. In addition, a scenario is sketched to incorporate the image processing system in the clinical epidural procedure, by proposing a manual procedure and a fully automated procedure with a mechanical device. The concept of the mechanical needle insertion device has been designed, along with the control system that enables the automated insertion procedure.

Chapter 7. Conclusions

This chapter draws conclusions to the thesis and presents possible works for future research.

Chapter 2

Image Preprocessing for Lumbar Ultrasound Images

2.1 Introduction

Ultrasound imaging is widely used in medicine for diagnosis purpose and increasingly being adopted in regional anesthesia for guidance purpose. Compared with other medical imaging modalities, e.g., magnetic resonance imaging (MRI), X-Ray and computed tomography (CT), ultrasound enjoys the following advantages:

- 1) It is inexpensive, compared with MRI and CT;
- 2) It is compact and portable;
- 3) It works in real-time;
- 4) It is non-invasive;
- 5) It does not require ionizing radiation, unlike X-Ray and CT.

Those advantages make ultrasound a proper imaging modality to assist epidural anesthesia, especially when the target patients are mostly pregnant [36]. One of the limitations of ultrasound image is the severe influence on the image due to random speckle noise. Speckle noise adversely hampers the interpretability of ultrasound images by decreasing the spatial resolution

of the image. Moreover, it overshadows and conceals the fine features of interest in the image, making it rather difficult to distinguish these features from the surrounding background with the human eyes. Therefore, image despeckling is among the most important steps in ultrasound image processing. In addition, since ultrasound waves are attenuated as they propagate through tissues, the deeper the anatomical target, the darker it appears on the ultrasound image. Time gain compensation (TGC) technique, which increases the amplification of ultrasound wave proportionally to the depth, is usually used in the ultrasound machine to compensate for the wave attenuation [37]. However, even after TGC compensation, it is still difficult to achieve an ideally distributed brightness across the entire ultrasound image.

Ultrasound despeckling is one of the most active research areas in medical image processing, with various techniques proposed to improve the ultrasound image quality. Adaptive filters, including Lee's filter [38, 39], Kuan's filter [40, 41] and Frost's filter [42], are widely employed to remove speckle noise because they are relatively easy to implement and control. Adaptive filters smoothen the image by computing a linear combination of the center pixel intensity with the average or weighted intensity of the filter window. Speckle noise is partially suppressed by the filter, however at the expense of blurring the image details. Another approach called Anisotropic Diffusion (AD) is developed for image despeckling [43, 44]. Anisotropic diffusion removes the speckle noise via the operations of partial differential equations. AD is effective for speckle noise removal, but there are significant problems associated with AD like blurring, loss of important structural details and generation of artificial smear [45]. In addition, wavelets has also been widely investigated for speckle reduction, as reported in [46–49]. Proper selection of threshold and parameters can achieve good results in speckle elimination.

The filtering algorithms mentioned above are effective for despeckling; however, those algorithms cannot solve the non-uniform luminosity problem of

ultrasound images. This problem can be solved by local contrast normalization algorithm. Local contrast normalization was initially proposed to improve the detection of micro-calcification clusters in mammograms by normalize the contrast locally [50]. This technique was later utilized on retinal images to normalize the luminosity and contrast [51]. It has also been reported that the local contrast normalization is able to improve the discriminational ability of individual features [52]. However, the local contrast normalization algorithm may strengthen the high frequency information unnecessarily, thus not able to remove the speckle noises.

In this chapter, the local contrast normalization algorithm is described in details and then Difference of Gaussian (DoG) enhanced local normalization for pre-processing of ultrasound images is proposed. The DoG enhanced local normalization is especially suitable for ultrasound image pre-processing as it not only eliminates the speckle noise, but also effectively overcomes the local intensity variance all over the images, thus alleviating the wave attenuation problem faced by ultrasound images. Furthermore, since the final target of the image processing is the realization of an automatic identification of key image features, removing the varying level of brightness across the image will eliminate a potential element that might degrade the image recognition accuracy. The details of the proposed algorithm will be presented in the following sections.

2.2 Local Normalization Algorithm

The idea behind the local normalization algorithm is based on the approximation of the perception of human eyes. The human perception of image features depends on the average local characteristics near a pixel, rather than the absolute signal magnitude at the pixel. In addition, the key image features are generally presented via a high spatial frequency;

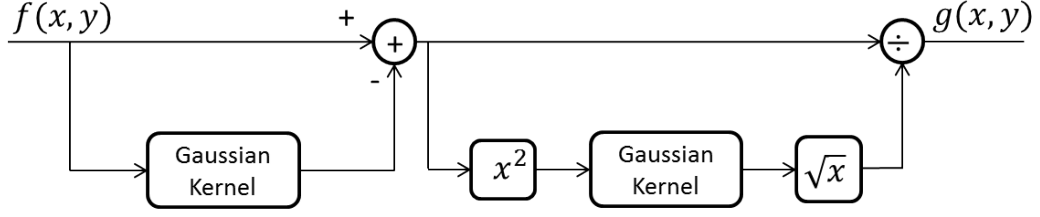


Figure 2.1: Processing Flow of Local Normalization Algorithm

while the low spatial frequency, due to uneven luminosity, will not seriously influence the perception of the image [53]. However, in computer-based image processing and recognition, poor and uneven illumination conditions will seriously influence the results of identification.

Local normalization is realized by first using an unsharp masking process to preserve the high frequency content in the image, and then normalizing the resultant image by dividing it with local standard deviation, thus the low frequency part induced by luminosity will be eliminated.

$$v(x, y) = f(x, y) - \sum_{i,j} w(i, j)f(x + i, y + j), \quad (2.1)$$

where $f(x, y)$ denote the original image; $w(i, j)$ represent the low pass Gaussian kernel:

$$w(i, j) = \frac{1}{2\pi\sigma^2} e^{-(i^2+j^2)/2\sigma^2}. \quad (2.2)$$

Then to obtain the local variance, the following equation can be used:

$$\delta(x, y) = \sqrt{\sum_{i,j} w(i, j)v(x + i, y + j)^2} \quad (2.3)$$

The locally normalized image is given in equation 2.4.

$$g(x, y) = v(x, y)/\delta(x, y) \quad (2.4)$$

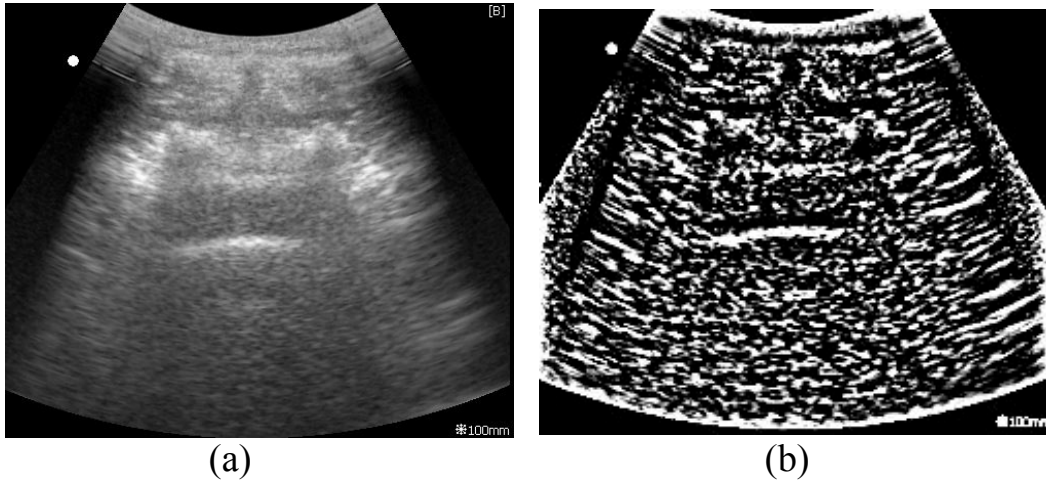


Figure 2.2: Processed Image After Local Normalization. (a). Original ultrasound Image (the test ultrasound image is collected from healthy volunteers with scanning frequency set as 5MHz and scanning depth as 10cm);(b). Processed result with Local normalization

To illustrate the process more thoroughly, the processing flow is presented in Fig 2.1. After the local normalization, the unevenly distributed background brightness, which is due to the ultrasound wave attenuation, is successfully overcome. The high frequency image content is preserved, as shown in Fig 2.2(b). However, since the first step of local normalization is unsharp masking, in consequence, speckle noise, as a high frequency component, is emphasized in the resultant image. Therefore, the main problem of speckle contamination is not yet relieved, and its presence will influence the interpretation of the ultrasound image.

2.3 Difference of Gaussian Enhanced Local Normalization Algorithm

In order to suppress the high frequency speckle noise, and also to overcome the low frequency background luminosity, the DoG algorithm is proposed to replace the unsharp masking procedure. DoG involves the subtraction of one Gaussian kernel filtered image from another Gaussian kernel filtered image

[53]. The first Gaussian kernel eliminates the high frequency speckle noise of ultrasound images, while the subtraction process with the second Gaussian kernel preserves the spatial frequency that lies between the range defined by the two Gaussian kernels.

In the proposed modified local normalization with DoG, the first part of local normalization is set as:

$$v(x, y) = \sum_{i,j} w_1(i, j) f(x + i, y + j) - \sum_{i,j} w_2(i, j) f(x + i, y + j). \quad (2.5)$$

in which $w_1(i, j)$ and $w_2(i, j)$ are the Gaussian kernels for the first and second filter respectively and,

$$w_k(i, j) = \frac{1}{2\pi\sigma^2} e^{-(i^2+j^2)/2\sigma^2}. \quad (2.6)$$

The modified processing flow is shown in Fig2.3. It is important to choose proper Gaussian kernel sizes and the σ value for the two Gaussian filters, in order to preserve the main features of the ultrasound images meanwhile eliminating the speckle noise. Generally, the first Gaussian filter is utilized to filter the high frequency speckle noise in the image, thus a proper Gaussian kernel size and σ value intended for effective noise filtering should be chosen. For the second Gaussian kernel, since it is desired that the difference of the two to preserve the main feature of the image, therefore, the second Gaussian filter should yield an even more blurred image than the first. Thus, the second Gaussian kernel should be assigned with a bigger σ value compared to the first Gaussian Kernel.

Comparing the results shown in Fig 2.4 where the Gaussian kernels are chosen with different sizes and σ values, the resultant images can be observed to vary significantly. The test images was acquired at the frequency of 5MHz and scanning depth of 10 cm, with the image size of 220×250 . As evident in

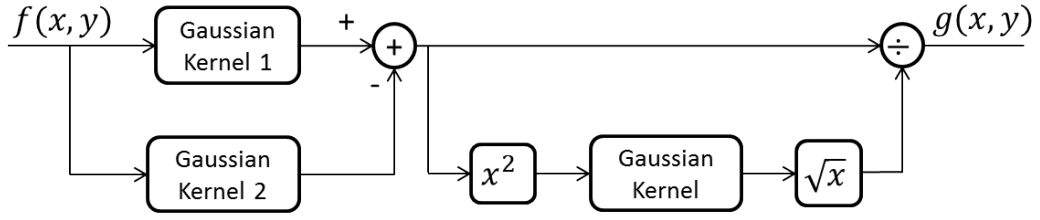


Figure 2.3: Processing Flow of Local Normalization Algorithm Modified with DoG

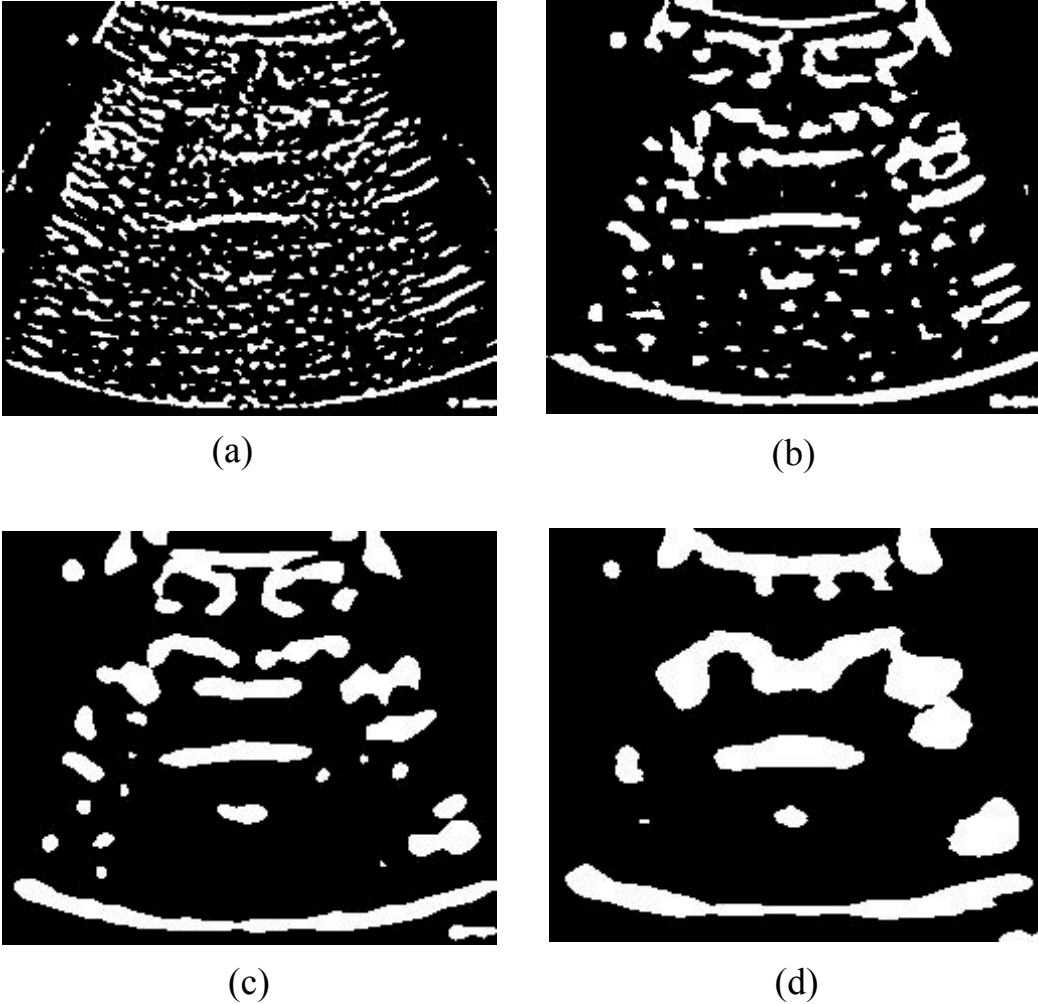


Figure 2.4: Processing Result of DoG Modified Local Normalization with Different Gaussian Kernels. (a): Kernel 1 $5 \times 5, \sigma = 1$; Kernel 2 $10 \times 10, \sigma = 4$; (b): Kernel 1 $10 \times 10, \sigma = 4$; Kernel 2 $15 \times 15, \sigma = 10$; (c): Kernel 1 $20 \times 20, \sigma = 4$; Kernel 2 $25 \times 25, \sigma = 10$; (d): Kernel 1 $35 \times 35, \sigma = 10$; Kernel 2 $35 \times 35, \sigma = 20$

the results in Fig 2.4(a), when the kernel size and σ value are chosen too small (Kernel 1 size 5×5 , $\sigma = 1$, kernel 2 size 10×10 , $\sigma = 4$), the speckle noise is not removed effectively. While in the results shown in Fig 2.4(d), the kernel size and σ value are chosen too large (Kernel 1 size 35×35 , $\sigma = 10$, kernel 2 size 35×35 , $\sigma = 20$), thus losing the important details and image features. Fig 2.4(c) presents an ideal processing result (Kernel 1 size 20×20 , $\sigma = 4$, kernel 2 size 25×25 , $\sigma = 10$), where the speckle noise is effectively removed and the image features are well preserved.

The results show that a proper selection of the kernel size and σ value can perfectly fulfill the purpose of the pre-processing step: strengthening the image main features, while suppressing the speckle noise and removing the local intensity variance. After the processing with DoG modified local normalization algorithm, what is presented to the anesthetists will be the anatomical structure of the ultrasound images, as shown in Fig 2.4. In this form, the images already greatly facilitate anesthetists in their interpretation of the images. Therefore, the proposed DoG modified local normalization algorithm achieves ideal despeckling result, serving as a suitable preprocessing step for ultrasound image classification.

2.4 Results

In this section, the result achieved by the proposed DoG enhanced local normalization will be compared with other filtering algorithms, including the widely used anisotropic diffusion, wavelet, Lee's filter and median filter. Two simulated test image of different contrast, respectively 10dB and 5dB, are employed for the comparison [54]. The test images are shown on Fig 2.5. The signal/background contrast are higher for the 10dB image and it is easier to differentiate the signal on the image. While for the 5dB image, the contrast is so low that it is more difficult to recognise the circles.

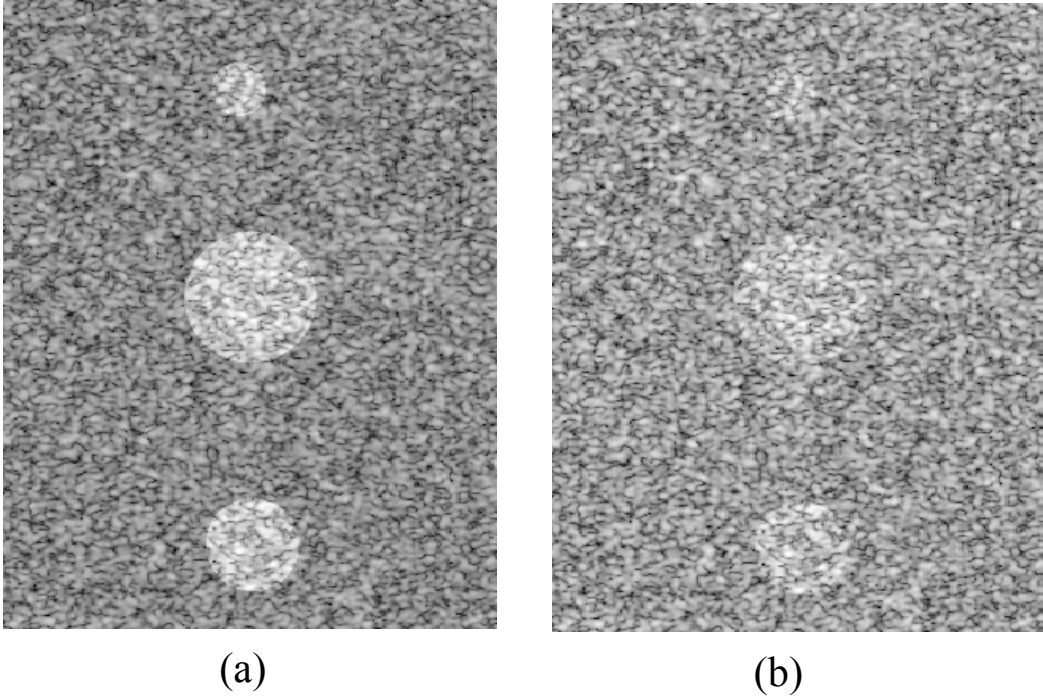


Figure 2.5: Simulated Test Ultrasound Image with Different Contrast. (a). Contrast = 10dB; (b). Contrast = 5dB

The algorithms are implemented with MATLAB. The implementation of anisotropic diffusion is based on Perona and Malik's paper [43] and Lee's filter is based on literature [38]. For wavelet and median filter, the Matlab Wavelet and Image Processing toolbox are employed respectively. The parameters used for the proposed algorithm is Kernel 1: 25×25 , $\sigma = 5$; Kernel 2: 35×35 , $\sigma = 10$. For the other filters, the parameters are optimized to obtain the best filtering result available for the specific filter. For anisotropic diffusion filter, the optimal result is obtained when conduction coefficient is set as 20, diffusion of speed is set as 0.25 and the program runs 50 iterations. For wavelet denoising method, the optimized filter is under soft threshold setting at 4 levels. For median filter and Lee's filter, the optimal filtering result is achieved when the window size is set at 13×13 and 15×15 respectively.

The processing result with different algorithms are shown on Fig 2.6 and 2.7 for test image with 10dB contrast and Fig 2.8 and 2.9 for the one with 5dB contrast. As can be seen on Fig 2.6, when the contrast is 10dB, all

the algorithms are able to suppress speckle noise quite well. The 3D mesh plot shown in Fig 2.7 illustrates more clearly of how different algorithms have improved the clarity of signals. The proposed DoG enhanced local normalization algorithm removes the speckle noise entirely and extracts the main signals, achieving better despeckling results than others. In the case of the 5dB images, the signals are seriously contaminated and can hardly be discerned from the background. The anisotropic diffusion, median filter, wavelet and Lee's filter, although effectively suppress the speckle noises, but it is still difficult to recognize the signals. The proposed algorithm successfully extracted the the circle signals; but because of the low contrast, the algorithm cannot remove all of the noise, resulting in several false positive points on the upper right part of the image.

The performance of different filtering algorithm is further evaluated from computational speed and peak signal-to-noise ratio (PSNR) aspects. PSNR measures the ratio between the maximum power of a signal and the power of noise. It is generally used as a quality measurement between the reference image and noise-corrupted image. The higher the PSNR value, the better the quality of the image. To compute PSNR, the mean square error (MSE) between the reference image and the corrupted image is first calculated, as in Eq 2.7.

$$MSE = \frac{\sum_{M,N}[f_1(x,y) - f_2(x,y)]^2}{M \times N} \quad (2.7)$$

In the equation, M and N represents the number of rows and columns for the image.

PSNR is then obtained by Eq 2.8. In the equation, R is the maximum fluctuation for the input image data type, e.g. R is 1 for float data type and 256 for 8 bit unsigned data type. In this thesis, the image data type is float,

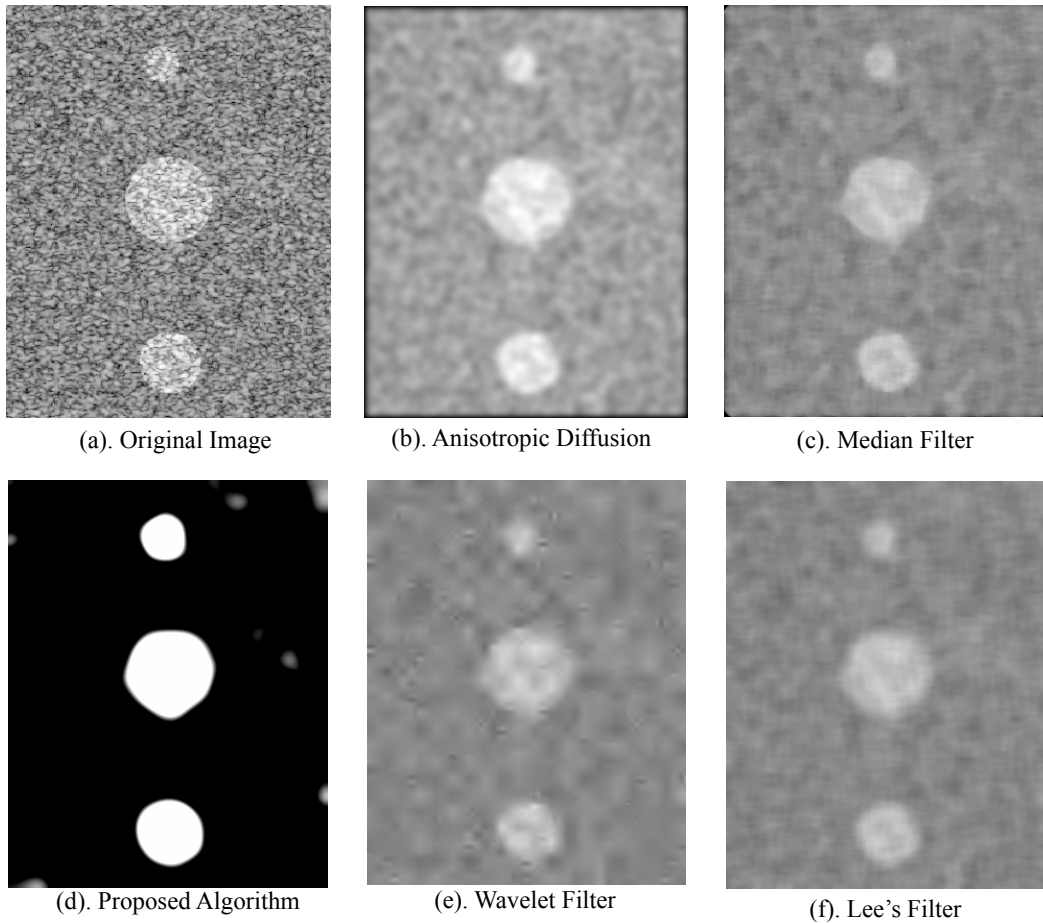


Figure 2.6: Comparison of Filtering Result for Test Image with Contrast of 10dB. (a). Original image; (b). Result obtained with anisotropic diffusion; (c). Result obtained with median filter; (d). Result obtained with proposed filter; (e). Result obtained from wavelet filter; (f). Result obtained from Lee's filter

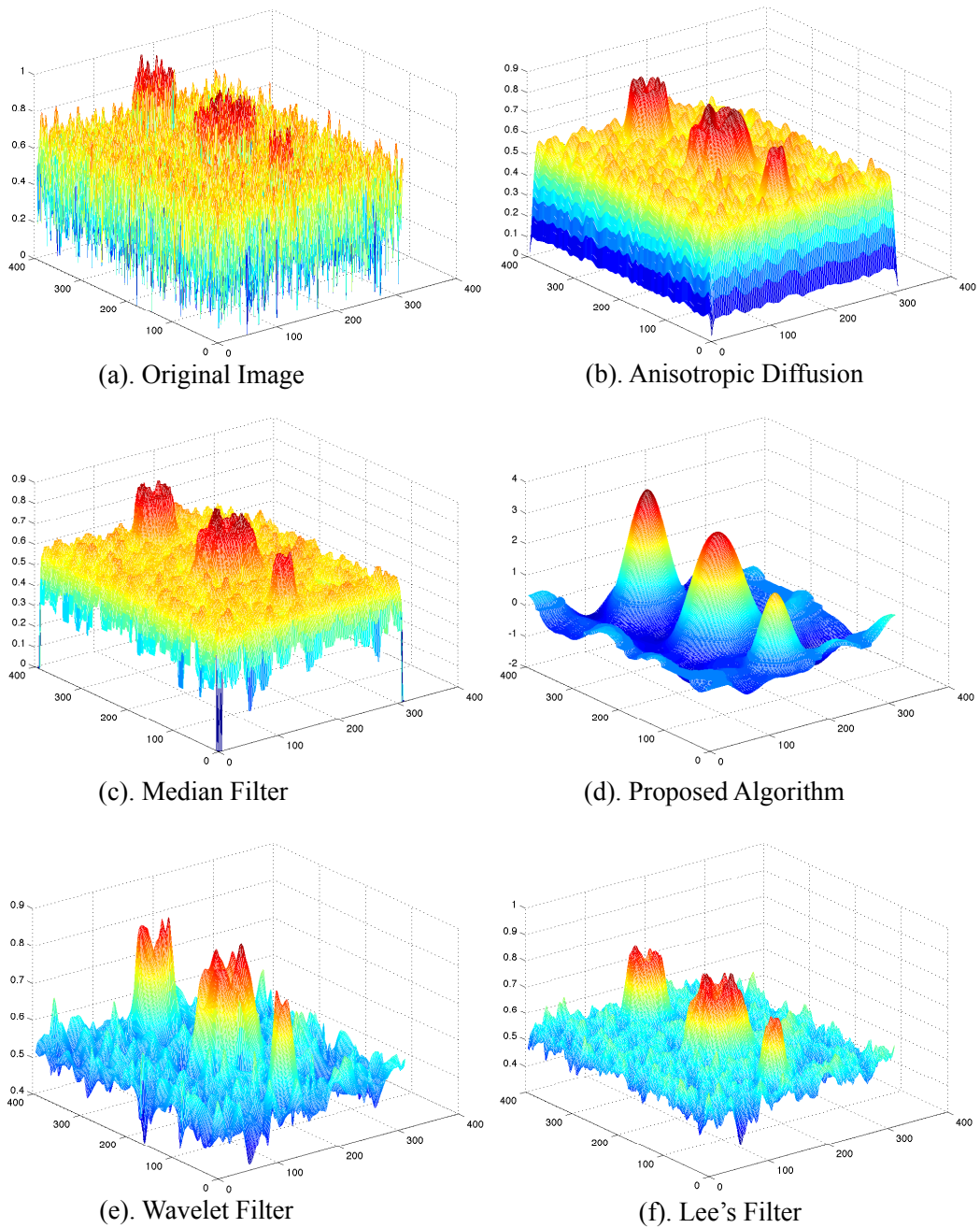


Figure 2.7: 3D Mesh Plot of Filtering Result for Test Image with Contrast of 10dB. (a). 3D mesh plot of original image; (b). 3D plot for result obtained with anisotropic diffusion; (c). 3D plot for result obtained with median filter; (d). 3D plot for result obtained with proposed filter; (e). 3D plot for result obtained from wavelet filter; (f). 3D plot for result obtained from Lee's filter

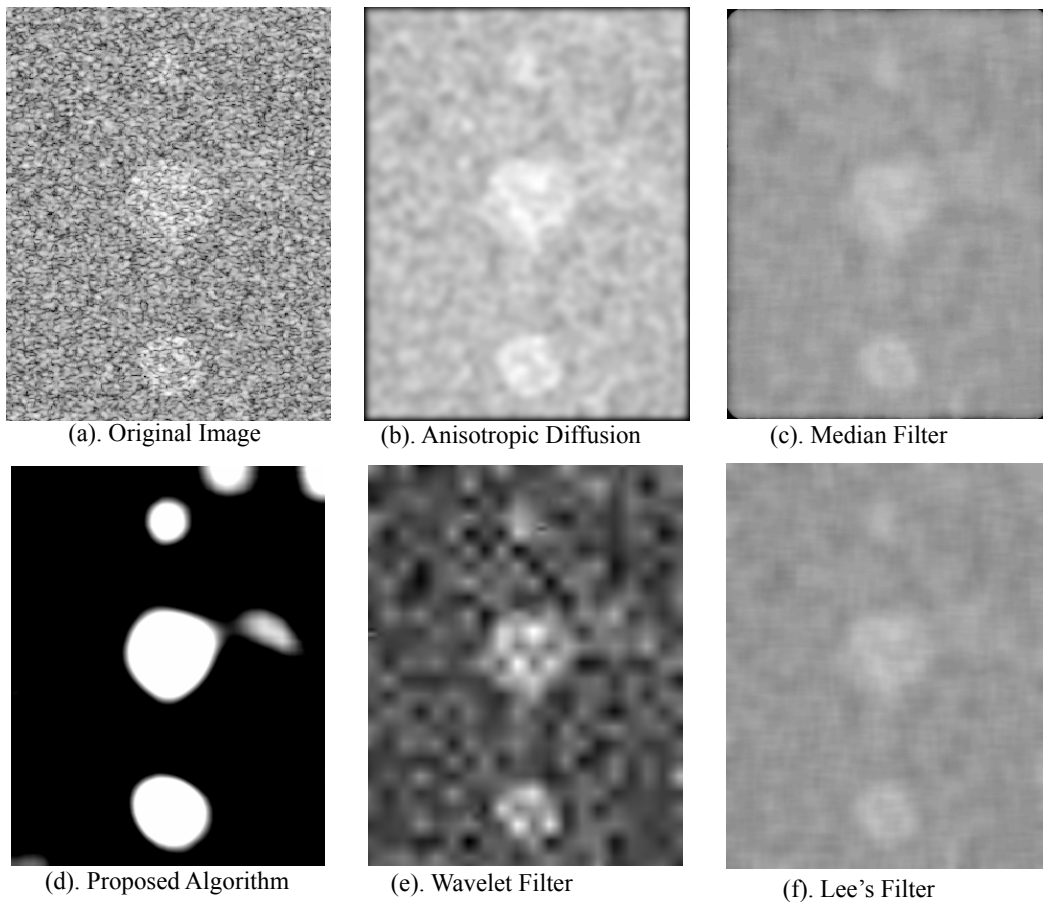
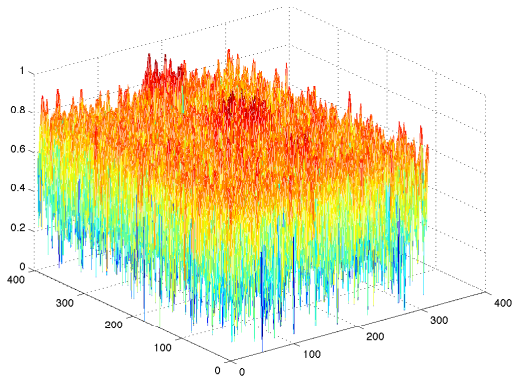
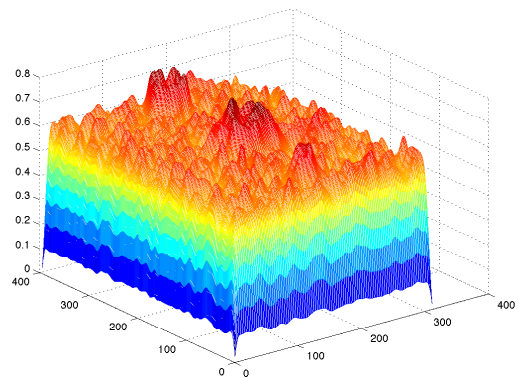


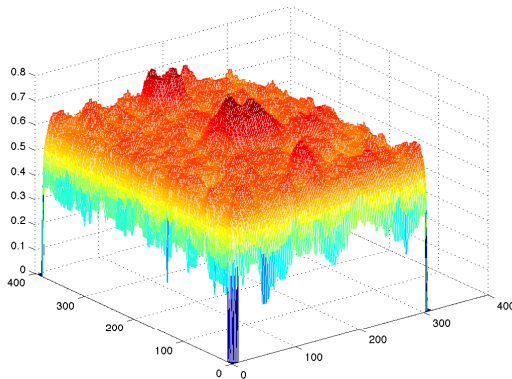
Figure 2.8: Comparison of Filtering Result for Test Image with Contrast of 5dB. (a). Original image; (b). Result obtained with anisotropic diffusion; (c). Result obtained with median filter; (d). Result obtained with proposed filter; (e). Result obtained from wavelet filter; (f). Result obtained from Lee's filter



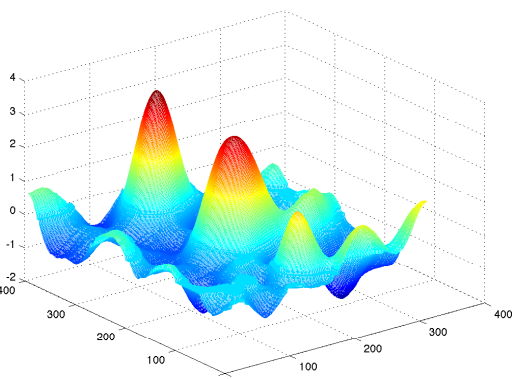
(a). Original Image



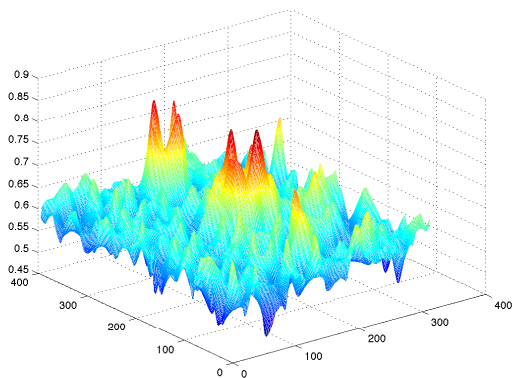
(b). Anisotropic Diffusion



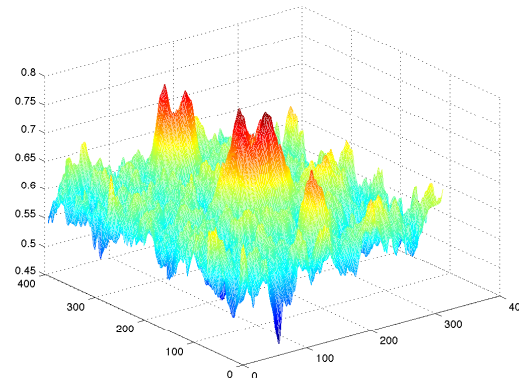
(c). Median Filter



(d). Proposed Algorithm



(e). Wavelet Filter



(f). Lee's Filter

Figure 2.9: 3D Mesh Plot of Filtering Result for Test Image with Contrast of 5dB. (a). 3D mesh plot of original image; (b). 3D plot for result obtained with anisotropic diffusion; (c). 3D plot for result obtained with median filter; (d). 3D plot for result obtained with proposed filter; (e). 3D plot for result obtained from wavelet filter; (f). 3D plot for result obtained from Lee's filter

Table 2.1: Performance Comparison Between Different Filtering Algorithms

	10dB Image	5dB Image	Time(ms)
Original Image	16.93	14.83	-
Anisotropic Diffusion	20.34	17.41	120.52
Wavelet Filter	20.36	17.45	32.08
Lee's Filter	21.13	17.85	5.81
Median Filter	20.54	17.19	149.36
Proposed Filter	24.86	21.09	29.29

thus R is set as 1.

$$PSNR = 10 \cdot \log_{10}\left(\frac{R^2}{MSE}\right) \quad (2.8)$$

Table 2.1 lists the detailed comparison of different filtering algorithms. The proposed DoG enhanced local normalization algorithm achieved maximum $PSNR$ among the filtering algorithms, both for the 10dB and 5dB test images. For the computational speed aspect, it takes 29.29 ms to process the test image of size of 396×311 , with kernel parameters of Kernel 1: $25 \times 25, \sigma = 5$; Kernel 2: $35 \times 35, \sigma = 10$ specifically.

The computational speed of the local normalization algorithm depends on the size of the image and Gaussian kernels. If the Gaussian kernel size is big, then the convolution between the image matrix and kernel matrix will take longer time to compute. Thus the bigger the kernel, the slower the computational speed. This problem can be solved by downsizing the original image into smaller image, then the kernel size required to filter the image will also shrink proportionally, therefore, accelerating the computational speed. It has been tested that if the original image is downsized to half of the original size, then the proper kernel size will be 15×15 and 20×20 . The computational

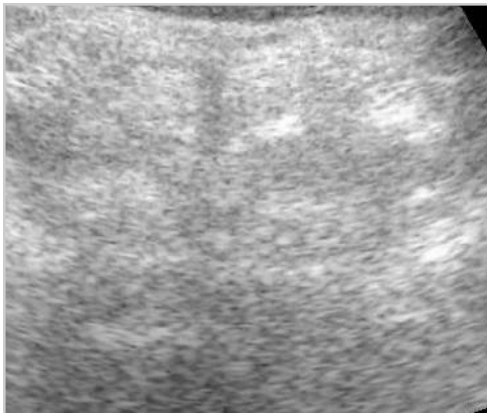
time is then shorten to 5.05ms.

The filtering result of the proposed algorithm is further tested on the clinical collected lumbar ultrasound images from pregnant patients. In the clinical settings, the lumbar ultrasound image may not be as clear as shown in Fig 2.2(a), which is obtained from volunteers. Fig 2.10(a) shows a clinical lumbar ultrasound image collected with frequency of 5MHz and scanning depth of 9cm. The clinical ultrasound image has low contrast and sometimes difficult to interpret. The filtering results obtained from comparison algorithms, e.g anisotropic diffusion and wavelet, although suppress the speckles to certain extent, are not good enough for interpretation. In contrast, the proposed algorithm is able to extract the anatomical structures, such as vertebra body and epidural space, from the given clinical lumbar ultrasound image.

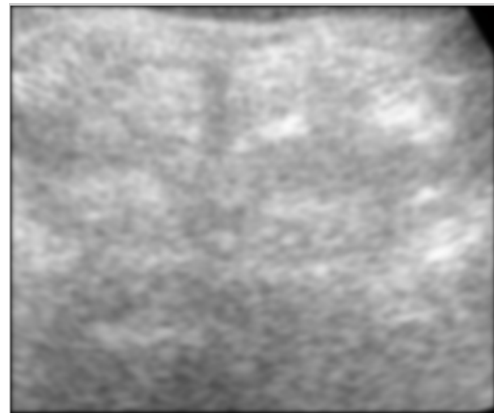
2.5 Discussions

As analysed in the above sections, the proposed DoG enhanced local normalization algorithm not only overcomes the non-uniform luminosity of ultrasound images resulted by wave attenuation, it also removes the high frequency speckle noises successfully, given that the kernel parameters are properly chosen. The results obtained by comparing with other filters indicate that the proposed algorithm is specially suitable for ultrasound image processing for the ultrasound image processing.

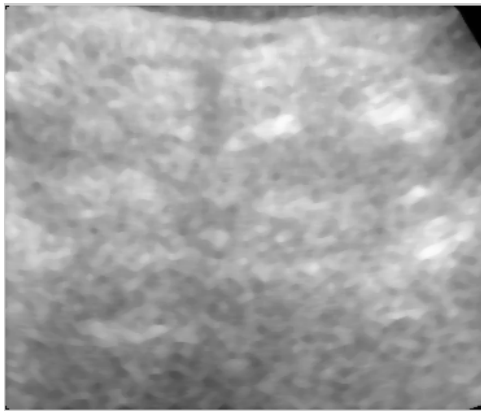
The choice of Gaussian kernel parameters are especially important in order to achieve desired despeckling effect. The proper kernel parameters are related to the size of the anatomical features to be extracted. They should be chosen based on the principal that the second kernel should have larger σ value and slightly bigger than or same size with the first kernel, so that the DoG procedure will be able extract the main anatomical structures/features of the image. For the case of lumbar ultrasound image pre-processing, the default



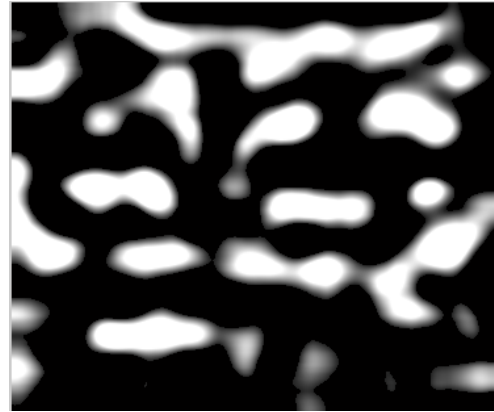
(a). Original Image



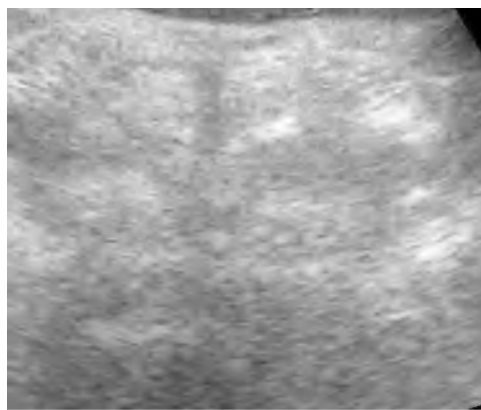
(b). Anisotropic Diffusion



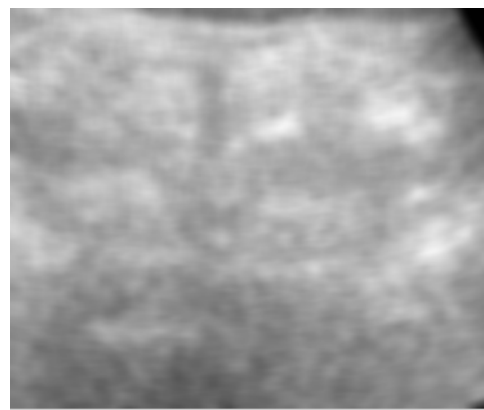
(c). Median Filter



(d). Proposed Algorithm



(e). Wavelet Filter



(f). Lee's Filter

Figure 2.10: Comparison of Filtering Result for Clinical Lumbar Ultrasound Image. (a). Original image; (b). Result obtained with anisotropic diffusion; (c). Result obtained with median filter; (d). Result obtained with proposed filter; (e). Result obtained from wavelet filter; (f). Result obtained from Lee's filter

value of the first kernel size may be set as $size = ImageSize/12, \sigma = size/5$ and the second kernel can be set as $size = ImageSize/10, \sigma = Size/3$. If the initial test with the default value shows that the speckle noises are not removed entirely, as shown in Fig 2.4(a), then need to increase the kernel parameters progressively until good despeckling effect is achieved; if the resultant image shows that major anatomical features are mingled together, as shown in Fig 2.4(d), it indicates that the kernel parameters are chosen too big and required to decrease the parameters.

However, there are limitations for the proposed DoG enhanced local normalization algorithm. In order to remove the speckle noise, the parameters of the Gaussian kernels are usually chosen large to achieve smoothing effect. This may lead to the losing of tiny features and shape deformation, as shown in Fig 2.8. If the target anatomical feature are too thin or too tiny that its size is comparable to the speckle noises to be removed, the proposed algorithm will eliminate the tiny features as speckle noise, thus not applicable. In addition, for applications where the speckle texture serves as important features, e.g., the liver cancer diagnosis, the proposed pre-processing algorithm may be counterproductive to the purpose. Nevertheless, for the case of lumbar ultrasound images, the target features, i.e. epidural space, vertebra body and articular processes, are much larger than speckle noises in size. Therefore, the proposed algorithm is applicable for lumbar ultrasound images.

2.6 Conclusion

In this chapter, DoG enhanced local normalization was proposed for lumbar ultrasound image pre-processing. The algorithm successfully eliminates the speckle noises and also effectively extracts the major anatomical structures revealed in the lumbar ultrasound image. In comparison with the general used ultrasound image pre-processing algorithms, the proposed algorithm achieves

better result in terms of PSNR. Therefore, the proposed algorithm is applicable for lumbar ultrasound image pre-processing.

Chapter 3

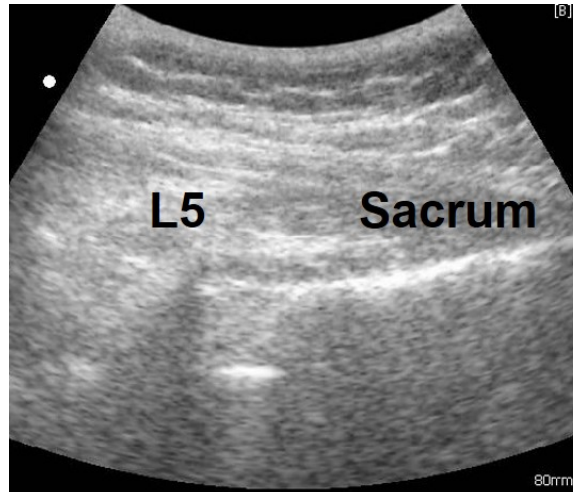
Lumbar Level Identification

3.1 Introduction

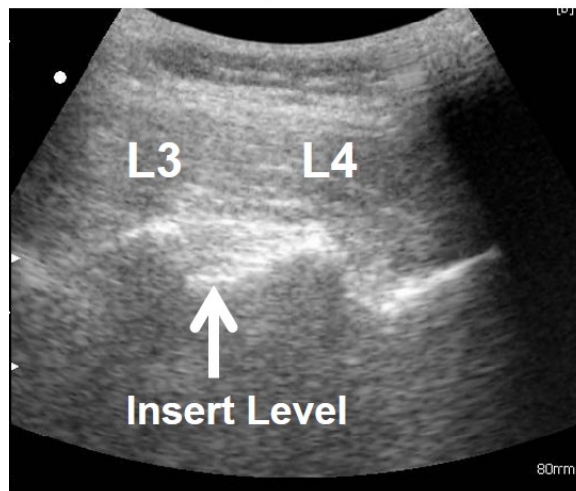
Lumbar level identification is an important procedure for epidural anesthesia, so as to select the spinous level that is most appropriate for needle insertion, usually in L3-L4 level, as shown on Fig 1.2 [5]. Conventionally, this procedure is implemented by palpation on the patients spine for certain anatomic landmarks [55]. However, it has been reported that only 30% success rate is achieved with the palpation method to identify the accurate spine level [56]. The case is clearly worse for patients with obesity issues, whose anatomical landmarks are more difficult to identify [57].

Ultrasound imaging, as a non-radioactive, convenient and inexpensive medical imaging modality, has been introduced to epidural anesthesia to assist epidural needle insertion since the 1950s [58]. Previous researches have confirmed the effectiveness of ultrasound imaging compared with traditional palpation method [23, 27, 29]. However, despite the benefits of ultrasound, the effective interpretation of ultrasound images remains a challenge, especially for anesthetists who received limited training in reading ultrasound images [58].

In order to assist the ultrasound image interpretation and facilitate the applicability of ultrasound in epidural needle insertion, automatic identification



(a)



(b)

Figure 3.1: (a).Ultrasound Image of the L5 and Sacrum. (b). Ultrasound Image of the L3-L4 Spinous Level.

of lumbar levels has been investigated by researchers. Kerby et.al [31] proposed to label the lumbar level automatically with panorama images obtained from the parasagittal plane. Rafi-Tari et.al [59] designed a simple system of using camera mounted on the ultrasound transducer to generate the 3D ultrasound volume, and then identify the spinous levels on the panorama image. An augmented reality system was further proposed by Ashab et. al [32] which is capable of generating panorama images, identifying spinous levels and projecting the result on patients' back with augmented reality.

The researches mentioned above are able to identify the spinous levels, however, they are either not fully automatic [31], demand the external modification of the transducer [59], or require the operator to choose the frames for image stitching, thus posing a requirement of ultrasound knowledge on the side of anesthetists [32]. In addition, all of the three papers mentioned above failed to recognize the importance of sacrum, the neglect of which will potentially bring error to the L5 identification and spinous level counting.

In this chapter, an ultrasound imaging processing procedure is proposed to realize the fully automatic real time spinous level counting, which incorporates automatic sacrum identification, panorama image stitching and spinous process identification. The identification results are imposed on the original ultrasound image in real-time while scanning, so that anesthetists are informed of which level the probe is located, without meticulously counting the spinous levels and read the ultrasound images. The system will provide simple guidance to the anesthetists on how to move the probe, thus require least basic knowledge on the part of anesthetists for ultrasound image interpretation. It is intended for anesthetists who received limited training on ultrasound interpretation and being utilized as a training tool to quickly get familiarized with epidural needle insertion.

3.2 Automatic Sacrum Identification

Sacrum is the starting point of the spinous level counting, followed by L5, L4, L3, L2 and L1. The interspinous level between L3-L4 is the level most appropriate for needle insertion, which provides largest interspinous gap and wider epidural space [5]. The existing researches of spinous level identification neglect the identification of sacrum on ultrasound image, assuming that sacrum is readily palpated. However, the lack of sacrum identification may lead to the misidentification of starting point, further resulting in missing levels.

In this section of the chapter, the automatic sacrum identification based on feature extraction and support vector machine (SVM) is proposed. When the scanning is commenced, the probe shall be placed in the longitudinal midline view near the sacrum. The algorithm will start with sacrum detection, till sacrum is identified successfully in continuous frames.

3.2.1 Feature Extraction

Before feature extraction, raw ultrasound images are pre-processed with DoG enhanced local normalization proposed in the last chapter, so as to remove the speckle noises and extract the anatomical structure. After pre-processing, local intensity variance induced by wave attenuation is also eliminated. Therefore, a potential element which might deteriorate the image classification is removed.

Sacrum appears to be a ‘*continuous hyper echoic line parallel to the skin*’ in the longitudinal ultrasound view, as shown on Fig 3.1(a) [19]. The feature is very obvious on the ultrasound image, thus morphological features will be sufficient to separate it from other anatomical structures. Firstly, local normalization is utilized to preprocess the raw ultrasound image and extract the key anatomical structures, and then the pre-processed image is binarized with Otsu method to obtain the blob information. Since the sacrum may be connected to the nearest L5 spinous level in the obtained binary image, thus

adversely influence the morphological analysis. The open operation followed by distance transformation is utilized to separate the connected S1 and L5 spinous level, to decrease the possibility that sacrum is merged to the L5 level. Morphological features, including blob length, area, angle, center, linearity, are extracted for every blob from the obtained binary image. The feature extraction procedure is illustrated in Fig 3.2. The linearity of each blob is simplified as the ratio between length and width of the containing rectangle.

The training and test database are established by randomly extracting stills from offline collected videos from 34 patients. The blob of sacrum will be labelled as '1', while the rest non-sacrum blobs will be labelled as '0'.

3.2.2 Support Vector Machine

After the feature has been extracted and normalized, SVM is employed to optimally classify the sacrum blobs apart from the rest blobs on the binary image. SVM is a supervised learning algorithm which seeks a decision boundary (or separating hyperplane) with maximal margin for the training set. The SVM model is trained with blobs data from randomly selected 17 cases (50%) and then tested on the rest 17 cases. The obtained SVM model is saved in the computer for real time sacrum detection.

3.3 Panorama Image Stitching

If sacrum is detected continuously on the ultrasound frames (e.g. 9 out of 10 continuous frames), the algorithm will consider the sacrum is successfully located and initiate the panorama image stitching procedure. The anesthetists will be guided to move the ultrasound transducer upward slowly and steadily. The panorama image stitching include three key procedures: motion estimation, image quality evaluation and image stitching.

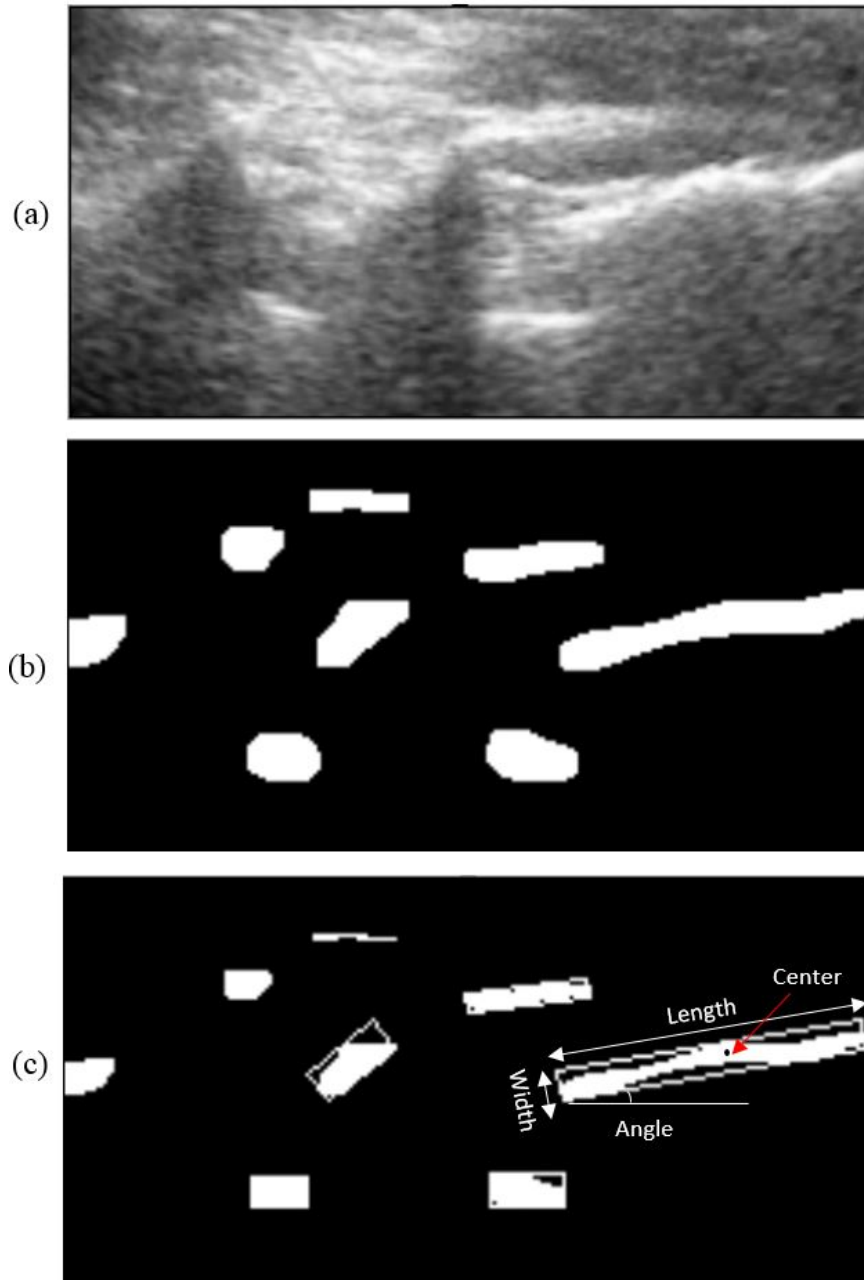


Figure 3.2: Morphological Feature Extraction for Sacrum. (a) Original grayscale image; (b). Binary image of the pre-processed image; (c). Morphological feature extraction for each blob.

3.3.1 Motion Estimation

Image stitching is a relatively time consuming operation, therefore it is necessary to estimate the probe motion and select the frames of certain distance to be stitched. During the ultrasound scanning, the transducer only takes translational movement, thus, it is reasonable to assume that the motion model is translational. In this chapter, phase correlation is utilized to obtain the relative movement of two continuous frames, because it is robust to noise, thus suitable for ultrasound image motion estimation.

Phase correlation is a Fourier-based approach which relies on the fact that ‘Fourier transform of a shifted signal has the same magnitude as the original signal but of linearly vary phase’ [60]. For two similar images $I_0(\mathbf{x})$ and $I_1(\mathbf{x} + \mathbf{u})$ with shift, the function of phase correlation is:

$$\begin{aligned} \mathcal{F}\{E_{PC}(\mathbf{u})\} &= \frac{\mathcal{F}\{\sum I_0(\mathbf{x})I_1(\mathbf{x} + \mathbf{u})\}}{|\mathcal{F}\{I_0(\mathbf{x})\}||\mathcal{F}\{I_1(\mathbf{x} + \mathbf{u})\}|} \\ &= \frac{\mathcal{I}_0(f)\mathcal{I}_1^*(f)}{|\mathcal{I}_0(f)||\mathcal{I}_1(f)|} \end{aligned} \quad (3.1)$$

where $\mathcal{I}_1(\mathbf{f}) = \mathcal{F}\{I_1(\mathbf{x})\}$, denoting the Fourier transform of the image.

Since

$$\begin{aligned} \mathcal{F}\{I_1(\mathbf{x} + \mathbf{u})\} &= \mathcal{F}\{I_1(\mathbf{f})\}e^{-2\pi j\mathbf{u}\mathbf{f}} \\ &= \mathcal{I}_1(\mathbf{f})e^{-2\pi j\mathbf{u}\mathbf{f}} = \mathcal{I}_0 \end{aligned} \quad (3.2)$$

Therefore,

$$\mathcal{F}\{E_{PC}(\mathbf{u})\} = e^{-2\pi j\mathbf{u}\mathbf{f}} \quad (3.3)$$

The final output of phase correlation is a spike located at the correct value of the shift of two images, as shown on Fig 3.3. Therefore, it is able to estimate the frame motion fast and conveniently.

The accumulated distance of the continuous frames are calculated, which,

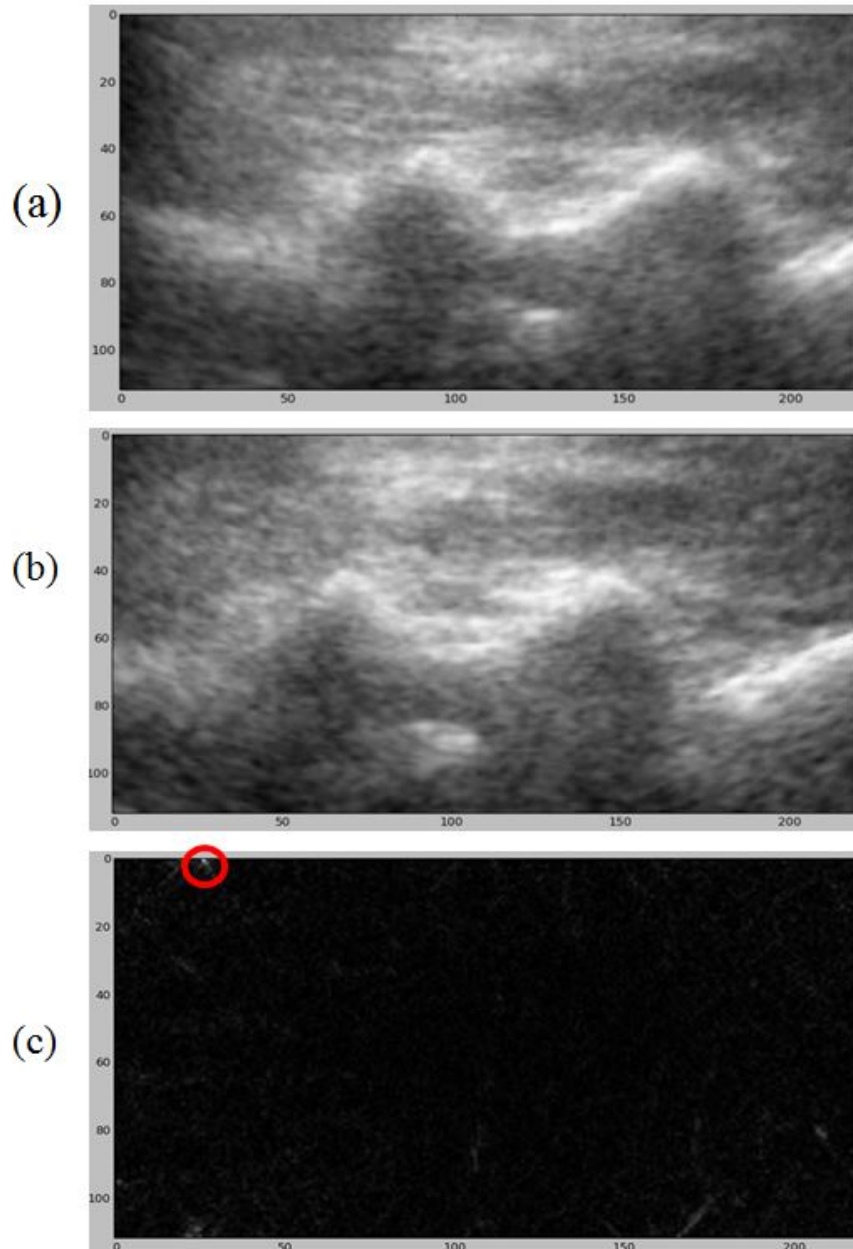


Figure 3.3: Phase Correlation Result of Two Similar Ultrasound Image With only Translation Movement. (a) and (b). Two similar ultrasound images of the spinous process; (c). Phase correlation result of the two images, with the maximum point circled, which represents the relative position between the two images.

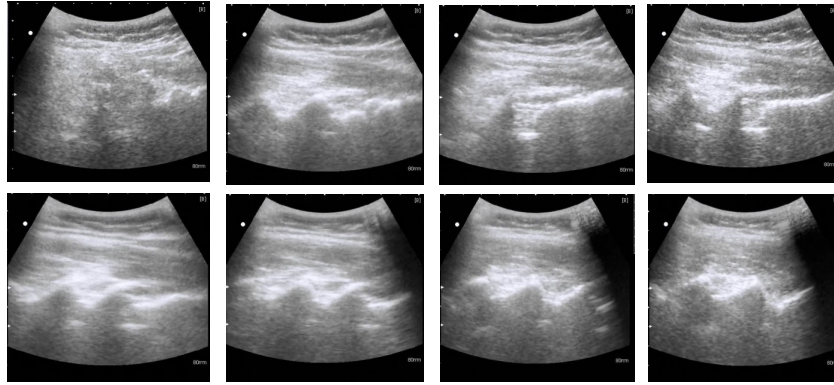
if higher than certain threshold, serves as an prerequisite for selecting frames to be stitched. However, if the accumulated distance is too large that there is no overlapping region between the panorama image and the new frame, the image stitching will be consider as a failure. For cases like this, the operator will be informed to repeat panorama image stitching and start scanning from sacrum again.

3.3.2 Frame Quality Evaluation

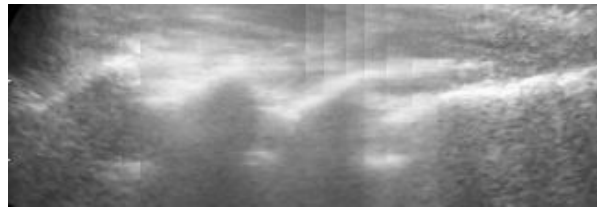
During the probe movement, it is inevitable that the probe may be slightly shifted and the image will go out of line, resulting in bad image quality. The frames of bad quality shall be excluded from image stitching, otherwise deteriorating the panorama image quality.

Three parameters are employed to evaluate the frame quality, respectively the template matching value of the spinous process, the cross correlation value of the previous stitched frame with the current frame and the stabilization of image features in the temporal domain.

The shape resembles the sinusoid peaks is utilized the the template (Fig 3.5(a)) and its matching value with the ultrasound frame serves as one parameter for the image quality evaluation. Since the spinous process shapes varies from one to another, once the spinous process is located with the given sinusoid template, the template will be updated with the detected spinous process shape, to ensure that the spinous process can be correctly identified in the continuous frames. Cross correlation of the current frame with the stored previous stitched frame will also be calculated, to ensure that the new frame going to be stitched agreeing with the panorama image. The stabilization of the image features is measured by the cross correlation value of previous and current frame. The higher the value, the more steady of the image features, thus excluding the bad quality frames resulted by accidental out-of-line of the probe.



(a)



(b)

Figure 3.4: Panorama Image Stitching. (a). Randomly selected ultrasound frames. (b). The resultant panorama image

Only when the three parameters are above certain threshold will the frames be considered good quality. Meanwhile, the accumulated distance obtained with phase correlation shall pass certain value. If those prerequisites are satisfied, the frame will be stitched onto the panorama image and related accumulator and saved stitched frame will be updated. Otherwise, the algorithm will drop the current frame and query for new frames to be stitched. With this motion estimation and frame quality evaluation approach, the algorithm ensures both the speed of panorama generation and quality of panorama image.

3.3.3 Image Stitching

After the motion estimation triggers the stitching process and the frames are evaluated to have good image quality, the frame will be selected as the one to be stitched to the panorama image. Since phase correlation has already estimated

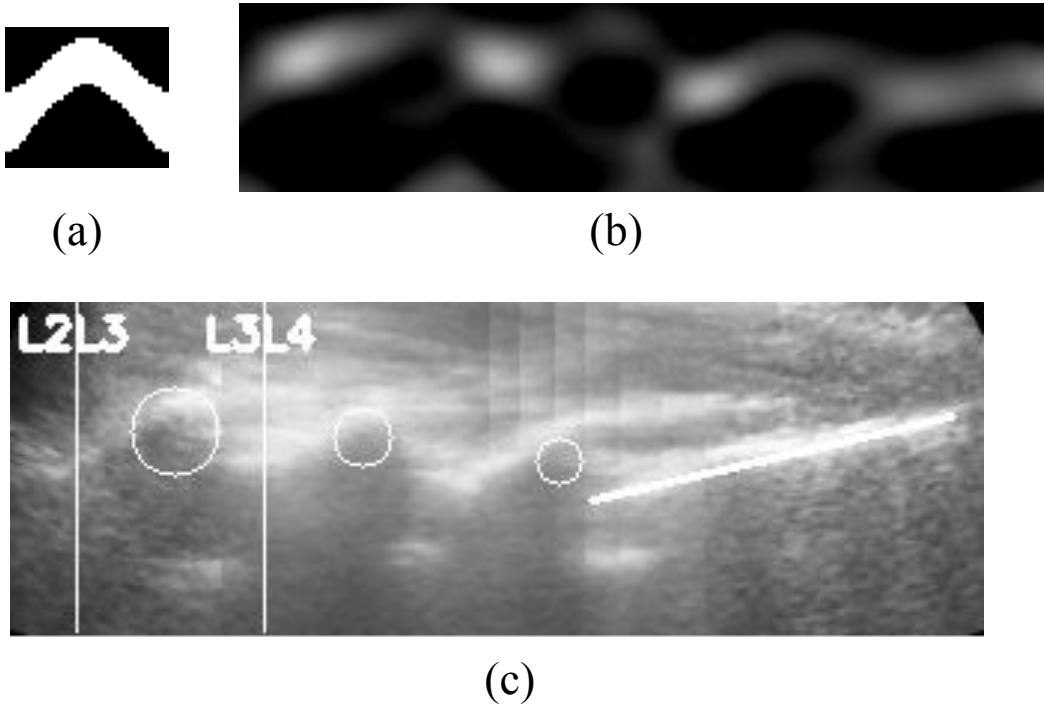


Figure 3.5: Spinous Level Identification. (a). Template used for spinous detection. (b). Template matching result of the panorama image. (c). Identified spinous levels, the circles marks the spinous processes, the vertical lines marks the interspinous region of L3-L4 and L2-L3, the sacrum is also marked with the white line.

the relative motion between the existing panorama image and the frame to be stitched, therefore, the image stitching process is simplified as aligning the new frame with the panorama image and then combining them together [60]. Fig 3.4 displays several frames randomly selected from the collected video and the final panorama image.

3.4 Spinous Level Identification

The target for level identification is to search for the L3-L4 interspinous region, which is the most appropriate level for epidural needle insertion. The spinous level identification is implemented based on the obtained panorama image. Template matching, the same sinusoid peak template, is used to identify the spinous processes. The local maximums of the template matching result are deemed as the spinous processes, if the local maximum is bigger than the given

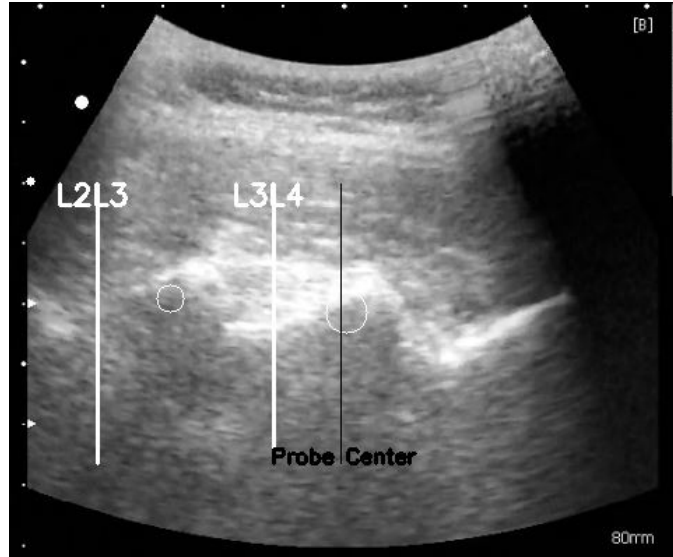


Figure 3.6: Spinous Level Identification Result on Original Ultrasound Image

threshold. Fig 3.5 shows the procedure of level identification.

The identified spinous level information will be imposed on the original ultrasound image and shown to the anesthetists, as shown on Fig 3.6. Probe center is marked on the image, so as to facilitate the anesthetists to align the L3-L4 level to the center of the probe.

3.5 Image Processing Procedure

The flow chart shown in Fig 3.7 illustrate the entire ultrasound image processing in the longitudinal midline view. To start the image acquisition, the operator holds the ultrasound transducer near sacrum with the midline view. A frame grabber is employed to acquire the ultrasound frames from the ultrasound machine and feed the video stream to a personal computer. The raw ultrasound images acquired will be pre-processed with local normalization first to remove the speckle noises and non-uniform illumination artifacts. In the initial stage, the trained SVM model will be utilized to search for the sacrum. If sacrum is identified in continuous frames, it will consider the sacrum is successfully identified and the flag for sacrum search will be set false,

eliminating sacrum searching in the following scanning. The algorithm will send out guidance for the operator to move the probe upward slowly and steady, initializing the panorama image stitching procedure. For the panorama image stitching, the relative motion of the frames is estimated with phase correlation. If the accumulated movement is bigger than certain threshold and the image quality is good enough, the frame will be stitched to the panorama image. After new frame is stitched to the panorama image, spinous processes identification and level counting will be conducted on the obtained panorama image. The spinous level information will be imposed on the original ultrasound frame to keep the operator well-informed. This procedure will repeat until L3-L4 interspinous region is aligned to the middle of the probe.

3.5.1 Materials and Image Acquisition

For the off-line model training and algorithm development, 34 ultrasound videos from 34 different subjects were collected. With the 34 collected ultrasound videos, 17 are randomly selected for the training set and the remaining 17 served as the test set for sacrum SVM model training and validation. The image processing and SVM training algorithms are implemented with Python programming language, with OpenCV, Scikit-Learn, Numpy and PyQT open source libraries installed.

3.6 Results and Discussions

3.6.1 Sacrum Identification

The SVM model for sacrum detection is trained with blobs from randomly selected 17 videos (50%) and tested with the rest 17 videos. The statistics of the training and test database for sacrum identification is listed on table 3.1. Table 3.2 lists the training and test result of the SVM model. The trained SVM model achieved an accuracy of 98.52% on the test set, indicating that

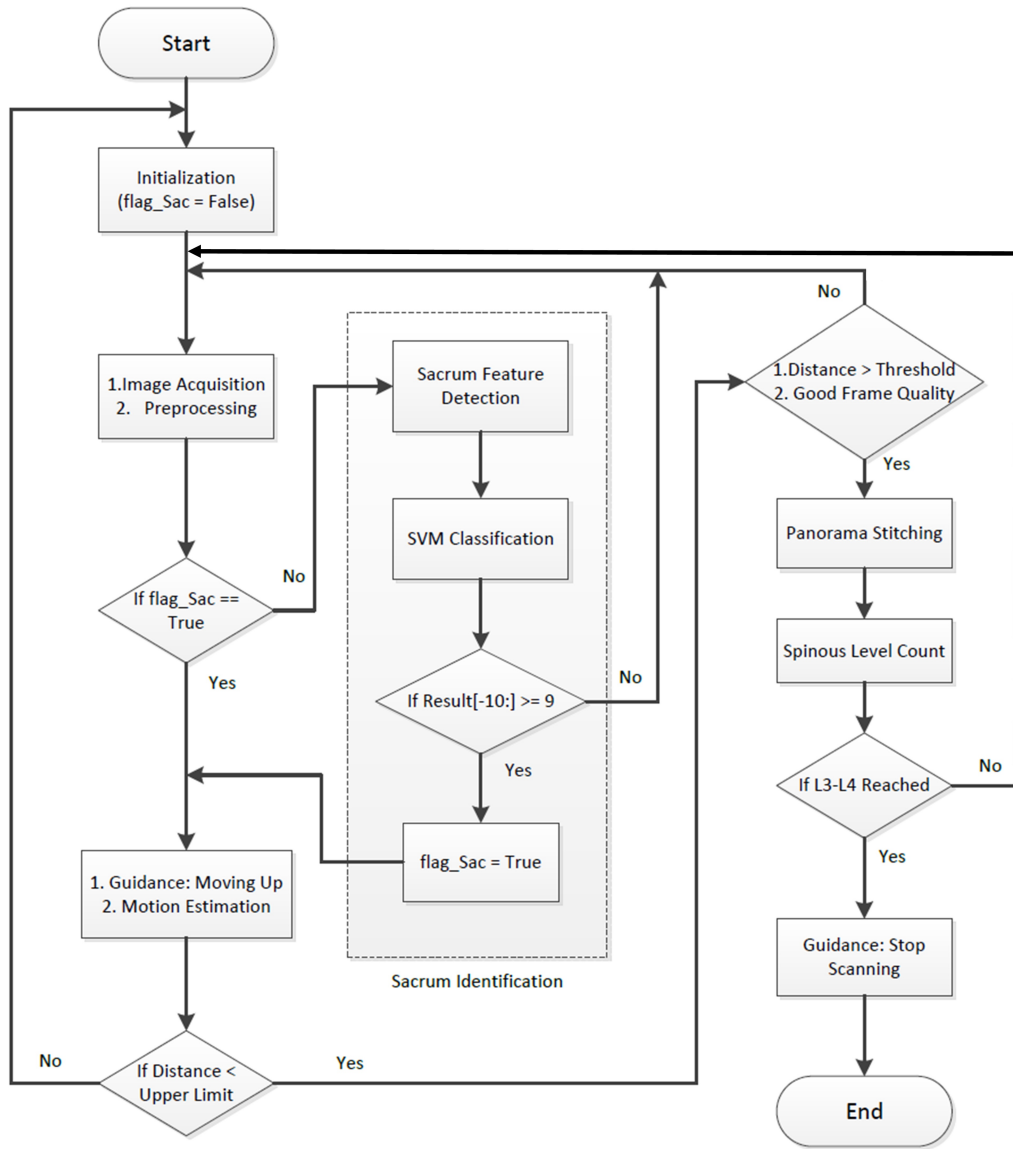


Figure 3.7: Flow Chart of Ultrasound Image Processing Procedure for Spinous Level Counting

Table 3.1: Statistics of Training Set and Test Set.

	Training Set	Test Set
Subject Number	17	17
Sampled Blobs	448	474
Interspinous	208	219
Bone Images	228	255

Table 3.2: Performance of SVM Classification for Sacrum Identification.

	Training Set (%)	Test Set (%)
Accuracy	99.55	98.52
Precision	99.04	97.75
Recall	100	99.08
F0.5	99.23	98.01

the model is well trained.

3.6.2 Result on Frame Quality Evaluation

Fig 3.8 displays the frames randomly extracted from one of the off-line video. The frame quality is evaluated based on the three parameters proposed in the previous section. In order to evaluate the quality selection criteria independently, the prerequisite for distance between the current frame and the existing panorama image is neglected. The evaluation parameter is listed on Table3.3. Of the nine frames displayed on Fig 3.8, (2)(5)(8) and (9) are selected as good quality frame. Frame (3) has the worst image quality, thus resulted in low score on all of the three parameters. Frame (1) shows no obvious spinous process and therefore get excluded. Frame(4) (6) and (7) is captured when the probe is moving in speed. The movement is reflected on the low temporal correlation parameter between the previous frame and the current frame. Therefore, the three parameters are able to reject the bad

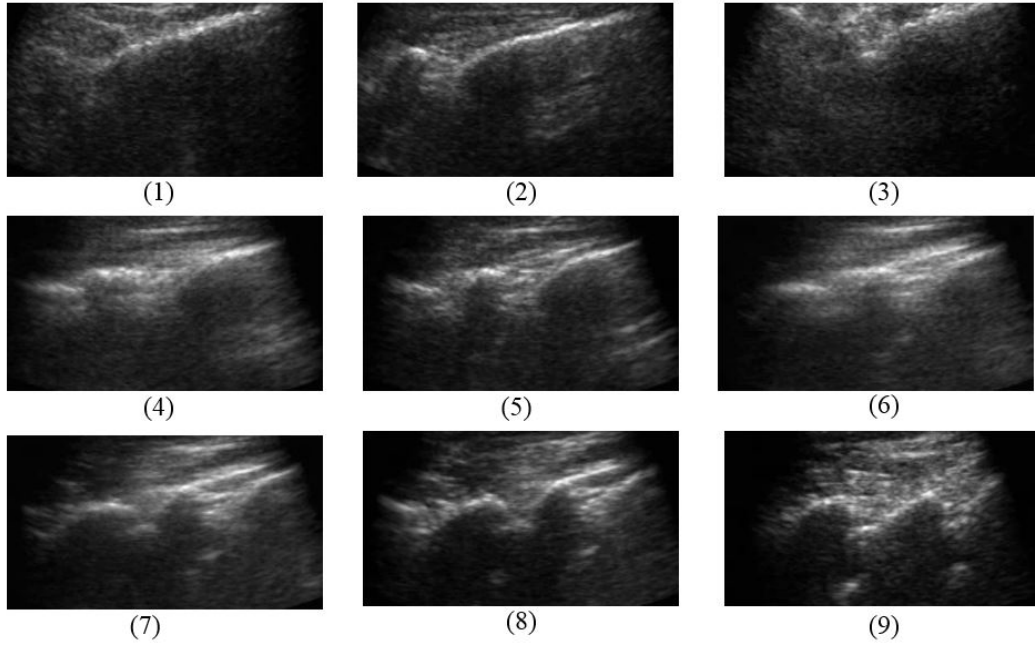


Figure 3.8: Frame Quality Evaluation for Image Series.

quality frames that occasionally appears in the video stream. In the image processing procedure, the stitching is conducted only when the accumulated distance between the current frame with the panorama image exceeds a given threshold. In this approach, the good quality frames that appears continuously can be selected at a distance, thus alleviating the computational burden of the image stitching procedure.

3.6.3 Image Stitching and Spinous Level Identification

For the offline collected ultrasound videos, the panorama image were successfully stitched on 33 out of 34 videos. The only failure case is induced by the unsuccessful saving of the whole video stream by the ultrasound machine, that the frames of the sacrum scanning part is missing in the saved video file. Since the sacrum is not detected, thus the panorama image stitching process is not triggered from the beginning.

The spinous level identification aims to locate the L3-L4 interspinous region. In the set of collected videos, L3-L4 region is successfully identified

Table 3.3: Parameters for Frame Quality Evaluation.

Image No.	Spinous Matching	Panorama Correlation	Temporal Correlation	Acceptable Quality
(1)	0.44	0.66	0.76	No
(2)	0.56	0.98	0.53	Yes
(3)	0.47	0.1	0.39	No
(4)	0.63	0.96	0.21	No
(5)	0.66	0.93	0.62	Yes
(6)	0.7	0.98	0.2	No
(7)	0.67	0.94	0.48	No
(8)	0.62	0.98	0.98	Yes
(9)	0.71	0.75	0.94	Yes

on all of the videos where panorama are successfully stitched previously, i.e., 33 out of 34 videos.

3.6.4 Computational Speed Tests

Table 3.4 lists the computational speed of major operations for the image processing procedure. For the most time-consuming procedure, where the frame is identified to be stitched to the panorama image, it takes 49.64 ms to process one frame. For the least time-consuming procedure, where the accumulated distance is less than the given threshold, it takes 15 ms to process one frame. Given that the image acquisition speed is 15FPS for real time online processing, the proposed image processing procedure is fast enough for real time application.

3.7 Conclusion

In this chapter, a lumbar ultrasound image processing procedure was proposed for spinous level identification in the longitudinal view. The algorithm starts

Table 3.4: Computation Cost of Video Processing with Matlab.

Operation	Computation Cost(ms)
Preprocessing	1.89
Sacrum Identification	7.52
Motion Estimation	4.39
Image Stitching	27.75
Spinous Level Counting	5.50
Maximum Processing Time Per Frame	49.64
Minimum Processing Time Per Frame	15.19

with automatic sacrum identification, by feature extraction and support vector machine. The continuous identification of sacrum will initiate the panorama image stitching process. Image quality is evaluated along with distance calculation, to ensure that the frames being stitched to the panorama image match certain standard. The spinous levels will be identified and divided based on the obtained panorama image. The identification results are imposed on the original ultrasound image in real time as the operator moving the probe. Simple guidance will also be provided to the operator on how to move the probe. The whole image processing procedure is fully automatic and requires the least ultrasound knowledge for anesthetists.

Chapter 4

Localization of Precise Needle Insertion Site with Cascading Classifier

4.1 Introduction

As mentioned in Chapter 1, the localization of epidural needle entry site with ultrasound imaging involves two continuous stages: counting the lumbar level in the longitudinal view and identify the accurate entry point in the transverse view [19]. The ultrasound probe is first positioned in the longitudinal orientation to search for the L3-L4 spinous level, the automatic image interpretation of which has been discussed in the previous chapter. Then the probe is rotated to the transverse view to further search for the precise location of the needle insertion site.

The objective of this chapter is to fill the gap of automatic ultrasound image interpretation of lumbar spine in the transverse view for pregnant patients. First, a primary version classifier based on position relationships of main anatomical features, called position correlator, was developed to identify the interspinous image. The position correlator achieved a success rate of

100% on ultrasound images obtained from lumbar spine of healthy volunteers. However, since the clarity of anatomical features of lumbar spine might degrade during pregnancy [61], the original position correlator designed for healthy volunteers may not be effectively applicable to the pregnant patients. In order to solve this problem, a cascading classifier is proposed to improve the image identification. The cascading structured classifier contains four layers and imposes stricter rules for the image classification, from aspect of position and intensity of anatomical features and black pixel rate along the midline. The proposed cascading classifier was further tested on ultrasound video streams collected from pregnant patients in an off-line manner and achieved much better performance than the position correlator.

4.2 Ultrasound Image Features of Lumbar Spine

Ultrasound imaging provides anatomical information on 2D B-mode images corresponding to the plane where the probe is located. Along with the movement of the ultrasound probe, the anatomical structures beneath the probe will change accordingly, leading to different image features. When the probe is placed directly on the spinous process, the ultrasound wave will be impeded by bones, creating a long triangular hypo-echoic acoustic shadow Fig4.1(a). The midline of the ultrasound image will be dark with a triangular dark window in the middle, which is the main feature of bony images. When the probe is moved to the interspinous region, more details beneath the skin can be noted, as shown in Fig 4.1(b). The ‘flying bat’ like shape indicates that the location of the probe is a suitable site for needle insertion [19]. The important anatomical features, i.e, epidural space, vertebra body and articular processes, will be revealed in the interspinous image.

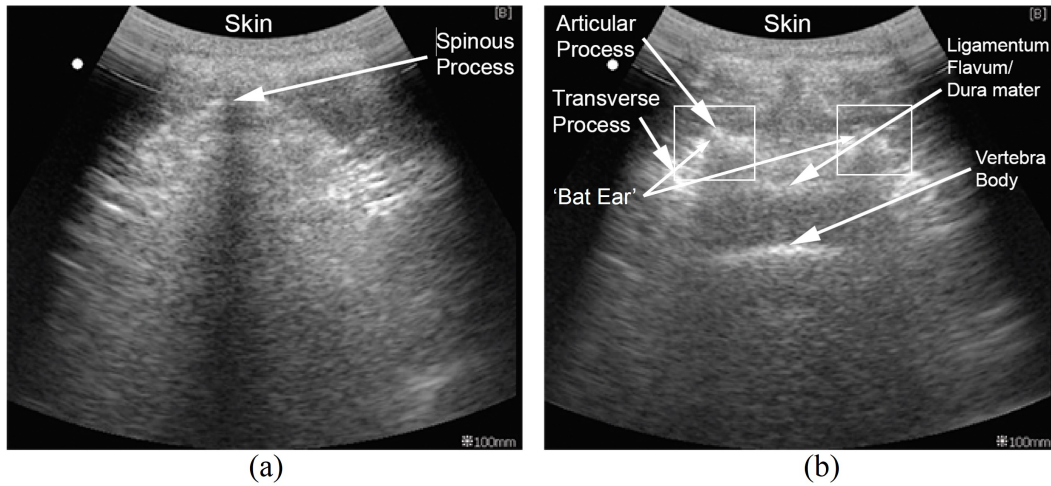


Figure 4.1: Ultrasound Image of Lumbar Spine. (a) Typical ultrasound image when the probe is placed above spinous process, featured by the triangular anechoic window; (b) Ultrasound image when probe is placed on interspinous space.

4.3 Position Correlator

The visibility of ‘flying bat’ shape is the criterion adopted by anesthetists to recognize interspinous images [19]. However, in computer vision, due to the variation and distribution extent of the ‘flying bat’ shape in the image, the recognition of the entire ‘flying bat’ shape is not a easy task. Although algorithms like active contour can be employed to fit the shape, it usually subjects to the limitation of slow computational speed; thus, not applicable for the real time recognition purpose.

In order to make the signatory feature easily recognizable, the ‘flying bat’ is decomposed into smaller and more easily distinguished and independent features to identify whether a certain position is suitable for needle insertion. The three features that are most important in identifying the needle insertion site are: the ‘bat ears’, which represents the combination of articular process and transverse process as marked on Fig 4.1(b), the epidural space (which actually includes both ligamentum flavum and dura mater, but usually seen as a single line in ultrasound images), and the vertebra body.

The separation of a single big feature into these three smaller features also

has the advantage that the distances between any two of the features can be allowed to vary, as long as the relative positions hold. This allows versatility for the approach to remain applicable to different patients, since the detailed spine structures will inevitably vary from one person to another, resulting in a different size of the ‘bat’. Thus, it is challenging to be able to use a single ‘bat’ as a signatory feature representative of everyone, but have three separated and smaller signatory features will be more robust to such uncertainties. Only when the probe is placed on the interspinous space, where it is suitable for needle insertion, will all the three features be manifested together. When the probe is placed above the spinous process, the image window is dark in the middle, thus none or less than three features can be identified. This decomposition of the conventional signatory feature is a key step contributing to the effectiveness of the proposed approach which will be highlighted in the following sections.

4.3.1 Template Matching Algorithm

In the quest for the three signatory features, the template matching algorithm is leveraged on to search for the features from the ultrasound image. Template matching, in essence, computes the cross correlation between templates and images. The template moves from pixel to pixel and the degree of similarity between the template and the area scanned by templates is computed. The group of pixels giving the maximal correlation results will be deemed as the desired feature.

$$g(x, y) = \sum_{i,j} T(i, j)I(x + i, y + j) \quad (4.1)$$

where $g(x, y)$ represents the matching result, $T(i, j)$ denotes the template and $I(x, y)$ denotes the target image.

Three signatory features, including the articular process, epidural space and vertebra body, were used as the representation of interspinous space. Among

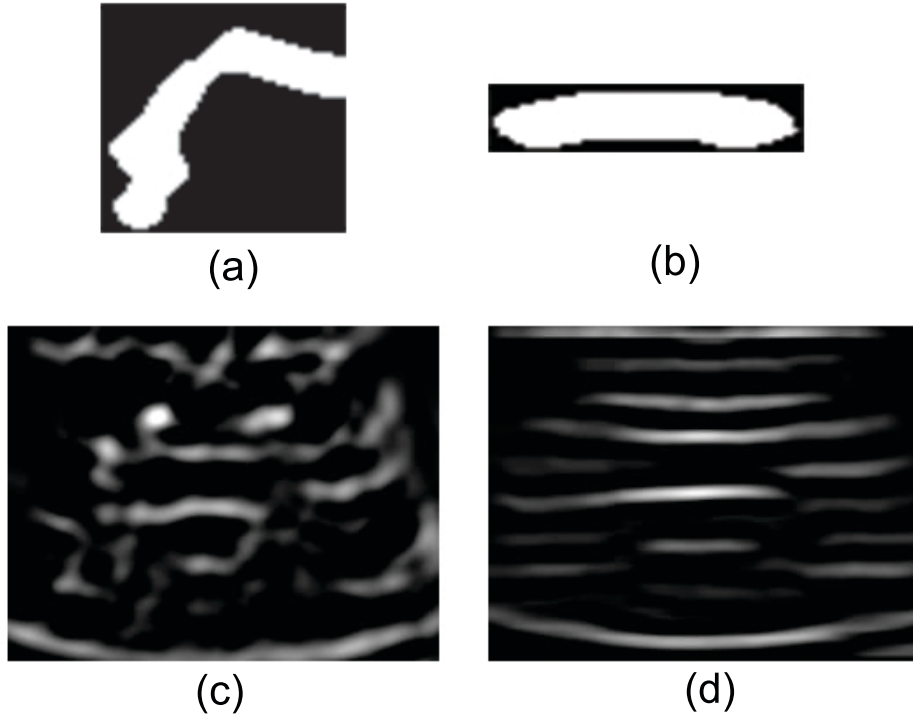


Figure 4.2: Ultrasound image processing using template matching. (a) Signatory template for articular process. (b) Signatory template for vertebra body. (c) Matching results for articular process. (d) Matching result for vertebra body.

the three sub-features, the appearance of the epidural space and the vertebra body both resemble a line. Thus, the same linear sub-template, as shown on Fig 4.2(b), is employed for the recognition of both vertebra body and epidural space. The signature of articular process is the ‘bat ear’ in ‘flying bat’ shape, as shown on Fig 4.2(a). Fig 4.2(c) and (d) lists the template matching result of the articular process and vertebra body for the interspinous respectively.

However, since the algorithm extracts the best match between the image and the feature template, there may be mismatches arising from look-alikes in the same image. As shown in Fig 4.3(b), which is the image of a bone, but the template matching algorithm may extract it as the vertebra body, if no differentiation regulation is applied.

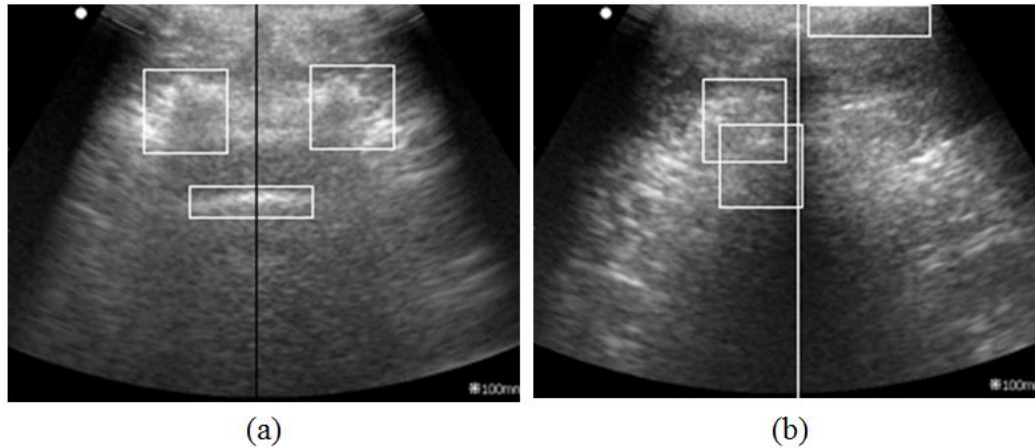


Figure 4.3: Template Matching Results for Interspinous Image and Bone Image. (a). template matching result for proper insertion site. (b). template matching result for images above spinous process.

4.3.2 Position Correlator

Although the target features are now smaller and easier to find in the image, another issue has occurred in its sensitivity to mismatches. Two solutions are proposed to solve this sensitivity problem. 1. A threshold can be used to limit the result of template matching output. A matching value which is higher than the threshold is considered to be the desired feature; while one lower than the threshold is dismissed as a mismatch. 2. The physical position relationship between the two features can be exploited to sieve out the mismatches. The ‘bat ear’ template on Figure 4.2(a), which represents the left and right articular processes, is always located higher up in the image than the vertebra body (template 2), following the anatomy structures of lumbar spine. Thus, a position correlator leveraging on this relative locations can be used to sieve out mismatches.

Even though the threshold method is widely employed when using template matching, it is not necessarily robust, since the thresholds for different persons will be vastly different. Even for the same person, the threshold is not constant if the scanning angle and position changes. It is not quite possible to find a threshold that fits all. However, the position correlation among the features

remains the same. Therefore, the position correlation approach is utilized to identify whether the identified feature is a good match. For matched results with the vertebra body area located higher than the articular process, the image is identified as a bone image. If the position correlation follows the anatomy, then the image will be identified as the interspinous space and the placement of the probe is a potential candidate for needle insertion.

The position correlator is a key function which makes up for the void created from the decomposition of the ‘flying bat’ to keep the identification results robust. In real experiments on a total of 239 ultrasound images collected from 5 healthy volunteers, comprising of 73 bone images and 166 interspinous images, the position correlator is able to successfully sieve out the 73 bone images which would otherwise be similarly interpreted as the interspinous space too.

4.3.3 Comparison of Identification Rate and Computation Time

Another important aspect to note is the effects of different local means of the image and the template on the interspinous image detection. The local intensity variance of the image and template significantly affect the correlation results, potentially shifting the search convergence from the best match point to the brightest region instead. Therefore, before the computation of the correlation statistics, the means of the templates and the local means of target images covered by templates should be first normalized. From the experiments conducted, it is observed that without the normalization step, the ratio of incorrectly identifications over total images scanned is 166/239 (69.4%). In these cases of incorrect identification, the algorithm is unable to distinguish interspinous images from bone images. Thus, the pre-processing stage is critical to improve the accuracy of template matching through a normalization

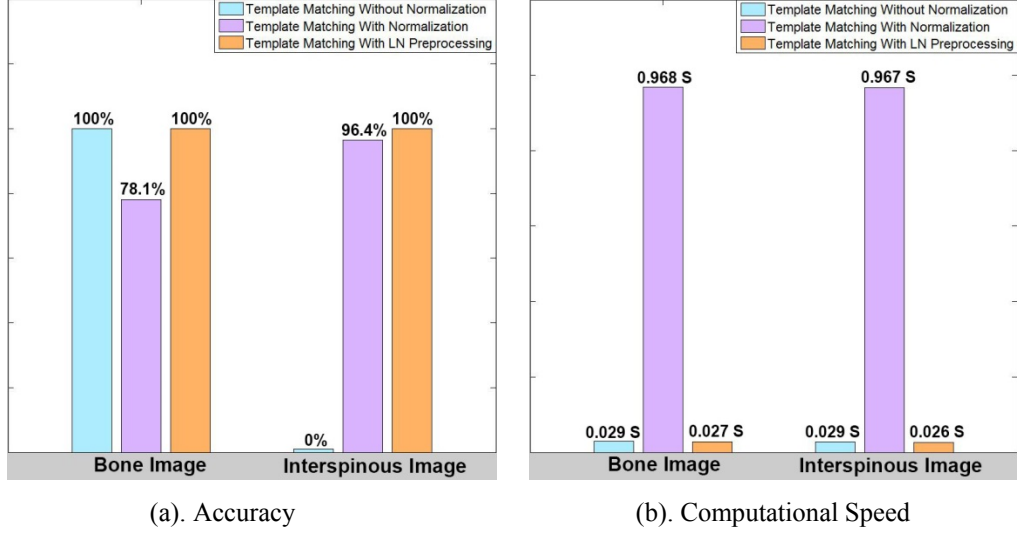


Figure 4.4: Identification Result for Template Matching. (a). Comparison of identification rate; (b). Comparison of computational time

process as in Equation 4.2.

$$g(x, y) = \frac{\sum_{i,j} T(i, j) I(x + i, y + j)}{\sqrt{\sum_{i,j} T(i, j)^2 \cdot \sum_{i,j} I(x + i, y + j)^2}}. \quad (4.2)$$

With the normalized correlation approach, the local standard deviation of target image under the template has to be computed at every pixel of the image. As a result, normalized template matching is generally a computationally expensive algorithm. For a 151×151 8 bit gray-scale ultrasound image, it consumes 0.968s to process an image with Matlab. This duration is rather long for a real-time recognition application processing a series of images acquired in quick succession.

To reduce the amount of computational time necessary, the DoG modified local normalization algorithm is used to overcome the local intensity variance of the ultrasound image, before template matching is computed. The results point to an even higher accuracy achieved compared to template matching with normalized correlation. The computational speed achieved is also 35 times faster than that with the normalized correlation approach. A thorough

comparison between those two approaches is illustrated in Fig 4.4.

The normalized template matching algorithm, combining the position correlator and DoG modified local normalization preprocessing proposed in Chapter 2, achieves excellent recognition results in the experiments conducted. In all of the 239 ultrasound images tested, the algorithm is able to find the features of interest successfully on interspinous images. The position correlator is able to effectively sieve out incorrectly matched feature on images that are collected above the bones. Therefore, collectively with these two algorithms, the proposed approach is able to automatically identify the interspinous images, at a speed which is amenable towards real-time applications, thus potentially reducing the anesthetists interpretation of ultrasound images to an easier one of following the guidance from the proposed system in the movement of the probe along the patients to reach the suitable site.

4.4 Cascading Classifier

4.4.1 Improved Position Correlator

With respect to the ultrasound images collected from volunteers, the proposed position correlator in the last section, which only is concerned with the relative positions of articular process and vertebra body, achieved 100% success rate on the 239 ultrasound images. However, the same position correlator performed poorly on the video streams collected from pregnant patients, since the visibility of key anatomical features decreases during pregnancy [29]. In order to improve the identification accuracy, an improved version of position correlator was developed, which takes into consideration more specific conditions.

Taking into account the anatomical structure of the lumbar spine, an improved version of the position correlator was formulated as shown in Fig 4.5.

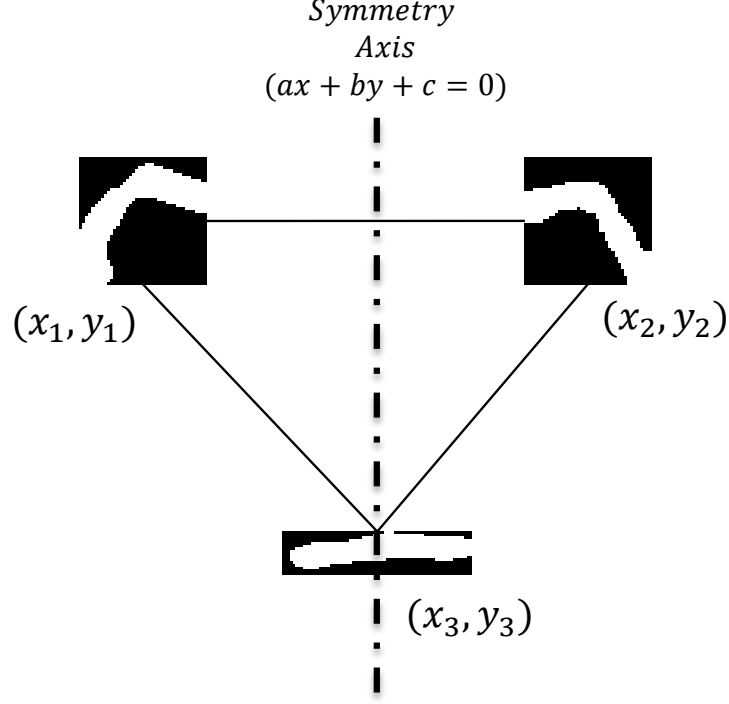


Figure 4.5: Position Correlator

The matched results for articular process (the left articular process is represented by (x_1, y_1) and the right one is represented by (x_2, y_2)) and vertebra body (position (x_3, y_3)) must fulfill the following criteria in order to be identified as interspinous images:

$$Cond(1) : a(x_1 + x_2)/2 + b(y_1 + y_2)/2 + c \approx 0 \quad (4.3)$$

$$Cond(2) : -b(x_1 - x_2) + a(y_1 - y_2) \approx 0 \quad (4.4)$$

$$Cond(3) : ax_3 + by_3 + c \approx 0 \quad (4.5)$$

$$Cond(4) : y_3 \geq \mathcal{D} \quad (4.6)$$

$$Cond(5) : y_3 \gg y_1 \quad (4.7)$$

$$Cond(6) : M \geq \alpha \quad (4.8)$$

Note: $ax + by + c = 0$ is the function for symmetry axis, known as midline for the spine structure, the detection of which will be discussed in the next section. M denotes the maximum matching result of vertebra body. \mathcal{D} and α

represent the depth threshold and matching result threshold for vertebra body as detected by template matching.

Equations 4.3 and 4.4 represent the relationship that the left and right articular process should be symmetrical to each other along the symmetry axis. Equation 4.5 indicates that the center of vertebra body should be located on or near the symmetry axis. Equations 4.6, 4.7 and 4.8 indicate that the vertebra body shall be located deeper than the articular process and the matching result shall be larger than a given threshold α .

4.4.2 Midline Detection

In order to locate the midline, a cost function $J(\vartheta, x_0)$ based on the summation of weighted pixel values within a predefined window was formulated. The window is scanned through the entire image within $[-45, +45]$ degrees. The position (x_0) and angle (ϑ) that produces the minimal cost is considered to be the midline of the image. This deduction is based on the fact that the bone image yields a dark window near the midline; and for the interspinous image this holds true most times.

To increase the accuracy of the midline detection in the interspinous images, a penalty which decreases its weight as a function of depth is imposed on the cost function. Because the vertebra body and epidural space usually appear at the deeper part of the interspinous image, a weight that decreases with depth will allow the appearance of the vertebra body to be penalized less toward the cost function, and thus the midline location can be calculated with higher accuracy for the interspinous images. Meanwhile, the weight change will not affect the bone images, because in the bone images, there are no white pixels

(value is 1) along the midline.

$$J(\vartheta, x_0) = \sum_{i=1}^n \sum_{j=-C}^C [0.5 + \exp(-0.05i)] \times f(i, i \tan \vartheta + x_0 + j) \times \sqrt{(1 + 0.3|\vartheta||x_0 - n/2|)}; \quad (4.9)$$

The cost function J is formulated with two variables, the degree of the line off the vertical direction ϑ and the starting point $(1, x_0)$. The first term of the Equation 4.9 is the penalty term for the appearance of white pixels at different depths. The third part is the penalty term if the detected midline is not near the middle of the ultrasound image or that it is not vertical. In Equation 4.9, $f(i, j)$ denotes the binary image of the pre-processed ultrasound image with a dimension of $n \times m$, i for depth direction and j for width direction; θ and x_0 denote the angle and intercept of the midline. The pair of parameters ϑ and x_0 that minimize the cost function will locate the midline, as shown in Fig 5.2. C represents the half size of the predefined window, the value of which can be optimally set between 5-10.

After the midline is obtained with the above cost function, the dark rate Δ within the predefined window is calculated with Equation 4.10.

$$\Delta = 1 - \frac{\min(J)}{2 * C * m} \quad (4.10)$$

Although the use of decreasing weight greatly improves the correct identification of the midline of interspinous images, it is noticed that for certain ultrasound images, a wrong midline may be identified by the cost function. This is often the result of the articular process being far away from the vertebra body in the horizontal direction. If the horizontal distance is larger than the predefined window, then the cost function would be minimized at the gap between articular process and the vertebra body, rather than at the midline. In order to rectify this incorrect identification, symmetry detection is employed. The ultrasound images of the lumbar spine should

be symmetrical along the midline. Therefore, a symmetry indicator can serve as the additional confirmation of the identification of the midline using the cost function approach.

Using the cost function to obtain the midline and then using symmetry detection to reconfirm its location improved the computational speed and accuracy, compared with alternate methods, i.e. full symmetrical detection.

The symmetry parameter of the image against the midline detected by the cost function is defined by the following equation:

$$S = \frac{\sum |f(x, y) - f(x', y')|}{mx_0} \quad (4.11)$$

where (x, y) and (x', y') represent the coordinates of one pair of pixels which are symmetrical to each other against the detected midline.

The midline detection adds another two conditions to the image classification, the symmetrical parameter and the dark rate:

$$Cond(7) : S > \mathcal{T} \quad (4.12)$$

$$Cond(8) : \Delta \leq \mathcal{R} \quad (4.13)$$

In the equation, the \mathcal{T} and \mathcal{R} denote the threshold for symmetrical parameter S and dark rate Δ , respectively.

4.4.3 Cascading Classifier for Image Classification

The position correlator with midline detection improved the recognition rate in pregnant cases, compared to the original position correlator in the last section. It was able to identify the interspinous images from 21 of the 36 ultrasound video streams, as long as the articular process and vertebra body were both clearly visible. However, among some of the collected pregnant cases, it was noticed that the articular processes were not visible or easily recognizable for certain cases, while only the vertebra body appeared, even on the best insertion

point locations. Under those extreme cases, the position correlator would fail to identify the interspinous images.

In order to strengthen the classifier and make it able to recognize the extreme cases, a cascading classifier was developed. The cascading classifier is composed of a series of classifiers so that if the image cannot be confidently classified by a certain classifier then it will be passed to the next classifier, until it is classified with a high confidence level. The structure of the proposed cascading classifier is shown in the Fig 4.6.

The first layer of the cascading classifier is the appearance of vertebra body. The criterion indicates that the vertebra body detector should be maximized at the lower part of the image and close to the symmetry axis. If the first criterion is not met, the image will be classified as a bone image. Otherwise it will be passed to the second layer, which will compute the maximal dark rate identified by the cost function. If the dark rate is lower than a certain threshold, indicating that there is a considerable number of white pixels within the predefined window, then the image will be identified as an interspinous image. If the second criterion is satisfied, then the image will be identified as an interspinous image; otherwise it will be passed to the third layer, the position correlator described in the previous section. If the criterion at the third layer is not satisfied, then the image will be passed to the fourth layer, which classifies the images based on the symmetry detection parameter. If the image symmetry parameter along the detected midline is higher than a certain threshold, then the image will be classified as an interspinous image. Otherwise, the image will be labeled as a bone image, as there are no further classifier layers.

4.4.4 Identification of Epidural Space

Epidural space is the target for epidural anesthesia, where the needle is placed and medication is delivered. The identification of the epidural space is also an

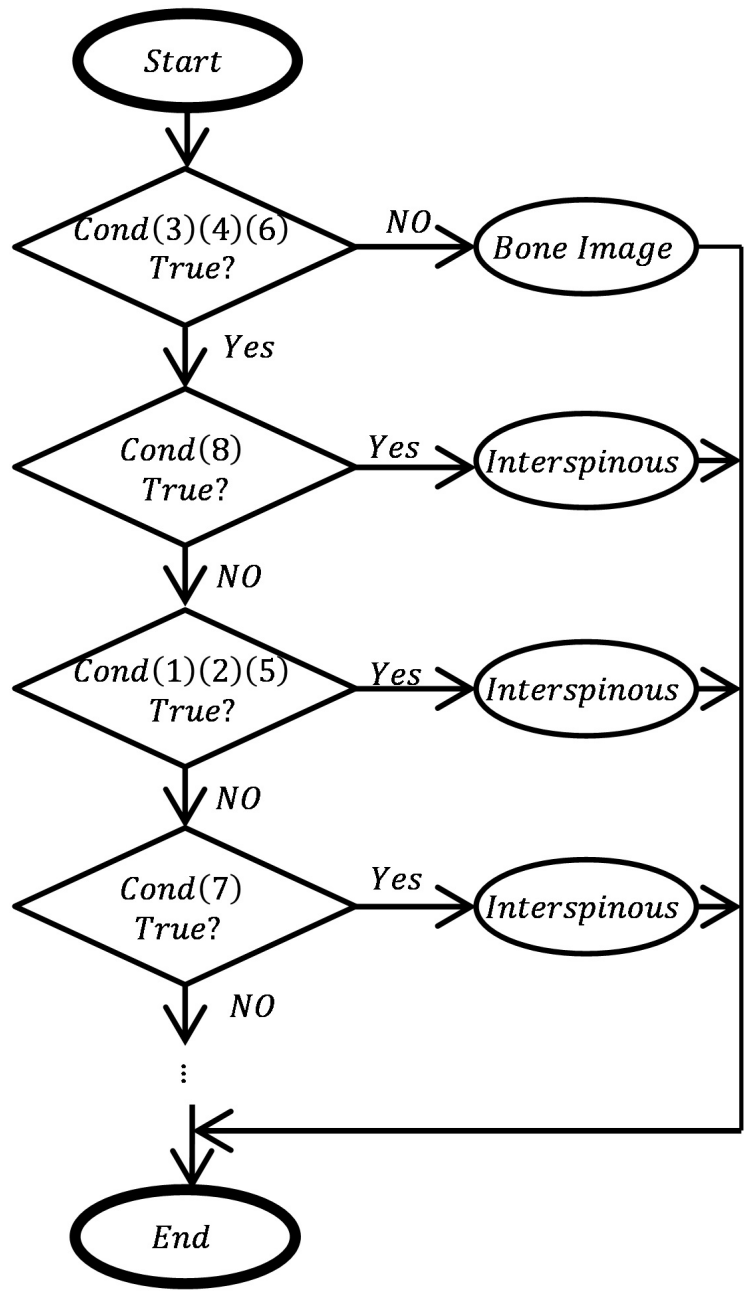


Figure 4.6: Framework of Cascading Classifier

important landmark for spinal needle insertion in case of spinal anesthesia. The epidural space is only visible on ultrasound images taken from the interspinous region. Once the processed image is identified to be an interspinous image with the proposed cascading classifier, it is then possible to search for the epidural space within a certain confine of the image.

The epidural space, according to the anatomical structure of lumbar spine, is located between the articular process and vertebra body. Moreover, like the vertebra body, the epidural space also appears as a linear feature in the ultrasound images. The signatory template used for vertebra body identification will also result in a large matching value at the epidural space, though less than that of vertebra body, as indicated by the matching results in Fig 4.7. In certain cases for the pregnant patients, the epidural space appears more obvious than the vertebra body and the template matching result will maximize at the epidural space instead of at the vertebra body. Under those cases, the algorithm will search for the two brightest lines in the matching results and identify the deeper one as vertebra body and the superior one as epidural space. Therefore, the epidural space can also be identified from the template matching results of the vertebra body.

4.4.5 Materials and Image Acquisition

The ultrasound video streams utilized in this research were collected from KK Women's and Children's Hospital, with institutional review board (IRB) approved and patients' consent obtained. Pregnant women scheduled for a caesarean procedure were recruited before they were sent to the operation theater (OT). For the data collection, an ultrasound system (Moddel U660, Canyearn Medical) and a 3.5 MHz curvilinear ultrasound probe (C3.5MHzR60, Canyearn Medical) were employed, with the scanning depth set to 8-10 cm. Contrast and gain were set as default, -10 and 80 respectively. The attenuation compensation was set with Time Gain Compensation (TGC) function, which

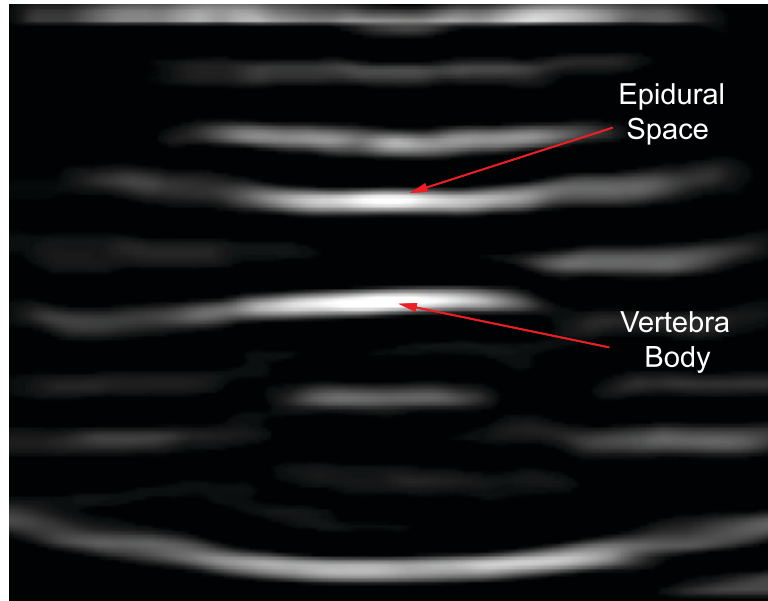


Figure 4.7: Search for Epidural Space

allowed for stepwise increase in gain to compensate for greater attenuation of ultrasound waves returning from deeper structures. TGC was set as proportional to the depth and remained unchanged for all of the cases collected. The ultrasound video streams were collected from the patients' lumbar spine in the transverse view (L3-L4 or L2-L3) at a constant speed of 15 Frames Per Second (FPS) and then saved as Windows Media Video (WMV) format for processing. The length of collected video streams ranges from 10-20 seconds, with 150-300 frames obtained from each participant. In total, 36 video streams are recorded from 36 different pregnant subjects. The ultrasound video streams were later processed with the described image processing algorithms off-line.

The image processing algorithm was implemented with the Matlab Computer Vision System toolbox and run on a personal computer (3.3GHz Core i5-3550 CPU and 8GB installed memory). Sector image were cropped and downsampled by a factor of 2, so as to improve the computation speed. An experienced sonographer participated in the research, helping to collect ultrasound video streams and identify whether an image or video frame was suitable for needle insertion, i.e., whether the image was an interspinous image

Table 4.1: Statistics of Training Set and Test Set.

	Training Set	Test Set
Subject Number	20	16
Image Number	800	640
Non Labelled	58	26
Interspinous	448	349
Bone Images	294	265

or a bone image. The labeling provided by the sonographer was treated as the ‘gold standard’ and then compared with the classification results produced by the algorithm, so as to evaluate the performance of the algorithm.

4.5 Results

There are four parameters (\mathcal{D} , α , \mathcal{T} and \mathcal{R}) in the cascading classifier which influence the performance of the classifier. In order to search for the parameters that achieve the optimal performance, 20 video streams were randomly selected from the 36 subjects as training set, and the remaining 16 video streams were selected as a test set. From each of the training videos and test videos, 40 images were randomly extracted, so as to evaluate the classifier’s performance qualitatively.

Each of the randomly selected ultrasound video frames were labeled by the sonographer: as 1 for interspinous images and as -1 for bone images. Frames located near the junction of interspinous image and bone image were labeled as 0, since it was difficult to assign these with a clear label. The label provided by the sonographer was utilized to tune the classifier’s parameters and evaluate the accuracy of the algorithm. The basic statistics of the training and test set are displayed in Table 4.1.

Parameters were tuned based on training set. The parameters that achieve

Table 4.2: Classification Result on Training and Test Set.

	Training Set	Test Set
Accuracy	94.80%	93.23%
Precision	95.90%	93.94%
Recall	95.46%	93.00%
F0.5	95.81%	93.75%

the optimal accuracy are chosen as the threshold for the cascading classifier, which corresponding to $\mathcal{D} = 4.5cm$, $\alpha = 0.45$, $\mathcal{T} = 0.6$ and $\mathcal{R} = 0.95$. The test result of the cascading classifier with the given parameters is displayed on Table 4.2.

The proposed cascading classifier was also tested on the 36 video streams themselves, trying to determine the best needle insertion location in real-time. A successful identification of needle insertion site is defined as follows: if the interspinous images appeared continuously, indicating that the probe is placed on the interspinous space, the classifier shall be able to identify the interspinous images in at least 5 consecutive images; while if the bone images appear continuously in the video streams, then the classifier shall not give positive results in more than two continuous frames. The classifier is not required to identify all the interspinous frames and bone frames, but the ones that appear continuously shall be correctly identified. Needle insertion points are successfully located on 20/20 of training videos and 16/16 of the test videos.

An example of related video frames are shown in Fig 4.8 with the identification results. The circle superimposed on the images indicates that the image is identified as an interspinous image by the algorithm. For the case 4.8(a), the anatomical structures revealed on the image are very clear and the ‘flying bat’ shape is easily recognizable. For the case 4.8(b) and 4.8(d), the ‘flying bat’ shape is not as obvious but discernable. For case 4.8(c) and 4.8(e), the ‘flying bat’ is hardly visible; however, the appearance of vertebra body

Table 4.3: Computation Cost of Functions with Matlab.

Function	Computation Cost(ms)
Preprocessing: DoG + normalization	9.0
Template Matching	13.1
Midline Detection	16.99
Symmetry Detection	18.98
Cascading Classifier	0.029
Processing Time Per Frame	59.9

indicates that the image is interspinous.

Table 4.3 lists the computational cost of major functions employed in the image processing procedure. Matlab (R2012a) was used for the implementation of the algorithm. Symmetry detection (18.98ms) and midline detection (16.99) are the two functions that consume most of the computational cost (60.07%). It takes 59.9ms to process one single frame, reaching the computational speed of 16.67 FPS. Given that video streams are collected at a frame rate of 15 FPS, the algorithm is fast enough for real-time video processing.

4.5.1 Precision and Accuracy of Epidural Space Measurement

The visibility of epidural space can decrease for some cases during pregnancy [29]. This was noted during the current study as well. Among the 36 ultrasound video streams, the epidural space was visible in 31 of them. Fig 4.8(e) shows a case where epidural space is not visible on the interspinous image. For the 31 video streams, epidural space was measured in two ways: manually by the sonographer and automatically with the algorithm. For the manual manner, the sonographer chose one frame which showed a clear epidural space and then measured the depth using the caliper function of the ultrasound machine. For the automatic manner, the algorithm first identified the interspinous image

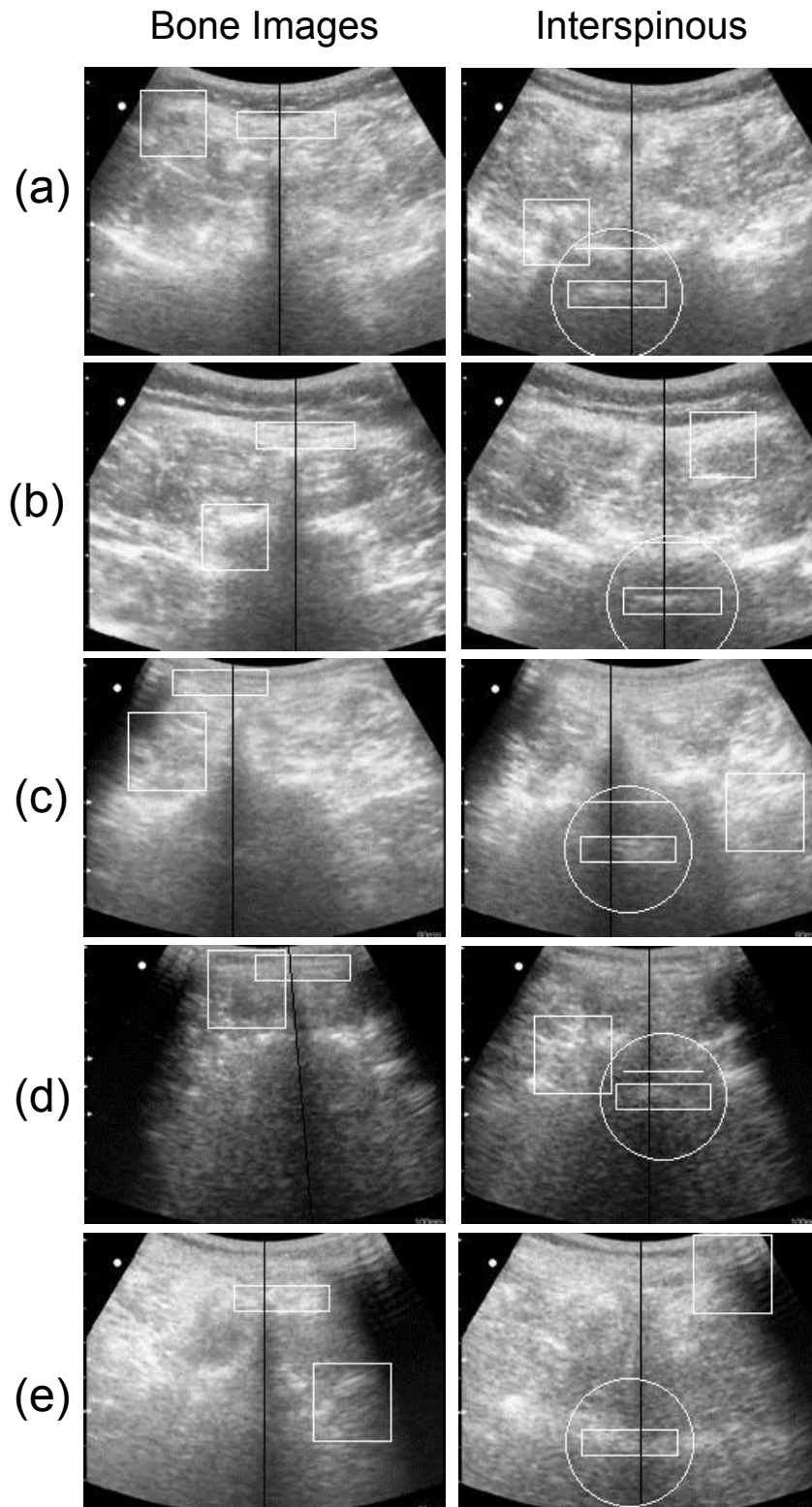


Figure 4.8: Identification Result of Randomly Selected Video Streams. (Note: In the image, the square box indicates the matching position for articular process and the rectangle indicates the position of vertebra body. In the right column of the images, the circle serves as a mark for the interspinous image and the white line above the vertebra body is the epidural space identified by the algorithm.)

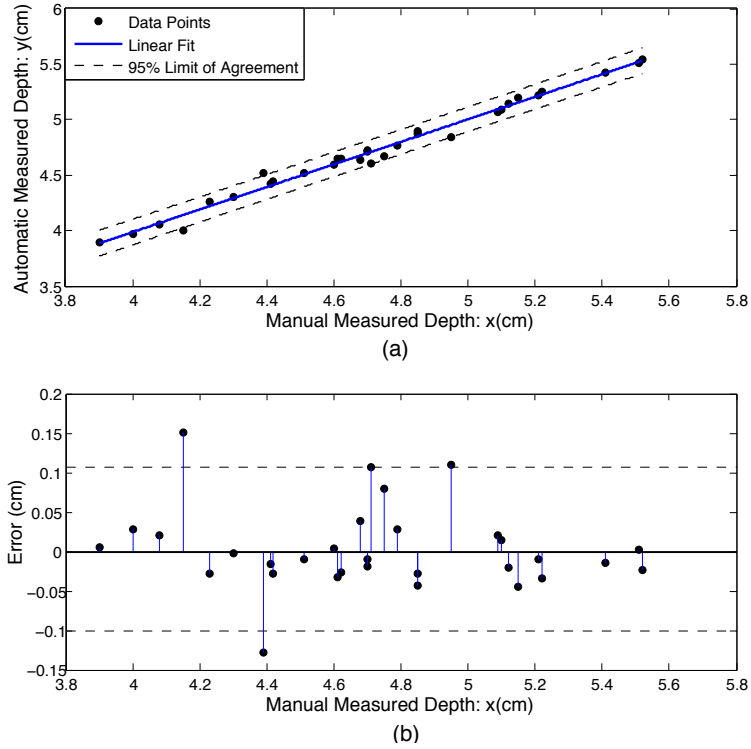


Figure 4.9: Comparison of Automatic vs. Manual Measured Epidural Depth. (a) Scatter plot; (b) Differences between automatic measurement and manual measurement

continuously and then epidural depth was measured by the mean of the epidural depth as it appeared in the interspinous images.

Fig 4.9(a) shows the results for both measurements. Linear regression analysis of the two methods result in the following relationship:

$$Automatic = 1.016 \times Manual - 0.078 \quad (4.14)$$

The coefficient of determination (R^2) is 0.9861 for the linear regression equation, indicating a high and linear correlation between the manual measurement and automatic measurement. As demonstrated by the plot in Fig 4.9(b), the error between automatic measured depth and manual measured depth ranges from -0.128 cm to 0.15 cm, with the average of 0.0028 cm, standard deviation of 0.0528 cm and 95% limits of agreement of -0.1008 cm to 0.1064 cm.

4.6 Discussions

The low resolution of ultrasound image and the corresponding decrease in clarity of the subtle anatomy structures pose a challenge in interspinous image identification for the pregnant population, resulting in a low recall rate with the position correlator. The cascading structured classifier developed in this chapter addresses this problem by using layers of weak classifiers. Important parameters, including matching values and positions of signatory templates, symmetry against midline and black rate within the predefined window along midline, serve as weak classifiers to discriminate bone images and interspinous images. The first layer of the cascading classifier ensures the appearance of vertebra body, which is the basic criterion for images to be identified as interspinous images; whereas the continuous layers increases the possibility for interspinous images to be picked up from the imaging pool. Therefore, the cascading classifier achieved a balance between precision and recall, further increasing the identification accuracy.

The error of intraobserver repeatability of ultrasound imaging measurement was reported to range from 4.75% to 7% [62]. Given that the average of measured epidural depth is 4.727 cm in this study, the error of manual measurement of epidural depth may fluctuate among [0.2245 cm, 0.3309 cm], which is higher than the difference between automatic measurement and manual measurement. Therefore, the automatic measurement is acceptable compared with the manual measurement.

In the image processing procedure, the incorporation of pre-processing alleviates the negative influence of image quality on the recognition result. The ultrasound image quality generally depends on the experience of sonographer and proper setting of machine parameters, e.g., contrast and gain. Pre-processing using DoG enhanced local normalization mitigates the dependence of classifier performance on good image quality. After the pre-processing, the divergence of image intensity induced by contrast and gain

is filtered, increasing robustness. In the five cases displayed in Fig 4.8, the gain parameter in case (d) was set to 67, while the rest was set at 80, leading to different image intensities. Nevertheless, the algorithm successfully identified all of the cases regardless of the difference in image intensity. Thus, anesthetists can use the ultrasound system for epidural needle insertion assistance without requiring extensive knowledge over the machine parameter setting and image interpretation.

Although it is not necessary for the operator to tune the optimal contrast and gain parameter to obtain the best image quality, scanning depth must still be properly chosen. The size of anatomy structures revealed on the ultrasound image will be different under different scanning depths, influencing the optimal choice of Gaussian kernels. If the depth is set excessively deep, then the anatomical structures will be very small and a large size Gaussian kernel will filter the tiny anatomical structure as noise, which is not desired. Since the epidural space is usually 3-8 cm below the skin and vertebra body is 1-2 cm deeper than the epidural space, thus the proper setting of scanning depth is suggested to be around 8-10 cm. During the data collection, the depth was set between 8-10 cm and the two Gaussian kernels remain unchanged for all the videos. The chosen Gaussian kernels are able to pre-process the raw ultrasound images properly with minor change in scanning depth.

Midline detection is another important feature of the video processing procedure. It not only provides the dark rate Δ for the cascading classifier, but also effectively detects the angle and position of the ultrasound probe against the spine midline. In the real-time procedure, a reference line that is vertical and corresponds to the middle of the probe can be superimposed on the image window, so that the operator can be guided to align the detected midline with the reference line. Therefore, while the cascading classifier locates the plane that is proper for needle insertion, midline detection will locate the spine midline, and the combination of the two techniques can locate the precise

insertion point.

The clinical workflow with the developed algorithm is envisioned as follows: (1), The operator holds the ultrasound probe in the transverse plane with an ultrasound system running the algorithm in the background in real-time, moving it along the patient's midline slowly, until a set of continuous interspinous images are detected. (2), At this point, the operator is prompted to adjust the angle and position of the probe until the detected midline is aligned with the reference line. (3), When alignment is accomplished, the location of the center of the ultrasound probe will correspond to a proper needle insertion point.

4.7 Conclusions

In this chapter, an image processing and identification procedure for automatic ultrasound image interpretation of lumbar spine in the transverse plane was proposed. An initially proposed position correlator was strengthened by using a cascading classifier approach. It includes a cost function based on minimal appearance of white pixels is formulated to locate the midline of the ultrasound image, and a symmetrical indicator to ensure the accuracy of the midline detection. This enhanced classifier effectively identifies the interspinous images with four layers of weak classifiers and successfully locates the proper needle insertion point on the 36 pregnant cases collected so far.

The automatic identification of interspinous images and bone images has been realized with the proposed algorithm. In the following chapters, the interpretation of lumbar ultrasound images will be realized in an automatic and real time manner by computers, so that anesthetists are not required to read ultrasound images which are not easily interpretable. It is expected that the use of the ultrasound system can be as easy as a direct sensor for needle site indicator, with the image processing and classification algorithms working

in the background in real-time. The difficulty associated with epidural needle insertion can thus be potentially alleviated by the developed approach.

Chapter 5

Image Classification with Machine Learning

5.1 Introduction

In the previous chapter, the identification algorithms for lumbar ultrasound images in the transverse view was proposed, including position correlator for healthy volunteers and cascading classifier for pregnant patients. The position correlator is a simple version of classifier which considers the position of detected anatomical features as the criteria to differentiate the interspinous image and bone image. It achieved high accuracy on images collected from healthy volunteers, the anatomical feature of which are clear and easier to recognize. However, since the clarity of anatomical features of lumbar spine might degrade during pregnancy [61], the original position correlator designed for healthy volunteers may not be effectively applicable to the pregnant patients. In order to improve the identification accuracy for pregnant women, a more sophisticated model with cascading structures were proposed. The cascading classifier contains four weak classifier layers and picks up the interspinous images from the image pool if the criteria in each layer is satisfied. The performance evaluation of the cascading classifier runs on ultrasound

images collected from 36 pregnant subjects (20 for training set and 16 for test set), and achieved an accuracy of 94.80% on training set and 93.23% on test set.

Although high success rate has been accomplished by using the cascading classifier, there are still several aspects needs to be improved. The cascading classifier contains four tunable parameters, including the reference depth of vertebra body \mathcal{D} , matching intensity of vertebra body α , symmetrical parameter \mathcal{S} and dark rate along the midline \mathcal{R} . A slight change in the parameters may seriously influence the performance of the classifier; thus, the cascading classifier is not very robust.

This chapter further extended the research of automatic identification for transverse lumbar ultrasound images by proposing a machine learning based approach to further increase the classification accuracy and make the classification algorithm more intelligent and robust. An intelligent image identification procedure is proposed, which includes feature extraction, feature selection and classification algorithm based on a support vector machine (SVM).

5.2 Materials and Image Acquisition

During the study, 46 ultrasound video streams were collected from 46 different subjects. After video streams were collected, the image database was obtained by extracting still images from the video streams. 40 images were randomly extracted from each of the video streams, constituting 1840 ultrasound images in the training and test database in total. In order to reduce label noise, the extracted images were labelled by two experienced sonographers independently: ‘1’ for interspinous images, ‘-1’ for bone images and other images not proper for needle insertion. Since two experts were involved in the labelling of image database, it was inevitable that they may have

different opinions on certain images, especially for the images located near the junction of interspinous and bone region. The labels assigned with unanimous categorization by the two experts were treated as ‘gold standard’ and used for SVM training and testing. On the contrary, the images with adversarial labels indicates that the two experts did not agree on the particular categorization of the image. The adversarial labels were regarded as label noise and removed from the database, so as to decrease the negative influence of faulty labels on supervised learning.

The feature extraction, feature selection and SVM training algorithms were implemented with Matlab (Version R2012a, The MathWorks, Natick, MA, USA) and run on a personal computer (3.3GHz Core i5-3550 CPU and 8GB installed memory). Sector images were cropped and downsampled by a factor of 2, so as to improve the computation speed.

5.3 Feature Extraction

Before feature extraction, raw ultrasound images were pre-processed with the DoG enhanced local normalization, so as to remove speckle noise and extract anatomical structures, with kernel parameters set as $20 \times 20, \sigma = 4$ for first kernel and $20 \times 20, \sigma = 10$ for second kernel [63, 64]. After pre-processing, local intensity variance induced by ultrasound wave attenuation was also eliminated. Therefore, a potential element which might degrade the image classification was removed.

Feature extraction procedure is extraordinarily important for image classification. Medical images generally suffer from limited data size, induced by the high cost of equipment and man power for image collecting and labelling [65, 66]. Therefore, the feature dimension is typically limited. Otherwise, the learning models will have high variance and cannot be optimally trained [67, 68]. In order to represent the lumbar ultrasound image with low feature

dimensions, the image features is extracted with two approaches: the template matching method to detect the key anatomical features and midline detection approach to obtain image features along midline.

5.3.1 Template Matching

The visibility of ‘flying bat’ shape is the criterion adopted by anesthetists to recognize interspinous images [19]. However, in computer vision, due to the variation and distribution extent of the ‘flying bat’ shape in the image, the recognition of the entire ‘flying bat’ shape is not an easy task. Although algorithms like the active contour model can be employed to fit the shape, it is usually subject to the limitation of slow computational speed; thus, not applicable for the real time recognition purpose [69]. In the previous research, the ‘flying bat’ shape is decomposed into three sub-features: the ‘bat ear’ (articular process), epidural space and vertebra body. The decomposed sub-features matched the articular process and vertebra body with high accuracy on images obtained from volunteers [63].

In this chapter, similar decomposition was employed. Template matching was used to obtain the matching position and matching value between the sub-features and the images. Among the three sub-features, the appearance of the epidural space and the vertebra body both resemble a line. Thus, the same linear sub-template (as shown on Fig 5.1(a)) was employed for the recognition of both vertebra body and epidural space. Of the two maximum matching blobs, the one that locates lower in the image is vertebra body and the superior one is epidural space, which follows the anatomical structure of the lumbar spine. In the interspinous images, the visibility of vertebra body and epidural space was clear and both of them can be correctly recognized. On the contrary, in the bone images, the maximum matching of the sub-template occurs at different regions in the image; and the matching values for both epidural space and vertebra body were low, as indicated by Fig 5.1(b). The

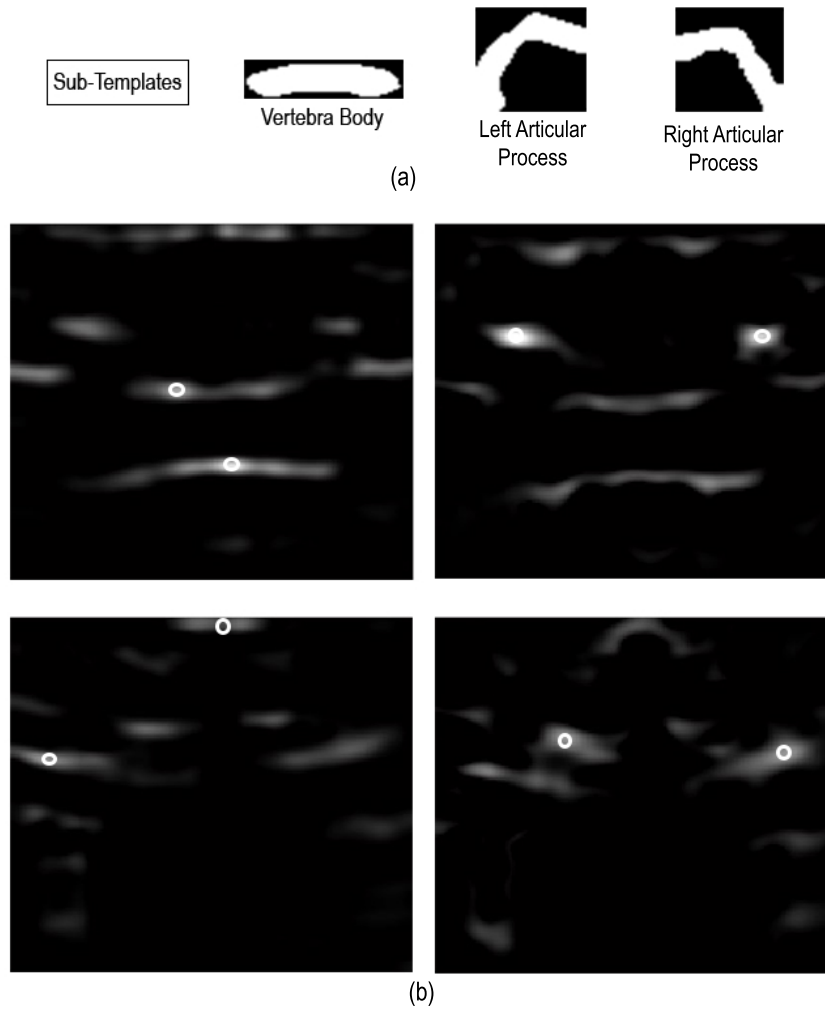


Figure 5.1: Feature Extraction with Template Matching. (a) Sub-templates for anatomical features, from left to right: vertebra body and epidural space, left articular process and right articular process; (b) Matching result of key anatomical features: The left column: matching result of vertebra body sub-template; the right column: matching result for articular process sub-templates; the upper row: interspinous image; the lower row: bone image. The optimal matching position is marked by a circle.

situation was the same for the matching of articular processes, except that the maximum matching of articular processes appears on the left and right side of the midline. Therefore, based on the matching position and matching value, it was possible to partially discriminate the interspinous images and bone images.

The parameters obtained with template matching can be utilized to constitute part of the feature vector for the purpose of image classification, including the retrospective depth measurement of epidural space (\mathcal{D}_1) and vertebra body (\mathcal{D}_2), their matching values (\mathcal{V}_1 and \mathcal{V}_2), matching position of two articular processes ($\mathcal{P}_3, \mathcal{D}_3$ for left articular process and $\mathcal{P}_4, \mathcal{D}_4$ for right articular process) and their matching values (\mathcal{V}_3 and \mathcal{V}_4).

5.3.2 Midline Detection

The image features along the midline of the ultrasound image is different for interspinous images and bone images. For the bone images, ultrasound is impeded by the spinous process, resulting in an anechoic region along the midline; while for interspinous images, the epidural space and vertebra body along the midline will be visible. Therefore, the appearance of black pixels along the midline serve as an important feature for the classification of interspinous / bone images.

For the detection of the midline, a cost function $J(\vartheta, x_0)$ based on the summation of white pixels within a predefined scanning window was formulated at Chapter 4 in Equation 4.9. The window was scanned though the entire image within $[-45, +45]$ degrees. The position and degree that gives the minimum cost function value will locate the midline, as demonstrated by Fig 5.2. In order to increase the accuracy of midline detection for interspinous images, a penalty which decreases its weight as a function of depth was imposed on the cost function, so as to allow the appearance of epidural space and vertebra body to be less penalized in the cost function.

After optimal ϑ' and x'_0 is obtained and the midline is located, the

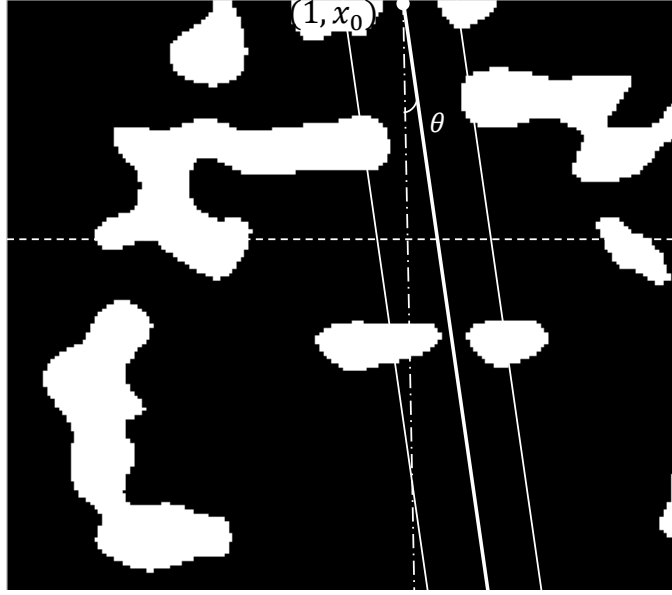


Figure 5.2: Feature Extraction with Midline Detection. (Note: the background image is the pre-processed binary image; The horizontal dashed line is the depth threshold used to calculate \mathcal{R}_w .)

proportion of black pixels within the predefined scanning window can be calculated using the following equation:

$$\mathcal{R}_b = 1 - \frac{\sum_{i=1}^n \sum_{j=-C}^C f(i, i \tan \vartheta' + x'_0 + j)}{n \times 2C} \quad (5.1)$$

The depth of epidural space was reported to range from 3-8 cm, indicating that the epidural space and vertebra body appear deeper than 3cm in the image [35, 70]. Thus, the proportion of potential epidural space and vertebra body within the scanning window can be calculated with:

$$\mathcal{R}_w = \frac{\sum_{i>=3cm}^n \sum_{j=-C}^C f(i, i \tan \vartheta' + x'_0 + j)}{n \times 2C} \quad (5.2)$$

Because of the presence of epidural space and vertebra body at the lower part of the interspinous image, the parameter \mathcal{R}_w is bigger than 0. On the contrary, for the images obtained from bone regions, the lower part of the image is black. Thus, \mathcal{R}_w approximates 0 for bone images.

After the midline is located via the cost function approach, a symmetry

measurement is utilized to doubly confirm the accuracy of midline detection. The introduction of the symmetrical parameter is based on the fact that the anatomical structure of lumbar spine exhibits mirror symmetry with respect to the midline. The symmetrical parameter \mathcal{S} is simply calculated with Equation 5.3 [71].

$$\mathcal{S} = \frac{\sum |f(x, y) - f(x', y')|}{nx'_0} \quad (5.3)$$

where (x, y) and (x', y') represent the coordinates of one pair of pixels which are symmetrical to each other against the detected midline.

\mathcal{R}_b , \mathcal{R}_w and \mathcal{S} add another three parameters for the feature vector. Therefore, combining the 10 parameters obtained from template matching and 3 parameters from midline detection, a feature vector of length 13 was formulated. A detailed description of template matching and midline detection on lumbar ultrasound image processing can be further examined in [71].

5.4 Feature Ranking and Feature Selection

A cross correlation method was employed to evaluate the ‘relevance’ of the features to the corresponding interspinous or bone label. The higher the correlation value (or the absolute value of the correlation value if the parameter is negatively related to the labels), the better the predicability of the feature [72].

The cross correlation between the i^{th} feature \mathbf{X}_i with label \mathbf{Y} is calculated as:

$$F(\mathbf{X}_i, \mathbf{Y}) = \frac{\sum_{j=1}^N (x_j - \bar{\mathbf{X}}_i)(y_j - \bar{\mathbf{Y}})}{\sqrt{\sum_{j=1}^N (x_j - \bar{\mathbf{X}}_i)^2 \sum_{j=1}^N (y_j - \bar{\mathbf{Y}})^2}} \quad (5.4)$$

in which $\mathbf{X}_i = \mathbf{X}(:, i)$.

Fig 5.3 shows the cross correlation value of the extracted feature

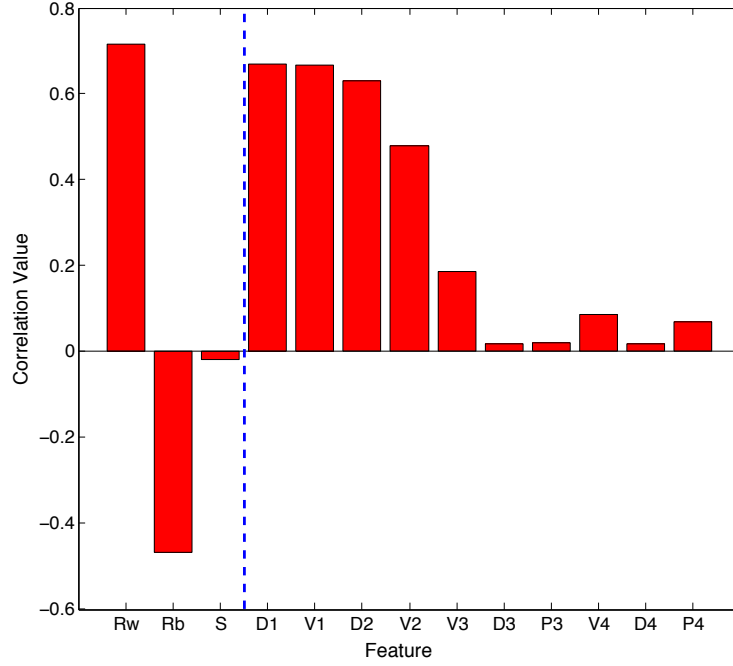


Figure 5.3: Ranking of Individual Features. (Note: The three parameters on the left side of the dashed line are generated from midline detection. The rest of the parameters on the right side are generated from template matching)

parameters. The features were then ranked according to their correlation value, resulting in the following feature order:

$$[\mathcal{R}_w, \mathcal{D}_1, \mathcal{V}_1, \mathcal{D}_2, \mathcal{V}_2, \mathcal{R}_b, \mathcal{V}_3, \mathcal{V}_4, \mathcal{P}_4, \mathcal{P}_3, \mathcal{S}, \mathcal{D}_4, \mathcal{D}_3].$$

The target of feature selection is to search for the best combinations of features which produces the optimal performance. It can also help to reduce the computation time by using a subset of features, instead of computing the whole set of parameters. In this thesis, although only 13 parameters were used as features, they were obtained with different approaches and the calculation for some of them, e.g. symmetrical parameter and template matching positions, were time consuming. If some of the parameters were not within the best feature subset, then the computational speed of image classification procedure can be accelerated.

In order to find the optimal feature subset with minimum dimension, forward search was utilized for the feature selection. Algorithm 1 lists the details of the algorithm [73].

Algorithm 1: Feature Selection with Forward Search

Input: Training Set: $\{\mathbf{X}, \mathbf{Y}\}$
Output: Optimal Feature Subset \mathcal{F}

- 1 **Initialization** : $\mathcal{F}_i = \emptyset$;
- 2 **for** $i \leftarrow 1$ **to** n **do**
- 3 **for** $j \leftarrow 1$ **to** n **do**
- 4 $\mathcal{F}_j = \mathcal{F}_i$
- 5 **if** $\mathbf{X}(:, j) \notin \mathcal{F}_j$ **then**
- 6 $\mathcal{F}_j = \mathcal{F}_j \cup \mathbf{X}(:, j)$
- 7 Train the classifier with feature subset \mathcal{F}_j
- 8 Select the best feature subset of i dimension: $\mathcal{F}_i = \mathcal{F}_{j, opti}$
- 9 Select the feature subset with optimal performance: $\mathcal{F} = \mathcal{F}_{i, opti}$
- 10 **end**

5.5 Support Vector Machine

After the best feature subset has been obtained and normalized, SVM was employed to optimally classify the interspinous images and bone images. SVM is a supervised learning algorithm which seeks a decision boundary (or separating hyperplane) with maximal margin for the training set [74]. In cases where the data is linearly non-separable, usually a soft-margin SVM is used, which allows for mislabeled training examples and makes the algorithm less sensitive to outliers.

For the given training samples, $\{(\mathbf{x}_i, y_i)\}_{i=1}^N$, the optimization problem is formulated as:

$$\begin{aligned} \min_{\mathbf{w}, b} \quad & \frac{1}{2} \mathbf{w}^T \mathbf{w} + C \sum_{i=1}^N \xi_i \\ \text{s.t.} \quad & y_i g(\mathbf{x}_i) = y_i (\mathbf{w}^T \mathbf{x}_i + b) \geq 1 - \xi_i, \quad \forall i \\ & \xi_i \geq 0, \quad \forall i \end{aligned} \tag{5.5}$$

In the equation 5.5, (\mathbf{w}, b) denotes the weight and intercept parameters of the separation hyperplane. ξ_i is the slack variable and measures the degree of misclassification of training data \mathbf{x}_i . Training data which were misclassified will have their corresponding $\xi_i > 1$. The parameter C is a regularization term

that controls the relative weighting between the two goals of achieving larger margin and decreasing classification error. A larger C corresponds to assigning a higher penalty to errors and classifying all training examples correctly.

The dual form of the optimization in Equation 5.5 is:

$$\begin{aligned}
 \max_{\boldsymbol{\alpha}} \quad Q(\boldsymbol{\alpha}) &= \sum_{i=1}^N \alpha_i - \frac{1}{2} \sum_{i=1}^N \sum_{j=1}^N \alpha_i \alpha_j y_i y_j \mathbf{x}_i^T \mathbf{x}_j \\
 \text{s.t.} \quad &0 \leq \alpha_i \leq C, \quad \forall i \\
 &\sum_{i=1}^N \alpha_i y_i = 0
 \end{aligned} \tag{5.6}$$

Quadratic programming can be employed to calculate $\boldsymbol{\alpha}$. α_i will be nonzero only for the support vectors, which includes the data points on the margin boundary and those on the wrong side of the margin boundary. While for the data points that is distant from the decision boundary, i.e. the non-support vector points, α_i will be zero.

After α is obtained, the \mathbf{w} parameter in the decision boundary can be calculated by:

$$\mathbf{w} = \sum_{i=1}^N \alpha_i y_i \mathbf{x}_i \tag{5.7}$$

The intercept parameter b will be calculated based on the support vectors, i.e, where $0 < \alpha_i \leq C$,

$$b = \frac{\sum_{i=1}^m (1/y_i - \mathbf{w}^T \mathbf{x}_i)}{m} \tag{5.8}$$

where m is the number of support vectors in the training set.

For the data points \mathbf{x} to be tested, it's decision function and class will be

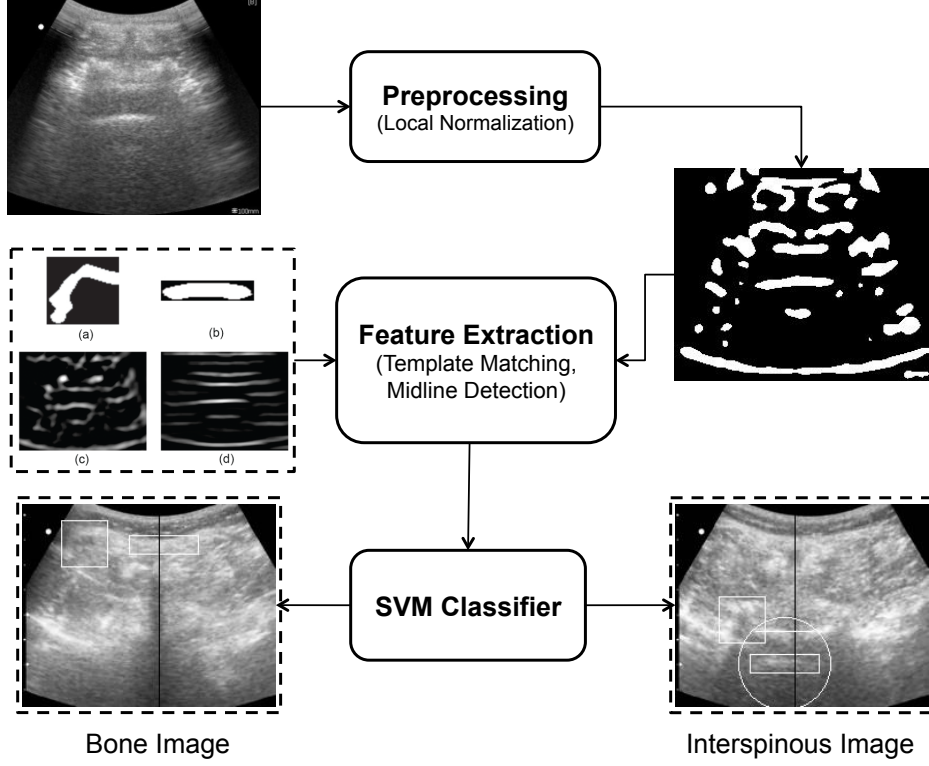


Figure 5.4: Image Identification Procedure for Lumbar Ultrasound Image

determined by:

$$\begin{aligned}
 g(\mathbf{x}) &= \mathbf{w}^T \mathbf{x} + b \\
 &= \sum_{i=1}^N \alpha_i y_i \mathbf{x}_i^T \mathbf{x} + b \\
 y &= \text{sgn}(g(\mathbf{x}))
 \end{aligned} \tag{5.9}$$

5.6 Image Identification Procedure

Fig 5.4 describes the entire image processing and identification procedure for the lumbar ultrasound images. Raw ultrasound images were first preprocessed by local normalization to filter the speckle noises; then the feature vector was extracted with template matching and midline detection. The best feature subset was then selected and normalized before passed to the SVM classifier. The SVM model, after properly trained with the training database, identified the labels of the images with the normalized feature vector.

5.7 SVM Performance Evaluation Criteria

In order to evaluate the performance of feature selection and SVM classification comprehensively, four commonly used parameters were utilized; specifically: accuracy, precision, recall and F-Measure. Accuracy denotes the correct rate of the classification result compared to the true label. Precision indicates the proportion of the predicted positive cases that are true positives, i.e, confidence of positive classification. Recall demonstrates the proportion of true positive cases that are correctly predicted by the classifier, i.e. sensitivity of the model to pick up the positive samples [75]. F-Measure combines precision and sensitivity and evaluates the weighted value of the two.

The mathematical definition of the four parameters is listed as follows:

$$Accuracy = \frac{TP+TN}{TP+FP+TN+FN} \quad (5.10)$$

$$Precision = \frac{TP}{TP+FP} \quad (5.11)$$

$$Recall = \frac{TP}{TP+FN} \quad (5.12)$$

$$F - Measure = (1 + \beta^2) \times \frac{Precision \cdot Recall}{\beta^2 \cdot Precision + Recall} \quad (5.13)$$

(Note: TP : True Positive; TN : True Negative; FP : False Positive; FN : False Negative.)

In Equation 5.13, β is a non-negative value that balances the weight of precision and recall. If $\beta < 1$, the F-measure will weigh precision higher than recall; vice versa for the case of $\beta > 1$. Concerning the application of needle entry site identification, the precision of positive identification is more important than the recall. Thus, a higher weight was imposed on the precision and β was chosen as $\beta = 0.5$ (i.e F0.5).

Apart from the four parameters mentioned above, the Receiver Operator Characteristic (ROC) curve is another commonly used criterion to evaluate the performance of binary decision problems in machine learning [76]. The ROC curve shows how the rate of correctly classified positive samples (true

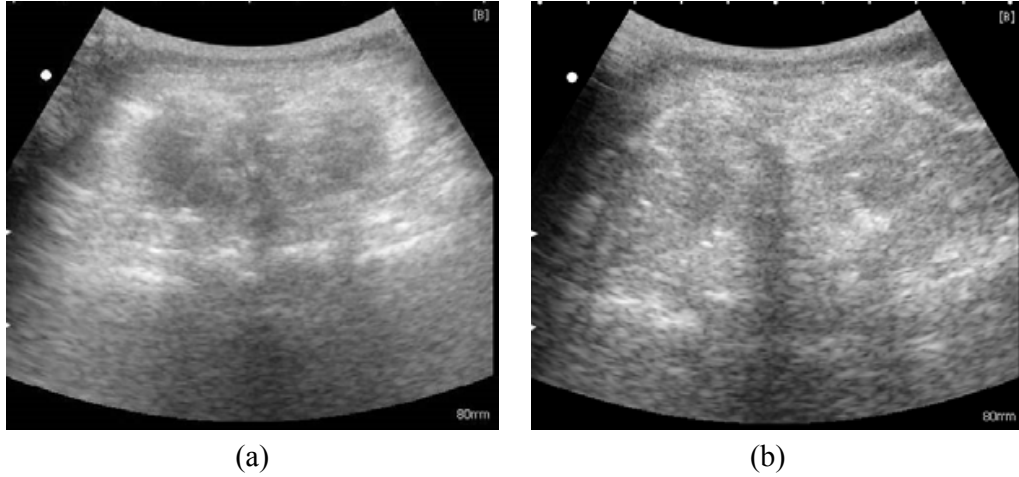


Figure 5.5: Two Representative Images with Adversarial Labels

positive rate) varies with the rate of incorrectly classified negative samples (false positive rate). The closer the area under curve (AUC) of ROC to 1, the better the predictive performance of the classifier.

5.8 Results

The two groups of labels provided by experts were compared and analyzed before passing to the SVM learning. 1799 (97.77%) out of the 1840 extracted images had consistent labels. The rest 41 (2.23%) images were assigned with opposite labels, thus excluded from the database. Fig 5.5 shows two representatives of the images with adversarial labels. On Fig 5.5(a), the epidural space and vertebra body is discernable, but vague and not clear. Compared with continuous interspinous frames, the interspinous feature of this image is not obvious; but it is certainly not a bone image. On Fig 5.5(b), the dark anechoic window casted by spinous process appears at the middle of the image window, indicating that it may be a bone image; but the epidural space and vertebra body are visible on the image. Images with adversarial labels were treated as label noise and excluded from the database.

For the purpose of SVM model training, 26 (57%) of the collected videos

Table 5.1: Statistics of Training Set and Test Set.

	Training Set	Test Set	Total Number
Subject Number	26	20	46
Image Number	1040	800	1840
Interspinous	540	410	950
Bone Images	471	378	849
Adversarial Label	29	12	41

were randomly selected as training set and the remaining 20 (43%) were used as test set [68]. The training and test sets were divided on the level of subjects instead of extracted images, which followed the assumption that in the clinical setting the detailed lumbar spine structure of individuals were not known nor examined with MRI or other imaging modalities before epidural anesthesia. Since 40 images were extracted from each video, there were in total 1040 images in the training set and 800 images in the test set. The SVM model was trained 10 times continuously, so as to evaluate the feature performance without statistical bias. The detailed statistical information for one of the training is listed in Table 1.

5.8.1 Results of Feature Selection

In order to avoid over-fitting along with the increasing of feature dimension, the feature selection procedure was implemented on the training set with Algorithm 1 and then validated on the test set.

As shown on the Fig 5.6 and 5.7, the trends of SVM performance, evaluated by the accuracy, precision, sensitivity, F0.5 and AUC, along with increase of feature dimension was similar for both training set (Fig 5.6) and test set (Fig 5.7). When the feature dimension was below 4, the SVM performance improved dramatically along with the increase of feature length. When the feature dimension was between 5 - 10, the SVM performance improved along

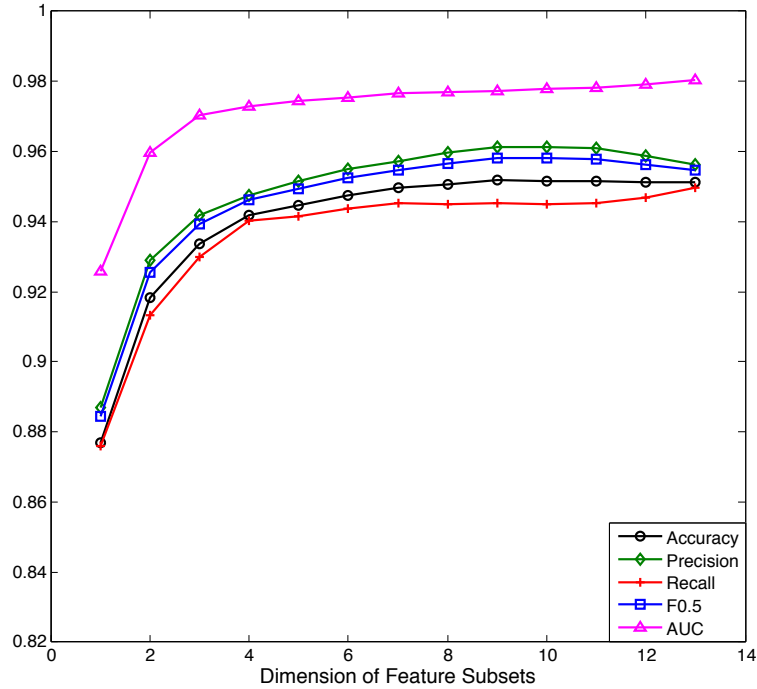


Figure 5.6: Trends of Accuracy, Precision, Recall, F0.5 and AUC along with Feature Dimensions for Training Set

with feature length, but at a much slower speed. The maximum performance was achieved when the feature dimension is 10; then the performance started to degrade with the increase of feature dimension. Therefore, the dimension of best feature set was chosen as 10, where the parameter of symmetry \mathcal{S} and matching depth of articular process $\mathcal{D}_3, \mathcal{D}_4$ were excluded.

5.8.2 Performance of Support Vector Machine

Based on the training set with the optimal feature set obtained in the last section, the soft SVM model was trained to get the optimal hyperplane. The trained model parameters were then validated on the test set. The only free parameter in the soft margin SVM model is the regularization term C . C was tested in the range from 0.1 to 100 at the interval of 0.1, and the best performance was achieved when setting $C = 1.0$. Fig 5.8 displays the general performance of the SVM model in the 10 continuous training.

Table 2 lists the best and worst SVM performance in the 10 trials. The

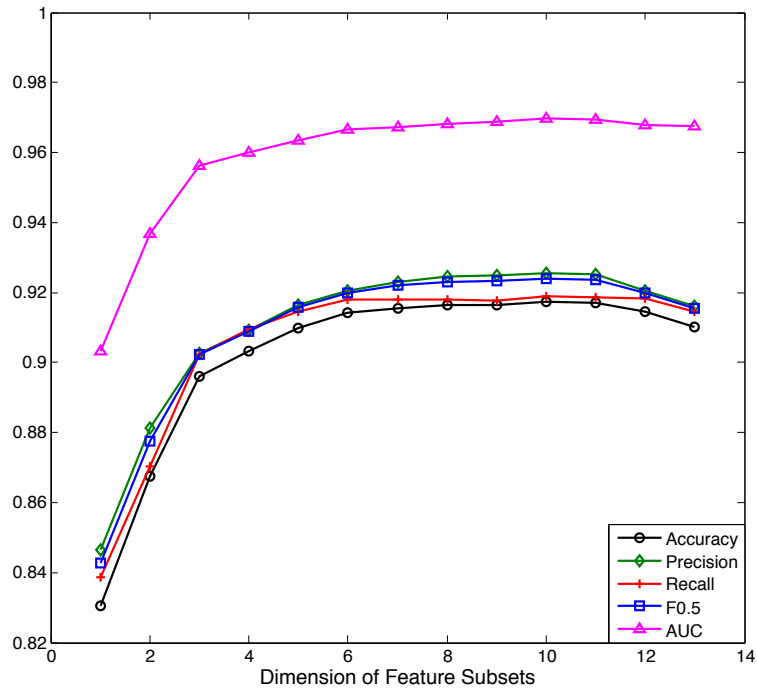


Figure 5.7: Trends of Accuracy, Precision, Recall, F0.5 and AUC along with Feature Dimensions for Test Set

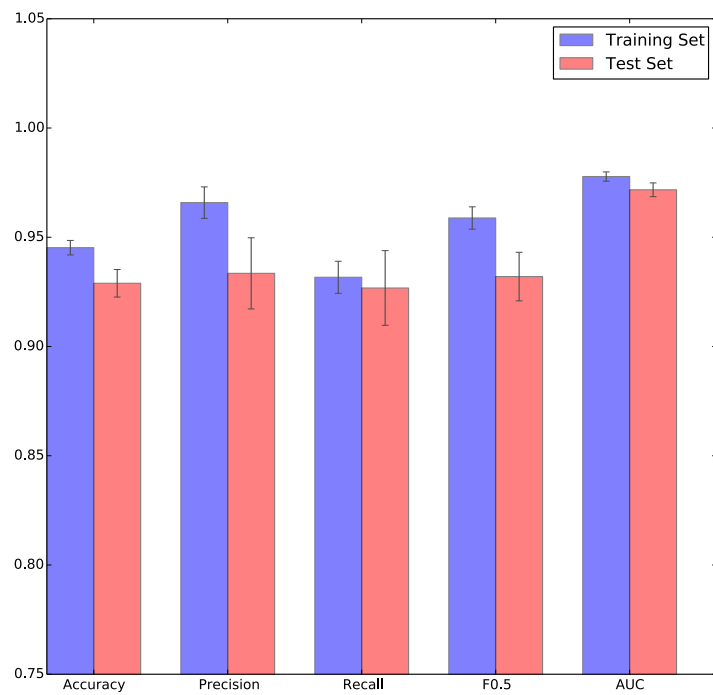


Figure 5.8: SVM Performance in 10 Continuous Training

Table 5.2: Best and Worst SVM Performance in the 10 Continuous Training

	Best Performance		Worst Performance	
	Training Set (%)	Test Set (%)	Training Set (%)	Test Set (%)
Accuracy	95.00	93.20	94.84	92.01
Precision	98.01	94.17	95.96	93.18
Recall	92.31	93.05	93.50	92.76
F0.5	97.70	93.95	95.45	93.10
AUC	98.08	97.55	97.71	96.18

highest accuracy in the test set was 93.20%, while the lowest was 92.01%.

Fig 5.9 and 5.10 shows the distribution of decision function value for training set (Fig 5.9) and test set (Fig 5.10) respectively. The red curve on the negative side of each image represents the distribution of bone classes and the blue curve on the positive side represents the interspinous class. The decision function value of training set has the maximum probability density at -2.3 for bone class and 1.9 for interspinous class. The probability density at the test set is maximized at -3.5 for bone class and 1.7 for interspinous class. Furthermore, decision function value of the wrongly classified data is analyzed for the test set, as shown in Fig 5.11. Most of the misclassified data has low absolute decision function value of around zero, within the range of $[-2, 3]$.

5.8.3 Video Processing

The trained SVM model with best performance was further tested on the collected ultrasound video streams to identify the interspinous region and bone region, with 10 features used. In the video processing, the interspinous region is defined by the continuous appearance of more than 5 interspinous images; while for the negative detections, if it is in the interspinous region, no more than 2 bone images shall be detected by the image; vice versa for bone region. According to the definition above, the trained SVM model was able

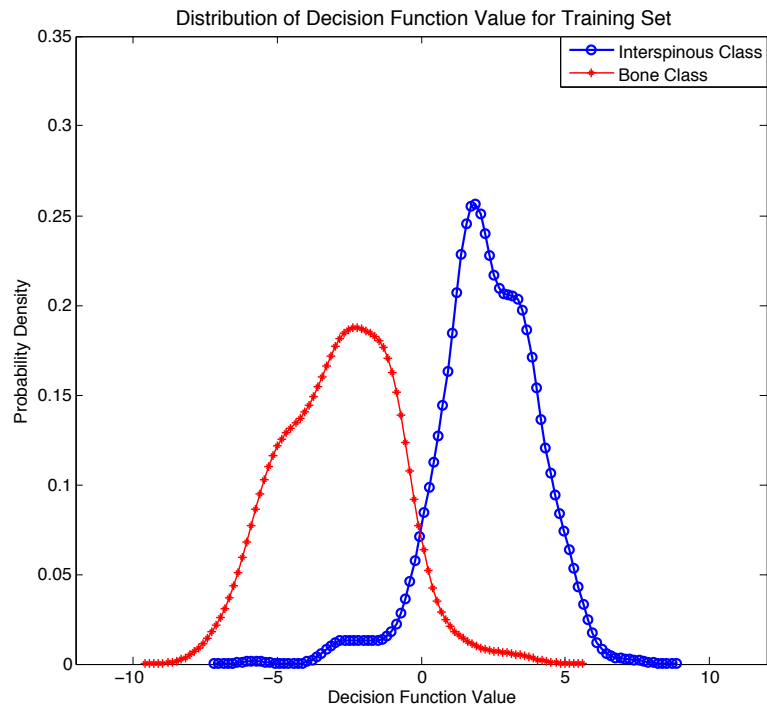


Figure 5.9: Probability Density Estimation of Decision Function Value for Training Set

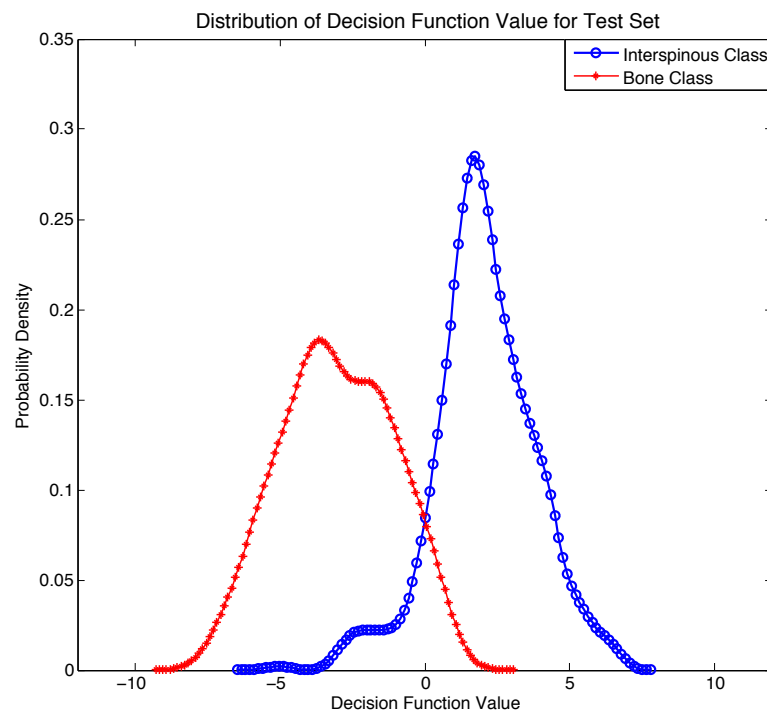


Figure 5.10: Probability Density Estimation of Decision Function Value for Test Set

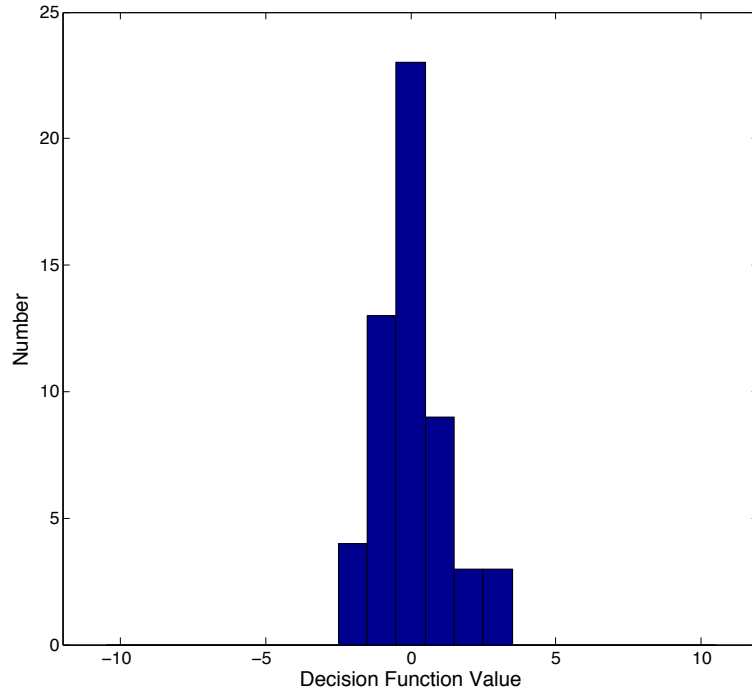


Figure 5.11: Histogram of the Decision Function Value for Misclassified Test Data

to identify the interspinous region and bone region correctly on 45/46 video streams collected.

An example of video frame identification result is provided in Fig 5.12. Only region-of-interest is extracted and shown on the image. The white vertical line is the midline identified by the algorithm. The circle on the right side of the images indicates that the image is classified as interspinous images by the SVM model, with vertebra body marked by rectangles and epidural space marked by white line. The digit on the upper left corner of each frame is the decision function value calculated with the SVM model. Fig 5.12(d) shows the failure case, which is from the same case as shown on Fig 5.5(b).

Table 3 lists the computation time for major operations in the pre-processing, feature extraction and SVM classification procedure. Matlab (R2012a, The MathWorks, Natick, MA, USA) was used for the implementation of the algorithm. The computation time for each frame was 52.77 ms. Given that the video was collected at the frame rate of 15 FPS, thus the computation speed is fast enough for real-time processing. Further improvement in

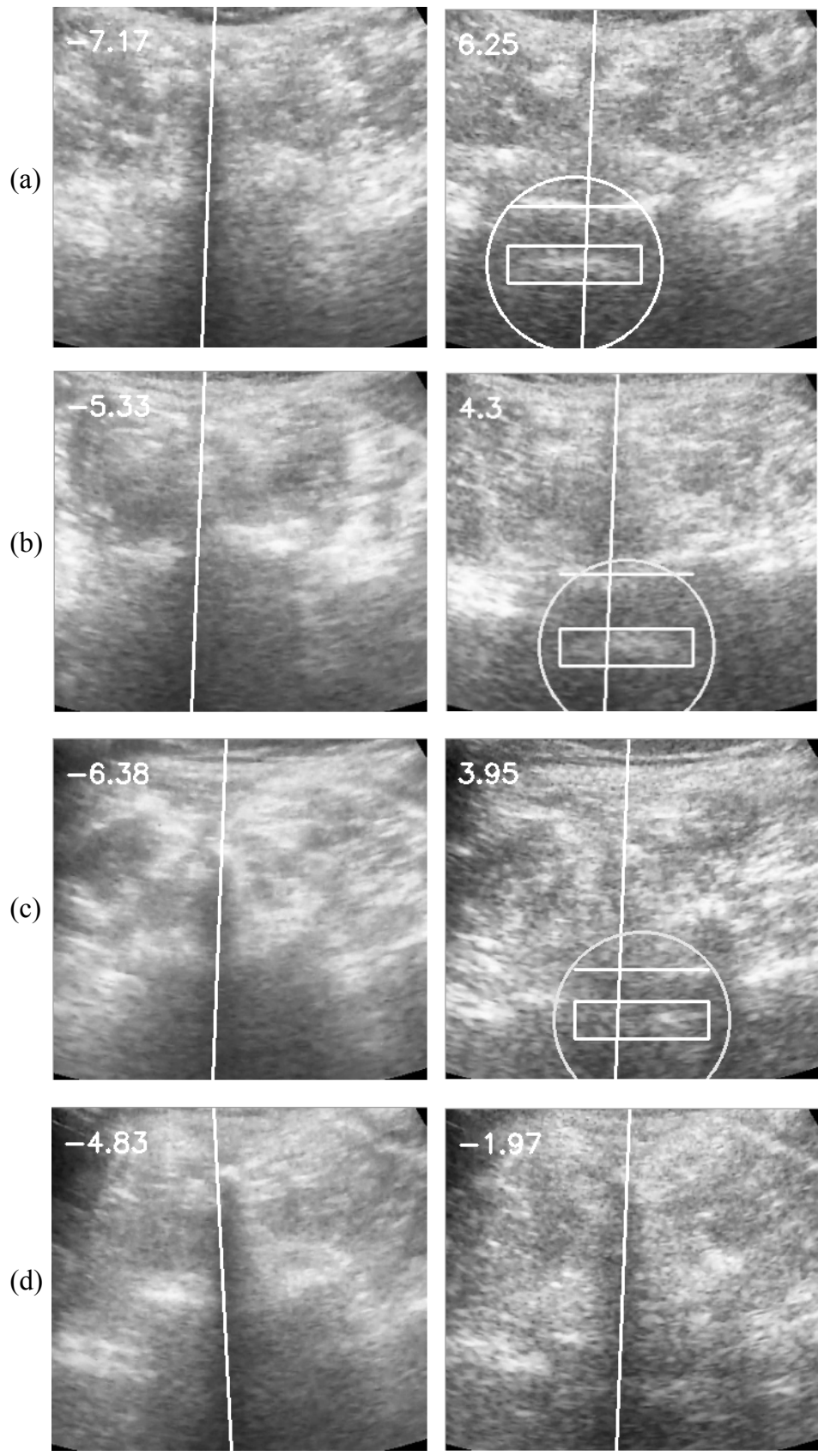


Figure 5.12: Classification Result of Selected Video Frames.

Table 5.3: Computation Cost of Video Processing with Matlab.

Operation	Computation Cost(ms)
Preprocessing	9.2
Template Matching	17.1
Midline Detection	17.84
SVM Classification	0.14
Others	8.49
Processing Time Per Frame	52.77

computational speed has been achieved by implementing the program using Python (Version 2.7.6) with Numpy (Version 1.8.1, [77]), OpenCV (Version 2.4.8, [78]) and Scikit-learn (Version 0.15.0, [79]) open source library, which shortened the computation time to 30.46 ms per frame. Therefore, the proposed image processing procedure is applicable to real time processing.

5.9 Discussions

The feature extraction method using template matching and midline detection utilized in this research provides a compact description for the ultrasound image obtained from lumbar spine in the transverse plane. It extracts the specific shape and midline features of the lumbar ultrasound images, which achieves high classification accuracy on the clinical data. However, the feature extraction method in this chapter may not be widely applicable for ultrasound images obtained from other body areas, considering the specific features of different anatomical structures.

Of the ten parameters generated from template matching, the parameters related to vertebra body and epidural space ($\mathcal{D}_1, \mathcal{V}_1, \mathcal{D}_2, \mathcal{V}_2$) have higher rank than the ones related to articular processes ($\mathcal{V}_3, \mathcal{P}_3, \mathcal{D}_3, \mathcal{V}_4, \mathcal{P}_4, \mathcal{D}_4$). Part of the reason leading to this phenomenon is revealed in Fig 5.1(b). In the left column of Fig 5.1(b), the template matching intensity and position for epidural space

and vertebra body is dramatically different on the interspinous image (the upper two images) and bone image (the lower two images). On the contrary, in the right column, the matching results of both articular processes don't differ much for the interspinous and bone images, revealing the reason for their lower ranking in the feature order.

Another feature extraction method used in this research is midline detection. On the bone region, ultrasound waves are impeded by the spinous process, thus creating the anechoic window along the midline. Hence, the proportion of black pixels serve as an important indicator for the identification of bone image. On the other hand, for the interspinous image, the epidural space and vertebra body appear at the bottom part along the midline; while for the bone image, no white pixels appear at the bottom part. Therefore, the appearance of white pixels under certain depth threshold indicates the image being classified as interspinous image, indicated by the large correlation value of the \mathcal{R}_w parameter. The symmetrical parameter was proposed so as to confirm the correctness of midline detection. A higher symmetrical parameter implies that the midline is correctly located. The symmetry parameter was not directly related to the image labeling, which is the reason why it had lower rank among the features.

Feature selection is a standard procedure for machine learning problems when the feature dimension is high, so as to avoid the 'curse of dimension' and decrease computational cost. Although the feature dimension used in this chapter is low, the feature selection procedure is still a necessary step and helps to select the best feature subset wisely. For the optimal feature subset obtained via feature selection, 10 out of 13 feature parameters were selected; whereas the symmetrical parameter \mathcal{S} and matching position of articular process \mathcal{P}_3 , \mathcal{P}_4 were excluded. The computational cost for symmetrical detection was 18.98 ms per frame, the discarding of which greatly improved the computation speed. Therefore, the system performance, including identification accuracy

and computational speed, were greatly improved by the feature selection procedure.

The SVM model is a supervised machine learning method, which requires that correct labels must be provided for every sample in the database. As an effort to decrease the label noise, two approaches were employed in this research. Firstly, the adversarial labels assigned by the two sonographers were removed from the training and test database. The images with adversarial labels has higher possibility of being misclassified, the removal of which will help to purify the database. Secondly, SVM with soft margin was utilized for the data training. Soft margin SVM is less sensitive to outliers and the sensitivity can be regulated by the regulation parameter C . The proper selection of C is able to balance the two goal of achieving high accuracy in the training set, but avoiding over-fitting for the outliers and mis-labeled data. Those two methods will help to decrease the adverse influence of the label noise.

For the test data, the value of decision function represents the distance of data to the optimal separation hyperplane obtained by SVM training. The higher the absolute decision function value, the higher the possibility that the data may be correctly classified. Therefore, the decision function value serves as an indicator for the confidence of classification. In the real-time processing, the value will be listed on the corner of the image to keep the operator informed of the identification confidence, as displayed in Fig 5.12. The optimal needle entry angle can be obtained by slowly tuning the angle of the probe, until the largest identification confidence is achieved.

The only video stream that SVM failed to locate the interspinous region in this research was the case shown on Fig 5.12(d). It is the same case shown on Fig 5.5(b) where sonographers disagreed on the label of the image. Although the image was excluded from training database as label noise, it was tested in the video processing procedure. The SVM model correctly identified the bone

region with high confidence. However, for the interspinous image, the dark shadow casted by spinous process influenced the template matching of vertebra body and epidural space; hence the SVM model was not able to recognize it. This was a typical case near the junction region of bone and interspinous, so that part of the ultrasound waves were obstructed, while the rest were able to reach the epidural space. It was speculated that the interspinous region might be correctly identified by the SVM model if the operator moved the probe downward or upward a little or that the probe angle was slightly adjusted upward to avoid the spinous process.

In conclusion, four contributions were achieved with this chapter. First, a set of features were extracted from the lumbar ultrasound images with template matching and midline detection methods. Secondly, the ‘predictability’ of extracted features were evaluated using cross correlation and the forward search approach was utilized for feature selection, so as to choose the feature subset with optimal performance. Thirdly, the SVM model was trained using the extracted feature sets, so as to generate the maximal margin for the classification. A high success rate was achieved with the proposed feature extraction and SVM classification algorithm on images collected from the pregnant patients. Finally, the trained SVM model was also tested on 46 videos and it successfully identified the interspinous region and bone region on 45 of the cases collected, with a computational speed fast enough for real-time processing.

5.10 Conclusions

In this chapter, a feature extraction, ranking and the selection procedure is proposed for the ultrasound images collected from lumbar spine. The important anatomical features, including epidural space, vertebra body and articular processes were extracted from the ultrasound images. Moreover,

the proportion of black pixels along with midline were also extracted with midline detection. Feature selection was further employed to select the feature subset with optimal performance and decrease computation cost. Based on the features extracted from training samples and test samples, a SVM was used to classify the interspinous and bone images with maximal margin. The trained SVM model was further tested on the ultrasound video streams collected from pregnant patients, and successfully identified the interspinous region / bone region on 45 out of the 46 videos collected.

Chapter 6

System Integration

6.1 Introduction

In the previous chapters, computer-aided automatic interpretation of lumbar ultrasound images, both in the longitudinal view and transverse view, has been discussed. The purpose of longitudinal view scanning is to identify the lumbar level of L3-L4. The algorithm will search for sacrum first, the identification of which will initiate the panorama stitching process when the operator moving up the ultrasound transducer. The spinous level dividing is performed on the generated panorama image by extracting the local maxima of template matching result. When L3-L4 level is identified, the algorithm will generate a signal to alert the operator that insertion level has been reached. The operator will then be guided to rotate the transducer to the transverse view, so as to locate the precise needle entry point. In the transverse view, along with the vertical movement of the probe, the algorithm will extract the features from the pre-processed ultrasound streams and identify whether the image is interspinous or bone image with the trained SVM model. When the interspinous images are detected continuously, the algorithm will deem it as proper needle insertion site and notify the operator to stop scanning and mark the position.

Although algorithms have already been developed in the previous chapters, there are remaining problems of applying the algorithms online to provide real-time in situ analysis and how to present the interpretation result in an intuitive and user-friendly approach. In this chapter, the interface between the ultrasound machine and computer will be developed, so as to realize the real-time image acquisition and on-line analysis of the ultrasound images. A graphical user interface will be developed to present the anesthetists with real-time image processing results and provide guidance for entry point localization. In addition, as an effort to realize the automatic epidural needle insertion, this chapter will also discuss the problem of improving the needle insertion procedure after entry site has been located. A mechanical system performing needle insertion procedure while preserving the entry site and entry angle detected by transducer will be proposed. A manual approach of using customized ultrasound transducer with thin slit which allows the penetration of epidural needle will also be proposed. This approach will realize the real-time ultrasound guidance for the whole needle insertion procedure.

6.2 Image Acquisition System Development

In order to realize the on-line image processing for the ultrasound images, the image acquisition system is required. Generally, the ultrasound machine is equipped with a video output port, which is capable of exporting the living stream to external devices. Different ultrasound machine may have different types of video port. The commonly used video output port types mainly includes: Video Graphics Array (VGA), Digital Visual Interface (DVI) and High-Definition Multimedia Interface (HDMI) etc.

The video signals from the video output port, whether analog or digital, are usually for displaying purpose, e.g., showing the video on an external monitor. In order to convert the video streams into a signal that is suitable

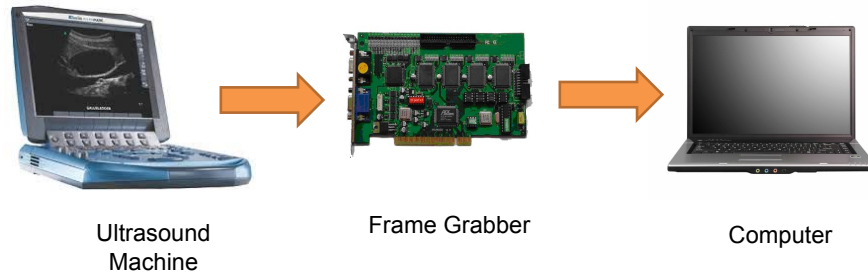


Figure 6.1: Image Acquisition System

for computer processing, a frame grabber (also called video capture card) is usually employed. Frame grabber is able to capture the individual, digital still frames from analog video signal (VGA etc) or digital video stream (DVI or HDMI etc). The system architecture of the image acquisition system is shown in Fig 6.1.

In this research, the video port of the employed ultrasound machine is the VGA port. The video frames are generated at 15 frames per second (FPS) with size of 800×600 . In order to captures the video without frame lost, the frame grabber are required to have an update rate above 15 FPS. The Epiphan DVI2USB 3.0 (Epiphan, Ottawa, Canada) is adopted as the frame grabber, which provides up to a speed of 60 FPS under the resolution of 800×600 . Moreover, the DVI2USB device is compatible with VGA, DVI and HDMI port; thus the device can be fed with ultrasound with different video output port. Further experimental tests with the acquisition system indicated that, the DVI2USB device is able to acquire the ultrasound video streams smoothly and accurately.

6.3 Graphical User Interface Design

In this section, the requirements and implementation of graphical user interface will be discussed. The target of user interface design is to present the anesthetists with real-time processing results of the video stream acquired by

the frame grabber; provide guidance to the anesthetists on how to move the transducer or to mark the position when optimal insertion site is located. The user interface is required to present the necessary information in a user friendly and readily understood approach, so that anesthetists can get the information conveniently.

In the procedure of searching for the optimal needle entry site, two different views are employed, the longitudinal view and transverse view, the details of which can be found in the introduction section. The information and guidance that needs to be imparted to anesthetists are different in those two views. The longitudinal view is mainly used for the identification of insertion level (L3-L4). The critical information in this view includes the identification of sacrum, which is the starting point for transducer scanning, and the level dividing of spinous process. The simplified guidance required includes: searching for sacrum in the sacrum area with probe hold vertically, moving up in the midline plane after sacrum is identified, stop scanning when L3-L4 is identified and rotate the transducer to the transverse plane. The target in the transverse plane is to locate the precise needle entry point. The information needs to be obtained in this view contains: the identification whether the current frame is bone image or interspinous image, and the depth of epidural space. Guidance required to be provided to anesthetists includes: holding the transducer horizontally and moving up slowly, aligning the probe center to the midline, stopping scanning when the optimal position is localized and marking the position on the patients skin with sterilized marker pen.

6.3.1 Longitudinal User Interface

The graphic user interface of the longitudinal view is designed as shown in Fig 6.2. Before scanning, the operator is required to place the transducer near the sacrum area and hold the transducer with marker pointed upwards. The scanning depth is set as 73 mm by default, which is suitable for most patients.

However, if the patients is estimated to have deeper vertebra body caused by obesity issues, then the operator may need to set the depth to around 91 mm. Different scanning depth influence the region of interest of the ultrasound image. Thus unless necessary, the scanning depth shall keep the default value without change. The preparation stage is stated clearly at the ‘Warning’ box, to inform the operator to perform the necessary machine and system tuning before scanning. After the preparation, the anesthetists can click the button of ‘Load Video’ to start ultrasound scanning, or by press the keyboard of ‘0’. All the operations can be invoked by either mouse or keyboard, to provide the anesthetists with shortcuts and multiple choices.

The user interface is composed of three major image displaying windows. The upper left one displays the original full size ultrasound image, as the one from ultrasound machine. The level dividing result will be imposed on the image to inform the anesthetists of the lumbar level where the transducer is located. The lower left window exhibits the panorama image stitching result as the transducer moving. The spinous identification and level dividing result are also marked on the panorama image. The right image window shows an illustration of the lumbar spine anatomy. The blue line indicates the lumbar level calculated by the algorithm and it will move along with the movement of transducer. This provides a direct notation for the anesthetists of the lumbar level where the transducer is located. The whole scanning procedure will be automatically saved by the system for the purpose of further examine.

The icon on the upper right corner of the user interface provides guidance to the anesthetists based on the processing results. Before the sacrum is located, it will be a ‘searching’ icon, so as to notify the anesthetists to keep searching in the sacrum area. After the system detected sacrum continuously, the icon will be changed to ‘moving up’ icon, as shown on Fig 6.2. After L3-L4 or L2-L3 lumbar level is identified, the icon will be changed to a green ‘Correct’ icon, to alert the anesthetists that the correct level has been reached. Fig

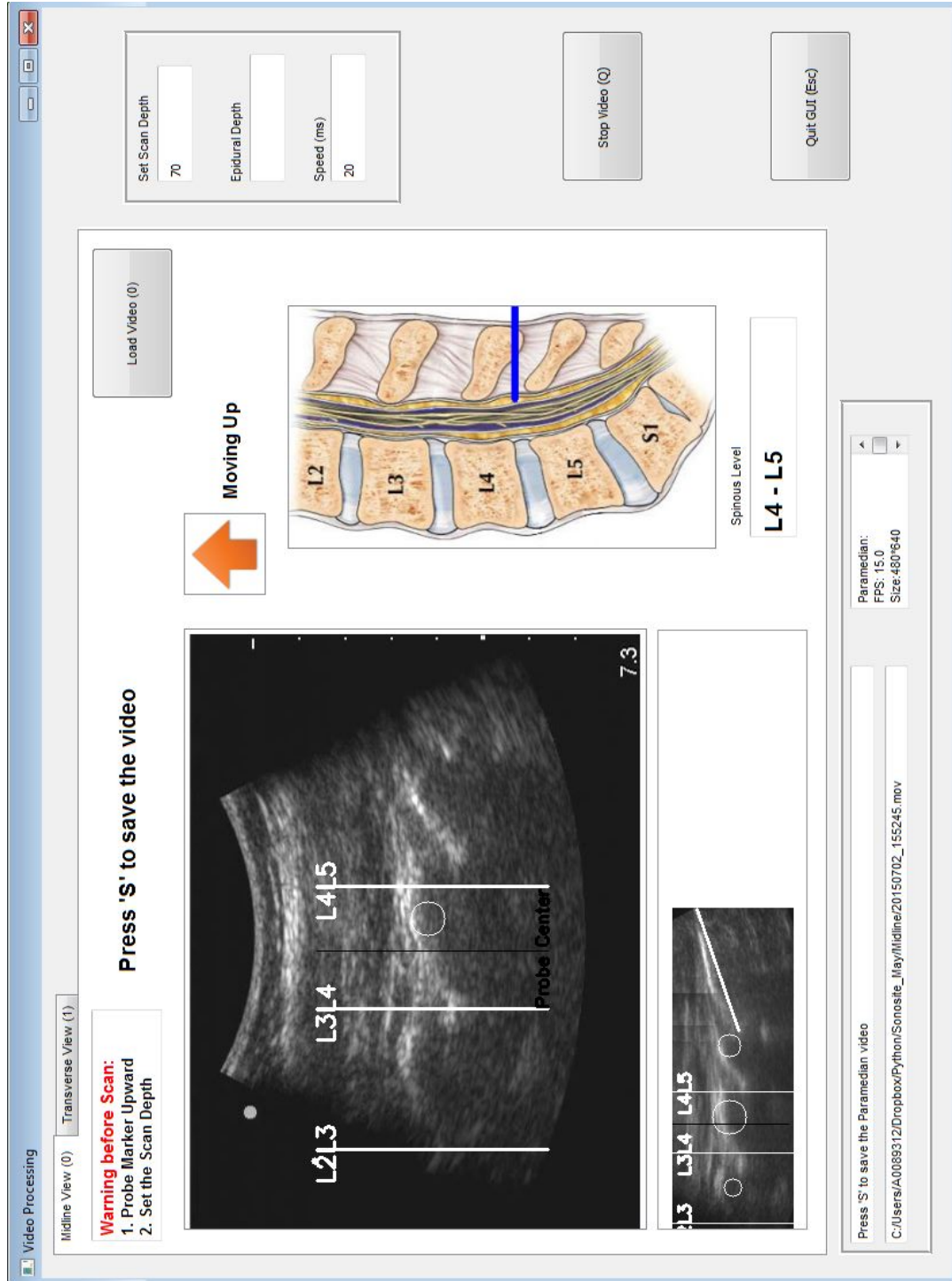


Figure 6.2: Graphical User Interface of Longitudinal View

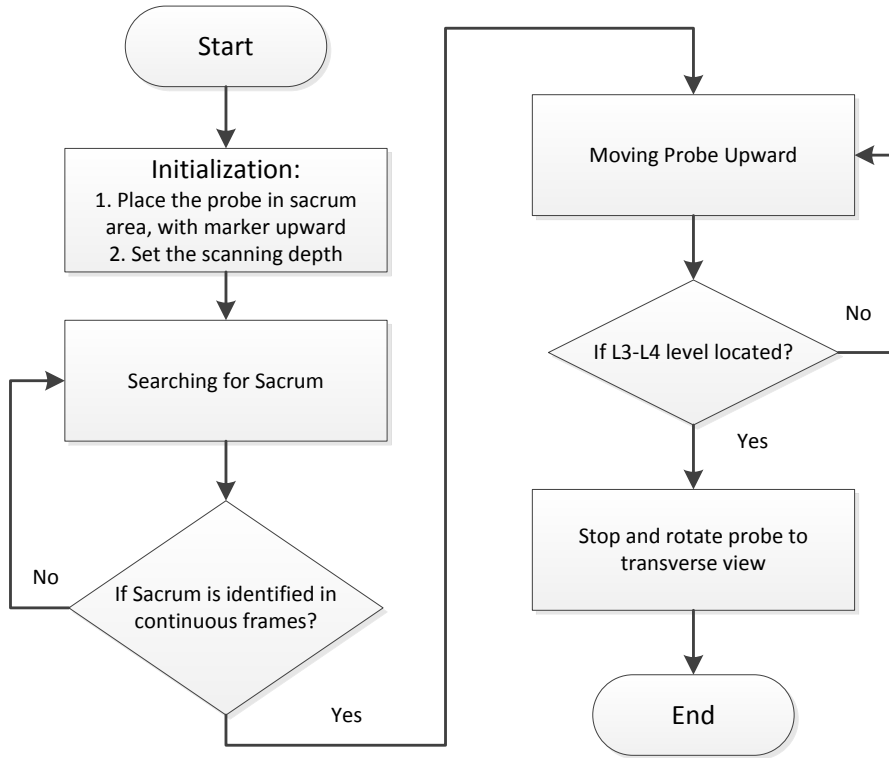


Figure 6.3: Working Flow of the Longitudinal User Interface

6.3 shows the working flow the longitudinal user interface. The processing algorithms working in the background in real-time along with the movement of transducer and providing result and guidance to the anesthetists.

6.3.2 Transverse User Interface

Fig 6.4 indicates the designed graphical user interface in the transverse view. After the transducer is rotated to the transverse view, the anesthetists will be guided to hold the probe with marker toward left, then the image acquisition will be initiated. The algorithm will identify whether the current frame is interspinous image or bone image.

The transverse view user interface contains two image windows. The left one shows the original ultrasound view acquired from ultrasound machine, with probe center reference line and detected midline marked on the image. The right window shows the cropped region of interest. The circle in the

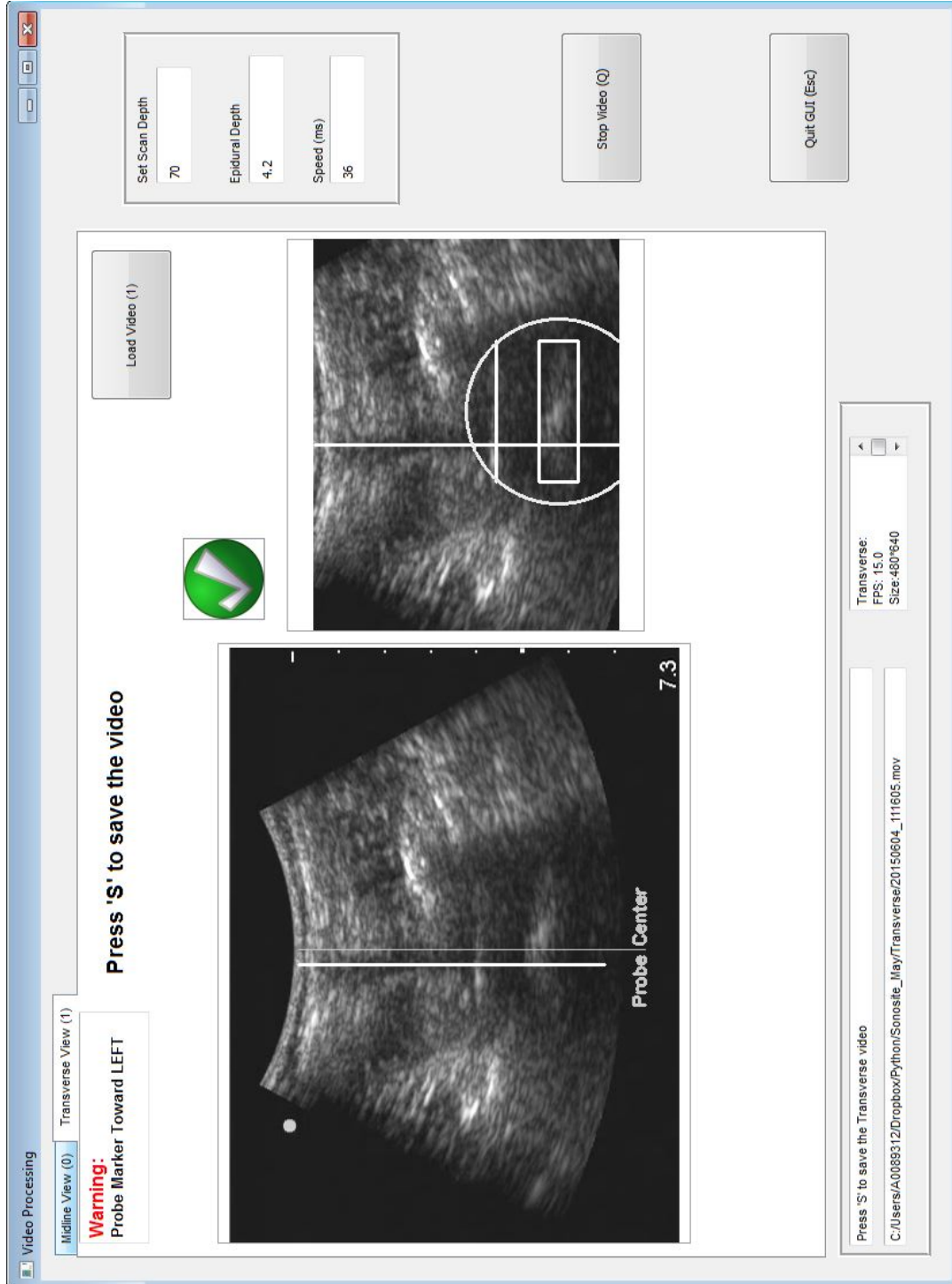


Figure 6.4: Graphical User Interface of Transverse View

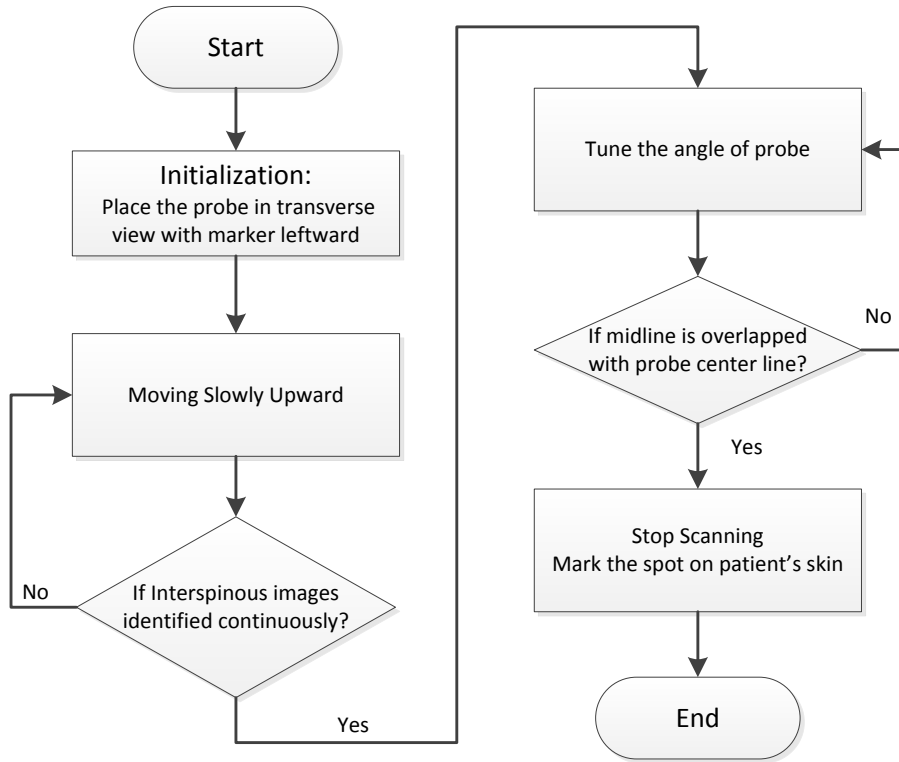


Figure 6.5: Working Flow of the Transverse View User Interface

center indicates that the image is being identified as interspinous image, and the brightness of the circle is proportional to the confidence of the detection, i.e. the higher possibility that the image is interspinous image, the brighter the circle. Vertebra body and epidural space will also be marked, as shown in Fig 6.4. If bone images are identified, the icon on the lower right corner of the window will be marked as ‘Wrong’ icon, indicating that this is the worst possible site for needle insertion. If the bone image and interspinous images are not detected continuously, but appeared over every other images, indicating that the transducer is located on the interval region between interspinous region and bone region, then the marker will be shown as ‘blank’, indicating that the algorithm cannot identify the bone/ interspinous region in this area. If the interspinous images are identified continuously, the icon on the lower right window will be changed to a green ‘Correct’ icon, indicating that this site is proper as needle entry site. The anesthetists will then be guided to align

the midline to the reference line of probe center, by aligning the white line (detected midline) shown on the left window to overlapping on the reference black line. The algorithm will further identify the epidural space and estimate the depth of epidural space, and then displaying it on the right dialog box for the information of anesthetists. After those procedures, the correct spot for needle entry is identified and the transducer is properly aligned. Then the anesthetists will stop scanning and mark the site on the patients skin with a sterilized marker pen. The detailed procedure is shown on Fig 6.5.

6.4 Result for Real-time Image Processing

The image acquisition system, together with the proposed algorithms and graphical user interface, has been tested in real-time on healthy volunteers at KK Womens and Childrens Hospital (Singapore), with IRB approval and individual participant's consent obtained. A Sonosite Titan ultrasound system (SonoSite, Bothell, WA, USA) and a 2MHz curvilinear ultrasound probe (SonoSite, Bothell, WA, USA) are used for the study. For the image acquisition, an Epiphan DVI2USB 3.0 video capture card (Epiphan, Ottawa, Canada) is adopted. As a primary test of the applicability of the system, 5 volunteers has been recruited so far.

During the study, the operator moves the probe as instructed by the interface, following the protocol in the section 'Appendix A'. An experienced sonographer is involved in the study to evaluate the landmarks identification accuracy of the program in real-time. For the longitudinal view, the key evaluation criteria is the correct detection of the sacrum and level counting of the L3-L4; for the transverse view, the key criteria is the accurate identification of interspinous image and precise measurement of epidural depth.

In the longitudinal view, the sacrum is successfully recognized for all of the 5 subjects. L3-L4 spinous level is successfully identified on 3 out of 5 cases for

the first scan (case (a)(b)(c)). For the other two cases, it takes two scans to locate the L3-L4 level (case (d)(e)). As shown on Fig 6.6, for the successful scans, the panorama images are properly stitched (left column) and L3-L4 is correctly identified and displayed on the frame in real-time (right column).

Fig 6.7 shows two representative frames of the cases (d)(e) for the failed first scan. The failure of first scan for the two cases is resulted by the fact that the volunteers are so skinny, such that the curvilinear probe cannot be properly covered by skin tissues, leading to the large area of anechoic window near the two ends of the frame. The frames with large black area are deemed as bad quality by the algorithm, thus cannot be properly stitched to the panorama image. On the second trial, the subject is requested to keep their back straight. Under this condition, the majority part of the probe is covered by body tissue; therefore, the panorama image is successfully stitched and L3-L4 level is correctly identified in the second trial.

After L3-L4 level is identified, the ultrasound probe is rotated to the transverse view to locate the precise needle entry site. The interspinous region identified by the algorithm accords to that identified by the sonographer for all of the 5 subjects. The epidural space is correctly identified for the 5 subject, to the precision of 0.1mm. The real-time transverse image processing result of the 5 subject is displayed on Fig 6.8. The left column shows the bone region images for the 5 subjects; the right column displays the identified interspinous region for the volunteers. The vertical white line is the midline identified by the algorithm. The circle on the right column denotes that the image is identified as interspinous image by the algorithm, with the brightness indicating the confidence of identification. The vertebra body recognized by the algorithm is marked by the rectangle; the horizontal line above the vertebra body denotes the epidural space identified by the algorithm.

The primary real-time results indicate that the program is applicable for needle entry site localization for volunteers. However, further test on more

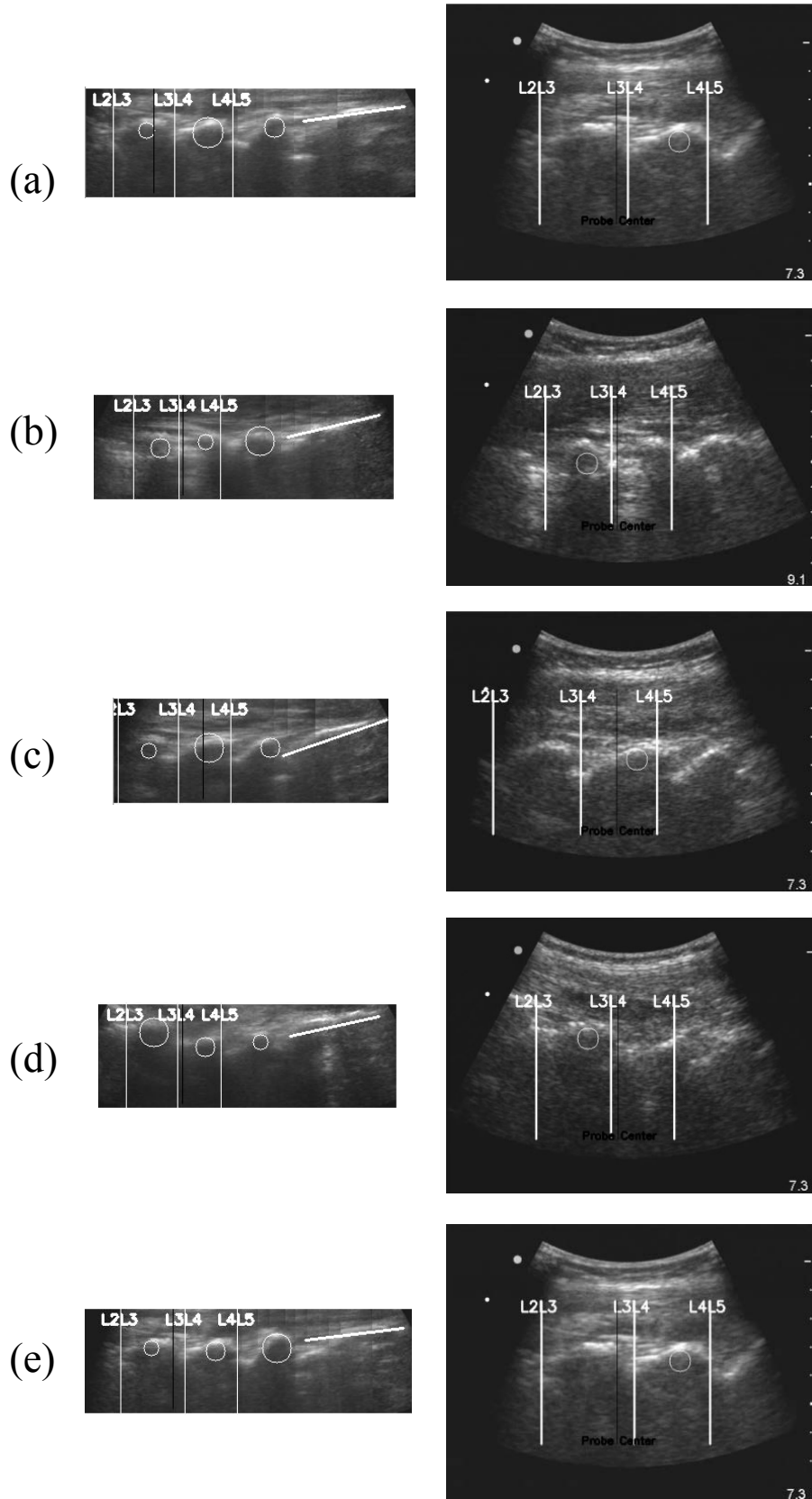


Figure 6.6: Real-time Image Processing Result of Longitudinal View for Volunteers. The left column lists the stitched panorama image; the right column displays the level dividing result on real-time frames.

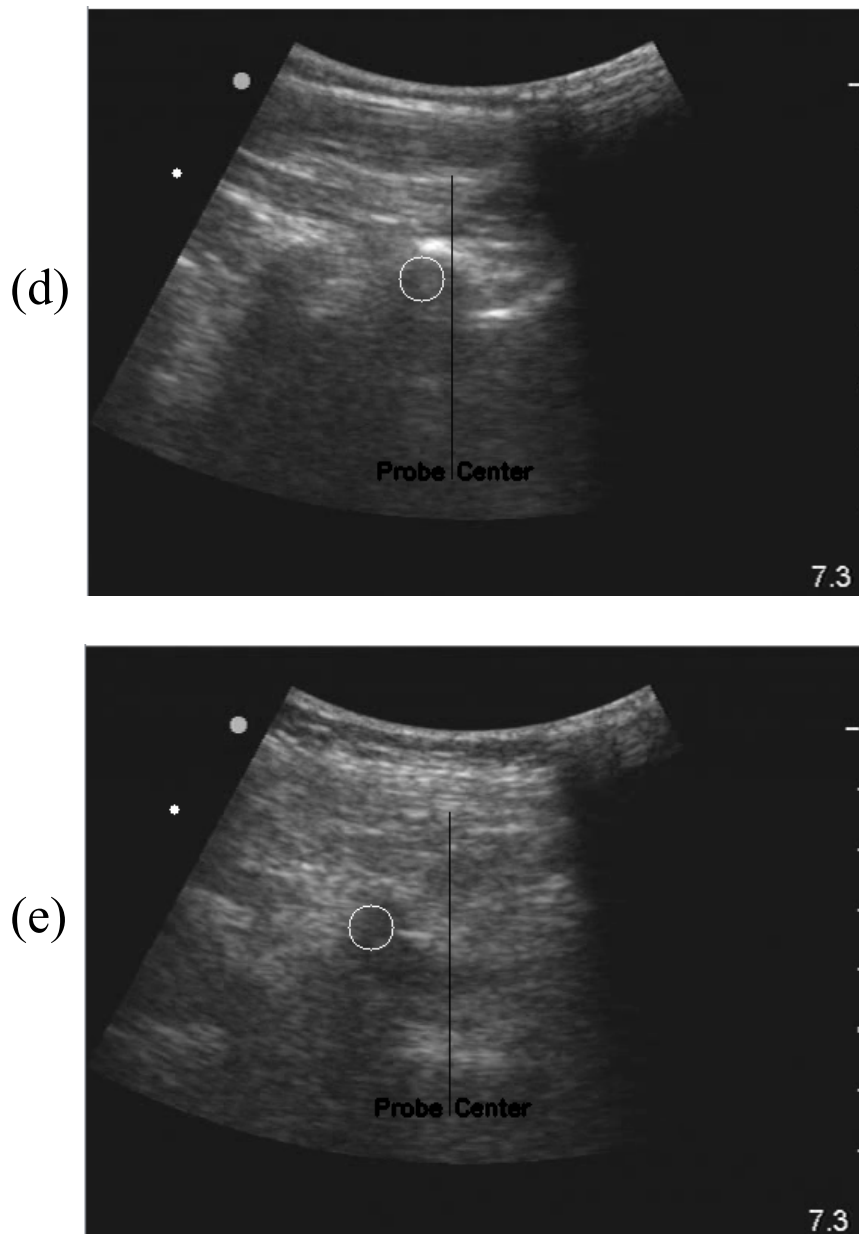


Figure 6.7: Representative Anechoic Region for the Two Failure Cases at First Scan.

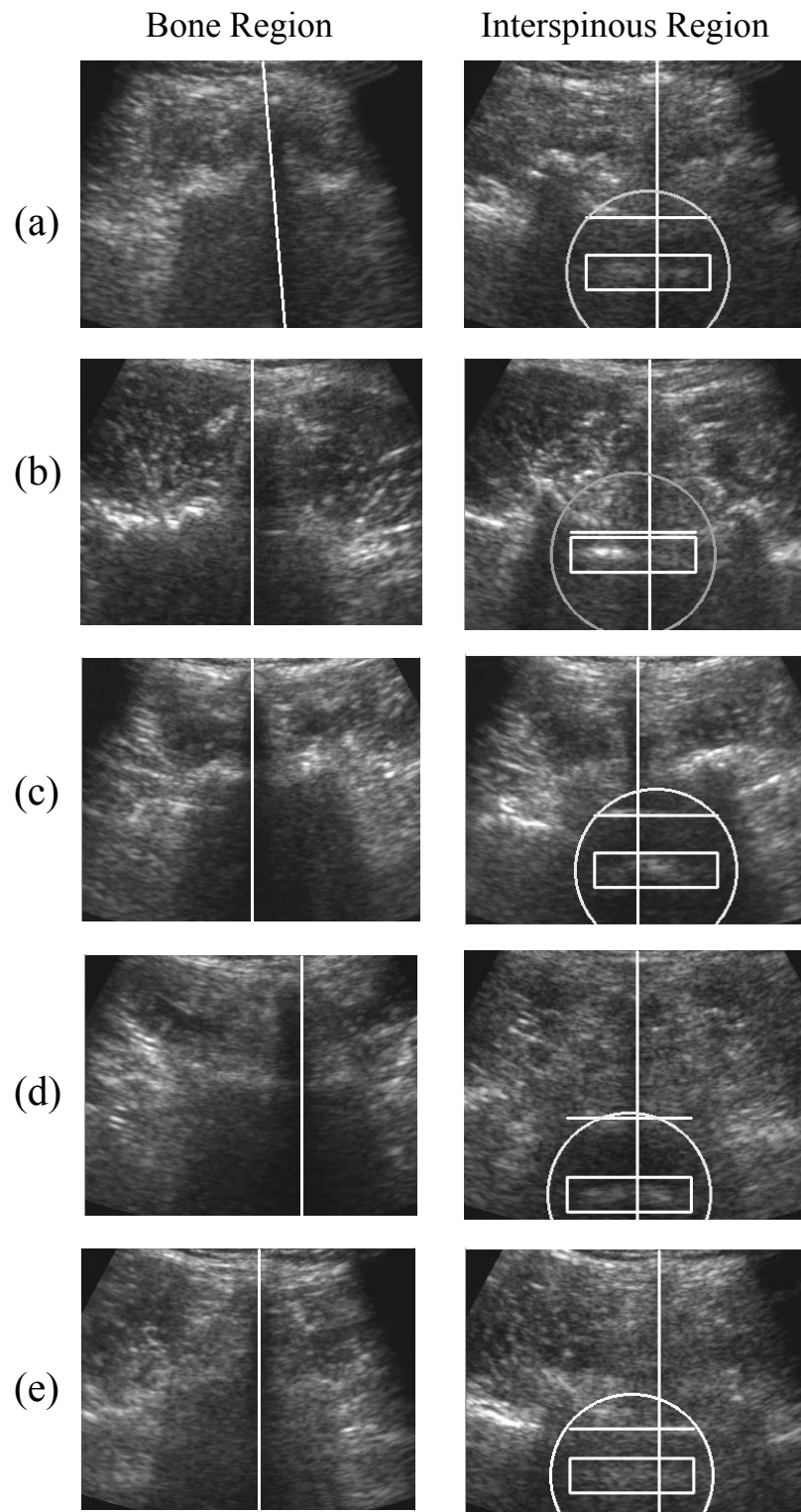


Figure 6.8: Real-time Image Processing Result of Transverse View for Volunteers.

subjects is required in order to fully validate the applicability of the system.

6.5 Manual Needle Insertion with Ultrasound Guidance

After the needle entry site has been located by the image acquisition and processing system, anesthetists will proceed with the epidural needle insertion procedure. In the clinical practice, anesthetists will first sterilize the lumbar area to avoid infection; then insert the needle at the identified point towards the epidural space. When the needle encounters ligamentum flavum, the dense tissue outside epidural space, the penetration force will increase; the anesthetists will connect the needle hollow with a syringe which filled with air or saline. Along with the carefully advancement of needle through ligamentum flavum, anesthetists are required to press the syringe to apply constant pressure. When the needle tip penetrates through the ligamentum flavum and enters the epidural space, the pressure inside the epidural space will be lower than the pressure inside the syringe, thus the saline will be released, so called ‘loss of resistance’ technique. This procedure is highly risky. The advancing force applied on the needle is high when the needle passing through ligamentum flavum; when the needle enters epidural space, the insertion force will drop quickly, thus it requires expert skills to stop the needle inside the epidural space, without penetrating the dura mater.

The insertion procedure described above is a blind procedure and it depends highly on the skills of the anesthetists. In order to make the needle insertion more secure, ultrasound is utilized to assist the needle insertion in real-time. Real-time ultrasound guided needle insertion has been widely employed in areas like biopsy. In EA, Trans et al. has proposed to use the ultrasound imaging in the longitudinal view to guide the needle insertion [80]. However, in Trans’ approach, since the needle is inserted in the longitudinal view and

not perpendicular to the skin, thus the insertion length are much longer than in the transverse view. Transverse view is widely adopted by anesthetists when inserting epidural needle, because the insertion distance is shortest in this plane. However, the problem with real-time ultrasound guided needle insertion in the transverse view is that the ultrasound probe itself will block the needle entry site.

In order to realize the real-time ultrasound guided needle insertion in the midline plane, the ultrasound probe needs to be customized so as to leave space for needle insertion. It is expected that the customized ultrasound probe has a hole or slit in the probe center, where the epidural needle can pass through. Such customized probe is available in the market.

Fig 6.9 illustrates the simulated ultrasound image with the customized probe during needle insertion. The probe center provides a fixed trajectory for needle insertion, and the trajectory can be easily planed before insertion, as shown by the dashed line in Fig 6.9. In addition, since the needle is inserted through the center of the probe, thus the needle is located in the same plane as the ultrasound image. Under this condition, the inserting needle resembles a bright line in the ultrasound image. The needle insertion procedure will thus be simplified to following the dashed line guidance till epidural space is reached.

6.6 Mechanical System Design

In this section, the concept of mechanical system which supports automatic epidural needle insertion will be proposed. The mechanical system aims to insert the needle to the epidural space after the optimal insertion site is located by the image processing algorithms. It is composed of a mechanical design system and control system.

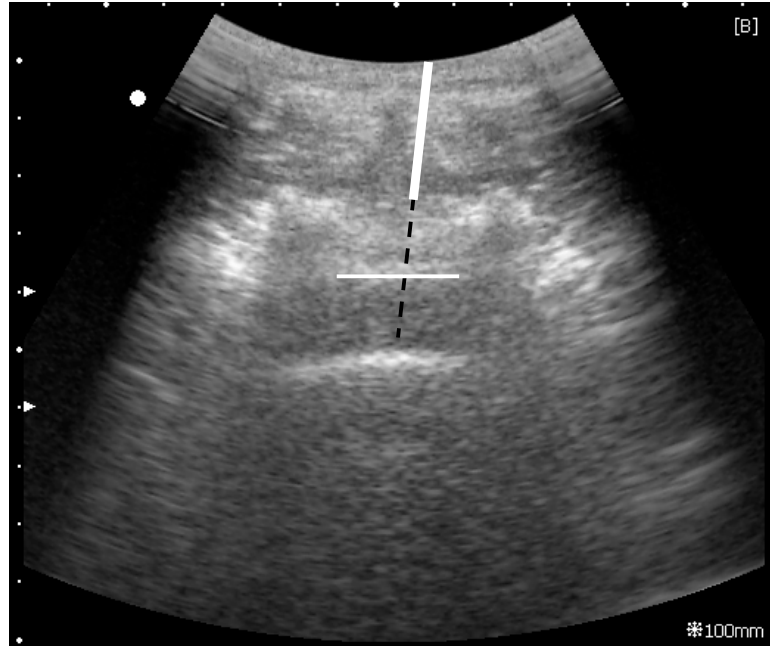


Figure 6.9: Simulated Ultrasound Image for the Customized Probe: the black dashed line represents the predicted needle trajectory, the thick white line is the detected needle path, the horizontal white line represented detected epidural space which is the target of needle insertion.

6.6.1 Mechanical Design

Fig 6.10 shows a theoretically feasible mechanical design of the insertion device. In the insertion system, the epidural needle is propelled by a precise linear motorized stage. Moreover, a highly sensitive force sensor is utilized to measure the exertion force on the needle, which will guide the needle to penetrate the correct distance into the lumbar spine to reach the epidural space. Additionally, the customized ultrasound probe is attached to the main structure and allows the needle pass through the slit, enabling the real-time image guidance and needle detection during the insertion process.

Two parameters can be used to identify and confirm the arrival of needle tip into the epidural space: pushing force (measured by force sensor integrated with the actuator) and reference epidural depth (automatically identified and measured by image processing algorithm). Moreover, under the real-time image guidance, the needle tip will be detected and tracked in real time. Relative position to the epidural space can be easily measured. Those

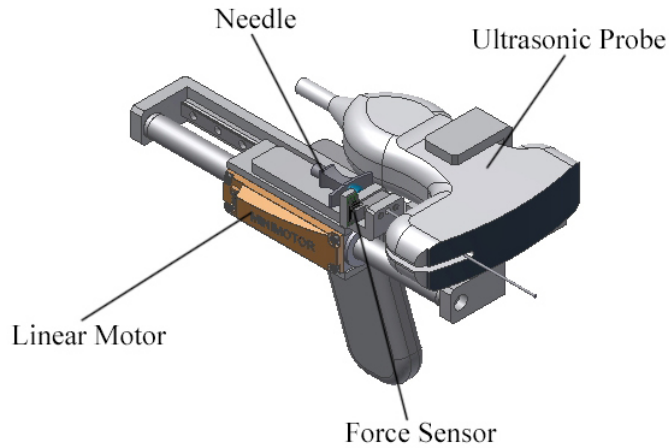


Figure 6.10: Mechanical System Design

parameters combined together will identify the epidural space accurately and prevent the dura mater from being punctured.

6.6.2 Control System

The role of control unit is to control the actuation of motor and sensor fusion, further, realizing the automatic procedure of epidural needle insertion. It consists of a sensor fusion algorithm for epidural space detection, a motion controller and a supervisory controller.

In the sensor fusion algorithm, two sensing modalities are employed. (1) Real time ultrasound image guidance is used to detect the needle tip, so as to estimate the insertion depth and its relative distance to the epidural space; and (2) The force sensor is used to measure the exertion force on the needle. As reported in related literatures, the insertion force will drop when the needle tip reaches the epidural space [81]. The real-time ultrasound guidance is more obvious and direct in indicating the needle insertion progress than the force sensor. But limited by the resolution of ultrasound imaging (1mm - 2mm), ligamentum flavum and dura mater usually appears as 1 layer in the image, while epidural space lies between those two layers. The ultrasound image guidance is very helpful in estimating the approaching of needle tip

near epidural space, but cannot fully confirmed the accurate puncture of ligamentum flavum and entry of epidural space, limited by the low resolution. At this point, the force sensor would be very helpful and effective. The force drop after ligamentum flavum getting punctured is very obvious and can be captured by the force sensor. This would trigger an immediate stop of the needle insertion. But the limitation of force sensor is that there may be force positives at different stage of needle insertion, e.g. when skin is punctured. Therefore, only the combination of the two sensing approaches can accurately and precisely confirms the arrival of epidural space.

The epidural space is located right after the ligamentum flavum (a dense tissue) and it is in a relatively narrow space. If the speed is too fast, the needle may not be able to stop immediately after it penetrates the ligamentum, which may lead to accidental dura puncture. Therefore, the insertion speed when the needle passing through the ligamentum flavum should be reduced in order to avoid dura puncture. On the contrary, the spinous ligament is softer and relatively further away from the epidural space; thus, the speed when the needle passes though the spinous ligaments can be faster, so as to speed up the procedure. Therefore, different speeds can be employed regarding different tissues, so that the execution time can be minimized. To this end, all the sensing information is connected to the motion controller. A supervisory control system is constructed which aims to control and manage the speed and the movements of the actuator precisely.

In the inner loop of the control system, a motion controller is used, which is able to achieve high level of performance for the motors. Thereby, precise motions can be realized for the insertion. Fig 6.11 illustrates a feasible control diagram for the system, which integrate the depth and the relative distance to epidural space information detected from ultrasound images as well as the sensory output from force sensor, so as to realize the speed control of the motor and the precise location control of needle tip inside the epidural space.

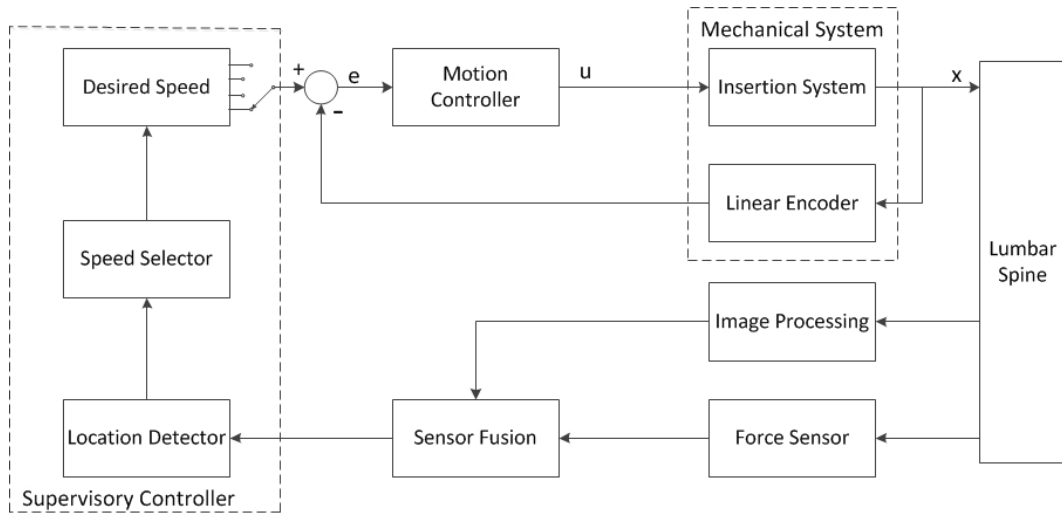


Figure 6.11: Control System Design

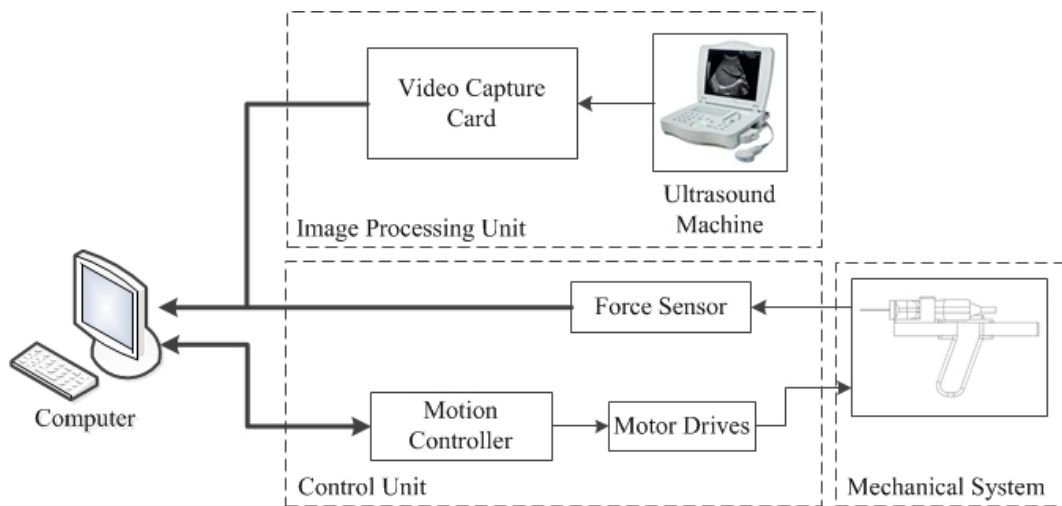


Figure 6.12: Proposed System Architecture

6.6.3 System Integration

Including the image processing system discussed in the previous sections, the proposed medical device comprises three sub-systems: image processing unit, mechanical system and control unit. The system architecture is shown in Fig 6.12 below.

Fig 6.13 indicates the system working procedure. The image processing unit will automatically interpret the ultrasound images and identify proper needle insertion site when the operator moves the probe along the lumbar spine. Then the whole system will be fixed in position and the mechanical system will

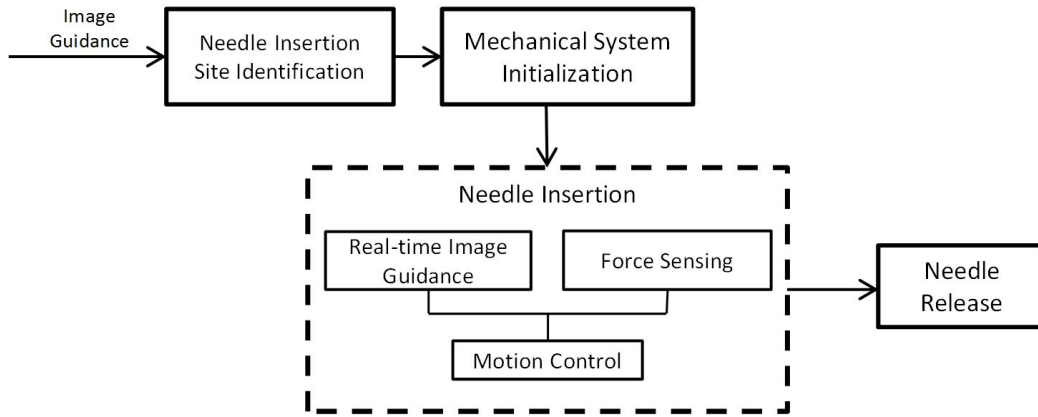


Figure 6.13: Proposed System Working Flow

be initialized. The needle insertion process is controlled with feedback from real-time needle detection and force sensing on the needle, until the needle tip enters the epidural space. Then the needle will be released with its tip inside the epidural space. Anesthetists can now precede with catheter insertion and the continuous anesthesia procedures.

6.7 Conclusion

In this chapter, on the basis of the image processing algorithms proposed in the previous chapters, a real-time ultrasound image acquisition and processing system with graphical user interface is developed. The image acquisition system is composed of three components: the ultrasound machine, frame grabber and computer. The frame grabber acquires the real-time image flow from the ultrasound machine and feeds it to the computer in a format that is proper for image processing. The graphical user interface integrates the image processing algorithms in both longitudinal view and transverse view, and presents the processing results to the operator in an easily understanding approach, with algorithms runs in the background. The developed real-time image processing system has been tested in a volunteer user study. The primary results on 5 volunteers achieves a success rate of 3/5 for first longitudinal scan

and 5/5 for second longitudinal scan. For transverse view, the success rate is 5/5 on first trial. Apart from this, a scenario where the developed system might be incorporated in the clinical practise is depicted. In the manual needle insertion, a customized probe with slit in the center can be employed to allow the needle passing through at the site located by the developed algorithm. A mechanical system and control system which support the automatic spinal needle insertion is also proposed in this chapter.

Chapter 7

Conclusions and Future Work

In this chapter, the summary of contributions for this thesis is drawn at first, followed by the suggestions for future work.

7.1 Summary of Contributions

Firstly, this thesis proposed a pre-processing algorithm, difference of Gaussian (DoG) enhanced local normalization algorithm, for lumbar ultrasound images. Ultrasound images generally suffer from low resolution, speckle noises and uneven brightness induced by wave attenuation problem, which negatively hampers the interpretability of ultrasound images. In order to solve the problem, the DoG algorithm was utilized to replace the unsharp masking procedure in the local normalization algorithm. The DoG enhanced local normalization algorithm is able to extract the key anatomical structures in the lumbar ultrasound image, remove the speckle noises, as well as eliminate the brightness variance problem encountered by ultrasound images. Compared with widely used ultrasound pre-processing algorithm, e.g., the median filter, Lees filter, anisotropic diffusion filter and wavelet filter etc, the proposed algorithm achieved better result in removing the speckle noise and getting higher PSNR value for the filtered images.

Secondly, this thesis improved the existing research work for computer

aided ultrasound image interpretation in the longitudinal view. Although there has been several researches conducted for the lumbar ultrasound image processing in the longitudinal view, they were either not fully automatic, required the external modification of probe, or required the operator to select the image frames for processing. In addition, one common problem faced by the existing researches is that they assume the sacrum being readily recognized by the operator, while neglect the importance of automatic identification with algorithm; therefore, introducing error in the starting point of spinous level counting. In this thesis, the sacrum is identified automatically with machine learning model. The level counting procedure started with sacrum searching, the continuous identification of which would initiate the panorama image stitching procedure. The image quality of the ultrasound stream is evaluated to determine the frames to be stitched on the panorama images, so as to remove the accidental out-of-line bad quality frames. The level dividing is realized by matching the spinous process template on the generated panorama image. Then the level counting information is imposed on the ultrasound stream in real-time as the probe is moved. Moreover, detailed guidance would be provided to anesthetists on how to move the probe, so as to locate the L3-L4 interspinous level efficiently. Therefore, the whole level counting procedure is fully automatic and realized in real-time, thus requiring the least ultrasound knowledge on the part of anesthetists.

Thirdly, as the first research for automatic lumbar ultrasound interpretation in the transverse view, this thesis proposed and developed two workable classifiers for interspinous image identification, with a high accuracy achieved for data collected from clinical IRB study. The purpose of transverse view scanning is to identify the interspinous region, i.e, position suitable for needle insertion. In order to differentiate the interspinous images (image suitable for needle insertion) and bone images (image not suitable for needle insertion), a cascading classifier was initially developed, which generalized the expert

knowledge in recognizing interspinous image. The cascading classifier is composed of four layers of weak classifiers and each weak classifier corresponds to one criterion for interspinous image recognition. It works in a cascading approach such that if the image cannot be confidently classified by a certain classifier then it will be passed to the next classifier, until it is classified with a high confidence level. With a proper selection of the four model parameters, the cascading classifier is able to classify the interspinous and bone images with a high accuracy. On the basis of the cascading classifier, in order to increase the robustness of the classification, a machine learning based classification algorithm is further proposed. The algorithm is consisted of feature extraction, feature selection and SVM training procedure. The important anatomical features, including epidural space, vertebra body and articular processes are extracted from the ultrasound images. Moreover, the proportion of black pixels along with midline is also extracted with midline detection. Feature selection is further employed to select the feature subset with optimal performance and decrease computation cost. Based on the features extracted from training samples and test samples, a SVM is used to classify the interspinous and bone images with maximal margin. The trained SVM model is further tested on the ultrasound video streams collected from pregnant patients, and successfully identifies the interspinous region / bone region on 45 out of the 46 videos collected. In addition, after the interspinous region is located, the epidural space, the space where the epidural needle will be placed, will be identified and measured automatically, providing a depth reference to anesthetists for the following needle insertion procedures.

Finally, as an effort to facilitate the application of the developed algorithms for anesthetists, a real-time image acquisition system and graphical user interface (GUI) are designed. The image acquisition system captures the real-time ultrasound stream from the ultrasound machine and feeds it to the computer for image processing, via a video capture card. The machine learning

based algorithm then processes the ultrasound stream, in both longitudinal view and transverse view, and presents the identification result on the GUI and provides detailed guidance to the anesthetists. The GUI simplify the usage of the developed algorithms by displaying the processing result in an intuitive and easily understandable approach; while the meticulous codes and algorithms are concealed in the background and remained a black-box for the anesthetists, therefore greatly facilitate the applicability of the algorithms for anesthetists. The developed image processing algorithms, together with the image acquisition system and GUI, enables the real-time image processing of the lumbar ultrasound images. An IRB study has been conducted to test the accuracy and applicability of the real-time image processing system on volunteers. The primary result on healthy volunteers shows that the system is able to identify the lumbar anatomical features accurately and locate the interspinous region correctly.

7.2 Suggestions for Future Work

The proposed image processing algorithms has been proved to be able to identify the lumbar anatomical structures and locate the interspinous region with high accuracy. User interface has also been designed to facilitate the usage of the algorithms for anesthetists. However, there are some limitations in this study and further research is required to overcome those limitations and extend the current research.

- The current research is based on ultrasound images and videos collected from limited number of volunteers and pregnant patients. Since the image processing procedure is based on machine learning algorithms, the expansion of the database will certainly increase the performance of the machine learning models. Future work can be done to collect lumbar ultrasound samples from more subjects with different demographic

features, i.e., body mass index, height and age etc., to establish a more comprehensive machine learning database.

- The real-time image processing system has currently been tested on healthy volunteers. Future study can be conducted to test the real-time system on patients in the clinical setting, to validate its applicability on clinical routine procedures.
- The current research realizes the automatic localization of needle insertion site. For a complete technical solution to the epidural needle insertion challenge, future research can be conducted to develop the mechanical system and control system that supports the epidural needle insertion procedure. Further research can also focus on providing guidance and real-time monitoring for the needle insertion procedure.
- As a meaningful extension to the current research, a training tool, which combines the ultrasound machine with lumbar spine mock-up, can be developed in the future to teach trainee anesthetists in learning how to read ultrasound images, as well as to locate the needle entry point with ultrasound.
- Current image processing algorithm is based on 2D lumbar ultrasound image. As 3D ultrasound is becoming a future trend for ultrasound research, future work can be conducted to extend the algorithms to 3D image processing.
- Extend the application of the machine learning based framework to other medical ultrasound applications, with the frameworks as shown on Fig 7.1. The modular framework used in this thesis can be easily extended to other medical ultrasound applications, given that training database of the specific anatomical ultrasound images is provided.

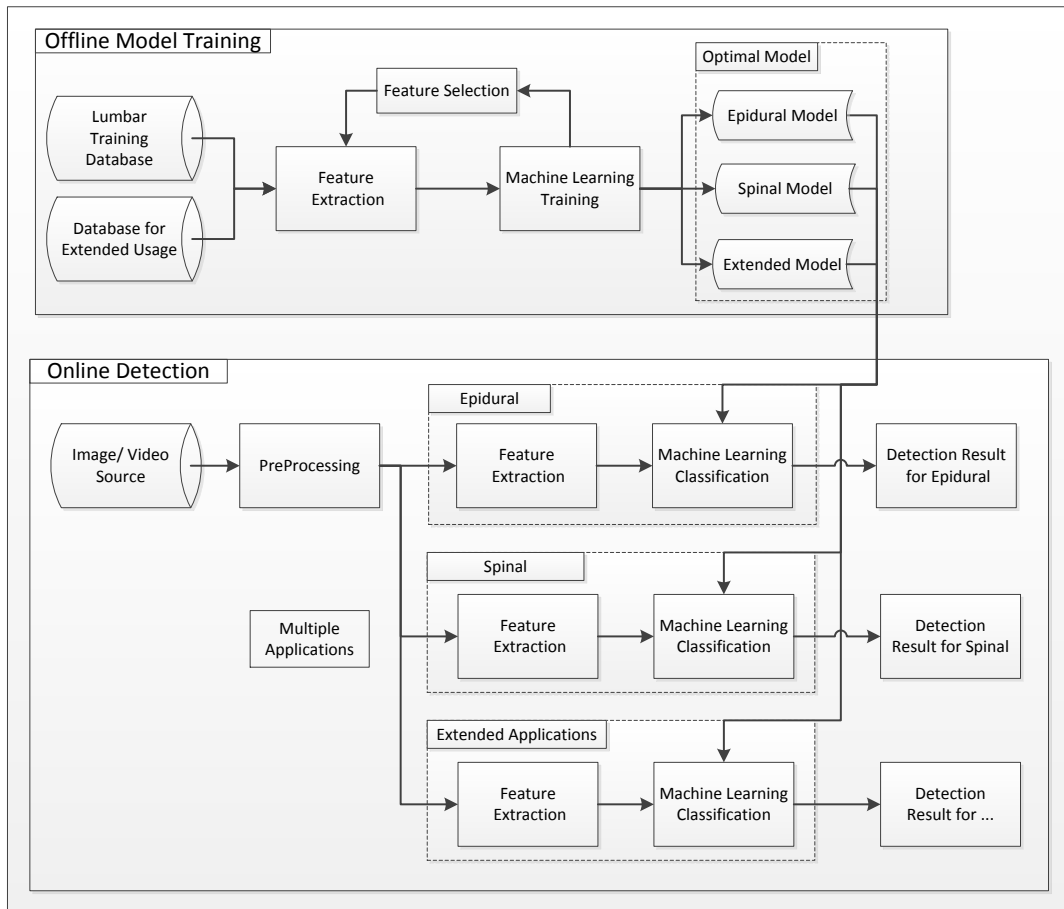


Figure 7.1: Framework of Machine Learning Based Ultrasound Image Identification Procedure

Bibliography

- [1] M. Osterman and J. Martin, “Epidural and spinal anesthesia use during labor: 27-state reporting area, 2008.” *National vital statistics reports*, vol. 59, no. 5, pp. 1–14, 2011.
- [2] N. E. Sharrock, S. B. Haas, M. J. Hargett, B. Urquhart, J. N. Insall, and G. Scuderi, “Effects of epidural anesthesia on the incidence of deep-vein thrombosis after total knee arthroplasty,” *Journal of Bone and Joint Surgery - Series A*, vol. 73, no. 4, pp. 502–506, 1991.
- [3] J. R. A. Rigg, K. Jamrozik, P. S. Myles, B. S. Silbert, P. J. Peyton, R. W. Parsons, and K. S. Collins, “Epidural anaesthesia and analgesia and outcome of major surgery: a randomised trial,” *Lancet*, vol. 359, pp. 1276–82, Apr. 2002.
- [4] J. Richardson, “Applied epidural anatomy,” *Continuing Education in Anaesthesia, Critical Care & Pain*, vol. 5, pp. 98–100, June 2005.
- [5] T. M. Halaszynski and M. W. Hartmannsgruber, “Anatomy and physiology of spinal and epidural anesthesia,” *Seminars in Anesthesia, Perioperative Medicine and Pain*, vol. 17, pp. 24–37, Mar. 1998.
- [6] N. a. Ebraheim, A. Hassan, M. Lee, and R. Xu, “Functional anatomy of the lumbar spine,” *Seminars in Pain Medicine*, vol. 2, pp. 131–137, Sept. 2004.
- [7] J. Andrés, M. A. Reina, and A. Prats, “Epidural space and regional

- anesthesia,” *European Journal of Pain Supplements*, vol. 3, pp. 55–63, Nov. 2009.
- [8] H. Ellis, “The anatomy of the epidural space,” *Anaesthesia & Intensive Care Medicine*, vol. 69, pp. 402–404, Nov. 2009.
- [9] M. Balki, “Locating the epidural space in obstetric patients-ultrasound a useful tool: continuing professional development.,” *Canadian journal of anaesthesia = Journal canadien d’anesthésie*, vol. 57, pp. 1111–26, Dec. 2010.
- [10] B. H. Meiklejohn, “Distance from skin to the lumbar epidural space in an obstetric population.,” *Regional anesthesia*, vol. 15, no. 3, pp. 134–6, 1983.
- [11] K. K. Ravi, T. K. Kaul, S. Kathuria, S. Gupta, and S. Khurana, “Distance from Skin to Epidural Space: Correlation with Body Mass Index (BMI).,” *Journal of anaesthesiology, clinical pharmacology*, vol. 27, pp. 39–42, Jan. 2011.
- [12] K. K. Srinivasan, M. Deighan, L. Crowley, and K. McKeating, “Spinal anaesthesia for caesarean section: an ultrasound comparison of two different landmark techniques.,” *International journal of obstetric anesthesia*, vol. 23, pp. 206–12, Aug. 2014.
- [13] P. Barash, *Handbook of clinical anesthesia*. Lippincott-Raven, 1997.
- [14] C. Konrad, G. Schupfer, M. Wietlisbach, and H. Gerber, “Learning Manual Skills in Anesthesiology: Is there a recommended number of cases for anesthetic procedures?,” *Anesthesia & Analgesia*, vol. 86, pp. 635–639, Mar. 1998.
- [15] D. L. Renfrew, T. E. Moore, M. H. Kathol, G. Y. El-Khoury, J. H. Lemke, and C. W. Walker, “Correct placement of epidural steroid injections:

- Fluoroscopic guidance and contrast administration,” *American Journal of Neuroradiology*, vol. 12, no. 5, pp. 1003–1007, 1991.
- [16] J. H. Levin, R. Wetzel, and M. W. Smuck, “The Importance of Image Guidance during Epidural Injections: Rates of Incorrect Needle Placement during Non-Image Guided Epidural Injections,” *Journal of Spine*, vol. 01, no. 02, pp. 2–4, 2012.
- [17] M. P. N. Lewis, P. Thomas, L. F. Wilson, and R. C. Mulholland, “The ‘whoosh’ test. A clinical test to confirm correct needle placement in caudal epidural injections,” *Anaesthesia*, vol. 47, no. 1, pp. 57–58, 1992.
- [18] P. Kumar and S. Francis, “Ultrasound-Guided Neuraxial Blocks : Recent Developments,” vol. 1, no. August, pp. 109–111, 2010.
- [19] J. Carvalho, “Ultrasound-facilitated epidurals and spinals in obstetrics,” *Anesthesiology clinics*, vol. 26, pp. 145–58, vii–viii, Mar. 2008.
- [20] O. a. Bamgbade, W. M. Khalaf, O. Ajai, R. Sharma, V. Chidambaram, and G. Madhavan, “Obstetric anaesthesia outcome in obese and non-obese parturients undergoing caesarean delivery: an observational study.,” *International journal of obstetric anaesthesia*, vol. 18, pp. 221–5, July 2009.
- [21] V. Faitot, R. Ourchane, S. Dahmani, M. Magheru, S. Nebout, F. Gomas, a. Katz, L. Salomon, and H. Keïta-Meyer, “An observational study of factors leading to difficulty in resident anaesthesiologists identifying the epidural space in obstetric patients.,” *International journal of obstetric anaesthesia*, vol. 20, pp. 124–7, Apr. 2011.
- [22] R. Whitty, M. Moore, and A. Macarthur, “Identification of the lumbar interspinous spaces: palpation versus ultrasound.,” *Anesthesia and analgesia*, vol. 106, pp. 538–40, table of contents, Feb. 2008.

- [23] T. Grau, R. W. Leipold, R. Conradi, E. Martin, and J. Motsch, “Efficacy of Ultrasound Epidural Anesthesia,” *Journal of clinical anesthesia*, vol. 8180, no. 01, pp. 169–175, 2002.
- [24] M. a. Peterson and J. Abele, “Bedside ultrasound for difficult lumbar puncture.,” *The Journal of emergency medicine*, vol. 28, pp. 197–200, Feb. 2005.
- [25] P. W. H. Peng and A. Rofaeel, “Using ultrasound in a case of difficult epidural needle placement.,” *Canadian journal of anaesthesia = Journal canadien d’anesthésie*, vol. 53, pp. 325–6, Mar. 2006.
- [26] R. Strony, “Ultrasound-assisted lumbar puncture in obese patients.,” *Critical care clinics*, vol. 26, pp. 661–4, Oct. 2010.
- [27] T. Grau, E. Bartusseck, R. Conradi, E. Martin, and J. Motsch, “Ultrasound imaging improves learning curves in obstetric epidural anesthesia: a preliminary study.,” *Canadian journal of anaesthesia = Journal canadien d’anesthésie*, vol. 50, pp. 1047–50, Dec. 2003.
- [28] M. C. Vallejo, a. L. Phelps, S. Singh, S. L. Orebaugh, and N. Sah, “Ultrasound decreases the failed labor epidural rate in resident trainees.,” *International journal of obstetric anesthesia*, vol. 19, pp. 373–8, Oct. 2010.
- [29] T. Grau, R. W. Leipold, J. Horter, R. Conradi, E. Martin, and J. Motsch, “The lumbar epidural space in pregnancy: visualization by ultrasonography.,” *British journal of anaesthesia*, vol. 86, pp. 798–804, June 2001.
- [30] J. A. Noble, N. Navab, and H. Becher, “Ultrasonic image analysis and image-guided interventions.,” *Interface focus*, vol. 1, pp. 673–85, Aug. 2011.

- [31] B. Kerby, S. Member, R. Rohling, V. Nair, and P. Abolmaesumi, “Automatic identification of lumbar level with ultrasound.,” *30th Annual International IEEE EMBS Conference*, vol. 2008, pp. 2980–3, Jan. 2008.
- [32] H. Al-Deen Ashab, V. a. Lessoway, S. Khallaghi, A. Cheng, R. Rohling, and P. Abolmaesumi, “An augmented reality system for epidural anesthesia (AREA): prepuncture identification of vertebrae.,” *IEEE transactions on biomedical engineering*, vol. 60, pp. 2636–44, Sept. 2013.
- [33] D. Tran and R. Rohling, “Automatic detection of lumbar anatomy in ultrasound images of human subjects,” *Biomedical Engineering, IEEE Transactions on*, vol. 57, no. 9, pp. 2248–2256, 2010.
- [34] C. Arzola, S. Davies, A. Rofaeel, and J. C. a. Carvalho, “Ultrasound using the transverse approach to the lumbar spine provides reliable landmarks for labor epidurals.,” *Anesthesia and analgesia*, vol. 104, pp. 1188–92, tables of contents, May 2007.
- [35] M. Balki, Y. Lee, S. Halpern, and J. C. a. Carvalho, “Ultrasound imaging of the lumbar spine in the transverse plane: the correlation between estimated and actual depth to the epidural space in obese parturients.,” *Anesthesia and analgesia*, vol. 108, pp. 1876–81, June 2009.
- [36] S. H. Contreras Ortiz, T. Chiu, and M. D. Fox, “Ultrasound image enhancement: A review,” *Biomedical Signal Processing and Control*, vol. 7, pp. 419–428, Sept. 2012.
- [37] J. A. N. Fernando L. Arbona, Babak Khabiri, “Introduction to Ultrasound,” in *Ultrasound-Guided Regional Anesthesia: A Practical Approach to Peripheral Nerve Blocks and Perineural Catheters* (J. A. N. Fernando L. Arbona, Babak Khabiri, ed.), ch. 2, pp. 10–23, New York: Cambridge University Press, 2010.

- [38] J. Lee, “Digital image enhancement and noise filtering by use of local statistics,” *Pattern Analysis and Machine Pattern Analysis and Machine Intelligence, IEEE Transactions on*, vol. PAMI-2, pp. 165–168, 1980.
- [39] J.-S. Lee, “Speckle analysis and smoothing of synthetic aperture radar images,” *Computer Graphics and Image Processing*, vol. 17, pp. 24–32, Sept. 1981.
- [40] D. T. Kuan, A. Sawchuk, T. C. Strand, and P. Chavel, “Adaptive restoration of images with speckle,” *Acoustics, Speech and Signal Processing, IEEE Transactions on*, vol. 35, no. 3, pp. 373 – 383, 1987.
- [41] D. Kuan and A. Sawchuk, “Adaptive noise smoothing filter for images with signal-dependent noise,” *Pattern Analysis and Machine Intelligence, IEEE Transactions on*, vol. PAMI-7, no. 2, pp. 165 – 177, 1985.
- [42] V. S. Frost, J. A. Stiles, K. S. Shanmugan, and J. C. Holtzman, “A model for radar images and its application to adaptive digital filtering of multiplicative noise.,” *IEEE transactions on pattern analysis and machine intelligence*, vol. 4, no. 2, pp. 157–166, 1982.
- [43] P. Perona and J. Malik, “Scale-space and edge detection using anisotropic diffusion,” *IEEE Transactions on Pattern Analysis and Machine Intelligence*, vol. 12, pp. 629–639, July 1990.
- [44] Y. Yu and S. T. Acton, “Speckle reducing anisotropic diffusion.,” *IEEE transactions on image processing : a publication of the IEEE Signal Processing Society*, vol. 11, pp. 1260–70, Jan. 2002.
- [45] M.-S. Lee, C.-L. Yen, and S.-K. Ueng, “Speckle reduction with edges preservation for ultrasound images: using function spaces approach,” *IET Image Processing*, vol. 6, no. 7, p. 813, 2012.

- [46] M. Swamy, M. Bhuiyan, and M. Ahmad, "Spatially adaptive thresholding in wavelet domain for despeckling of ultrasound images," *IET Image Processing*, vol. 3, pp. 147–162, June 2009.
- [47] R. Vanithamani and G. Umamaheswari, "Wavelet based despeckling of medical ultrasound images with bilateral filter," in *IEEE Region 10 Annual International Conference, Proceedings/TENCON*, pp. 389–393, Ieee, Nov. 2011.
- [48] O. V. Michailovich and A. Tannenbaum, "Despeckling of medical ultrasound images.," *IEEE transactions on ultrasonics, ferroelectrics, and frequency control*, vol. 53, pp. 64–78, Jan. 2006.
- [49] M. Alexander, R. Baumgartner, a.R. Summers, C. Windischberger, M. Klarhoefer, E. Moser, and R. Somorjai, "A wavelet-based method for improving signal-to-noise ratio and contrast in MR images," *Magnetic Resonance Imaging*, vol. 18, pp. 169–180, Feb. 2000.
- [50] W. J. Veldkamp and N. Karssemeijer, "Normalization of local contrast in mammograms.," *IEEE transactions on medical imaging*, vol. 19, pp. 731–8, July 2000.
- [51] M. Foracchia, E. Grisan, and A. Ruggeri, "Luminosity and contrast normalization in retinal images.," *Medical image analysis*, vol. 9, pp. 179–90, June 2005.
- [52] a.D. Fleming, S. Philip, K. Goatman, J. Olson, and P. Sharp, "Automated microaneurysm detection using local contrast normalization and local vessel detection," *IEEE Transactions on Medical Imaging*, vol. 25, pp. 1223–1232, Sept. 2006.
- [53] N. Halyo, Z.-u. Rahman, and S. Park, "Information content in nonlinear local normalization processing of digital images," *Proceedings of SPIE -*

- the International Society for Optical Engineering*, vol. 4388, pp. 129–142, 2001.
- [54] E. Nadernejad and M. Karami, “Despeckle filtering in medical ultrasound imaging,” *Contemporary Engineering Sciences*, vol. 2, no. 1, pp. 17–36, 2009.
- [55] M. J. Paech, R. Godkin, and S. Webster, “Complications of obstetric epidural analgesia and anaesthesia: a prospective analysis of 10,995 cases.,” *International journal of obstetric anaesthesia*, vol. 7, pp. 5–11, Jan. 1998.
- [56] G. Furness, M. Reilly, and S. Kuchi, “An evaluation of ultrasound imaging for identification of lumbar intervertebral level,” *Anaesthesia*, vol. 57, pp. 277–280, Mar. 2002.
- [57] E. H. Ellinas, D. C. Eastwood, S. N. Patel, A. M. Maitra-D’Cruze, and T. J. Ebert, “The effect of obesity on neuraxial technique difficulty in pregnant patients: a prospective, observational study.,” *Anesthesia and analgesia*, vol. 109, pp. 1225–31, Oct. 2009.
- [58] P. Ecimovic and J. P. R. Loughrey, “Ultrasound in obstetric anaesthesia: a review of current applications.,” *International journal of obstetric anaesthesia*, vol. 19, pp. 320–6, July 2010.
- [59] H. Rafii-Tari, P. Abolmaesumi, and R. Rohling, “Panorama ultrasound for guiding epidural anesthesia: A feasibility study,” *Information Processing in Computer-Assisted Interventions*, vol. 6689, pp. 179–189, 2011.
- [60] R. Szeliski, “Image alignment and stitching: A tutorial,” *Foundations and Trends in Computer Graphics and Vision*, vol. 2, no. 1, pp. 1–104, 2006.
- [61] Y. Lee, M. Tanaka, and J. C. A. Carvalho, “Sonoanatomy of the lumbar spine in patients with previous unintentional dural punctures during labor

- epidurals.,” *Regional anesthesia and pain medicine*, vol. 33, pp. 266–70, Jan. 2008.
- [62] P. V. Balint and R. D. Sturrock, “Intraobserver repeatability and interobserver reproducibility in musculoskeletal ultrasound imaging measurements,” *Clinical and Experimental Rheumatology*, vol. 19, pp. 89–92, Jan. 2001.
- [63] S. Yu, K. K. Tan, C. Shen, and A. T. H. Sia, “Ultrasound guided automatic localization of needle insertion site for epidural anesthesia,” in *2013 IEEE International Conference on Mechatronics and Automation, IEEE ICMA 2013*, pp. 985–990, 2013.
- [64] S. Yu, K. K. Tan, C. Shen, and A. T. H. Sia, “Development of an ultrasound image processing approach to enable automated needle localisation for epidural anesthesia,” *Int. J. of Mechatronics and Automation*, vol. 4, no. 2, pp. 137 – 146, 2014.
- [65] H. Müller, N. Michoux, D. Bandon, and A. Geissbuhler, “A review of content-based image retrieval systems in medical applications-clinical benefits and future directions,” *International journal of medical informatics*, vol. 73, pp. 1–23, 2004.
- [66] J. Yao and R. M. Summers, *Machine Learning in Computer-Aided Diagnosis*. IGI Global, 2012.
- [67] D. Brain and G. I. Webb, “On The Effect of Data Set Size on Bias And Variance in Classification Learning,” *Proceedings of the Fourth Australian Knowledge Acquisition Workshop (AKAW '99)*, pp. 117–128, 1999.
- [68] M. Sordo and Q. Zeng, “On Sample Size and Classification Accuracy: A Performance Comparison.,” *Lect Notes Comput Sc*, vol. 3745, pp. 193–201, 2005.

- [69] J. Denzler and H. Niemann, “Evaluation The Performance Of Active contour Models For Real Time Object Tracking,” *Asian Conference on Computer Vision*, vol. 2, no. Informatik 5, 1995.
- [70] S. K. Palmer, S. E. Abram, A. M. Maitra, and J. H. von Colditz, “Distance from the skin to the lumbar epidural space in an obstetric population.,” *Anesthesia and analgesia*, vol. 62, no. 10, pp. 944–946, 1983.
- [71] S. Yu, K. K. Tan, B. L. Sng, S. Li, and A. T. H. Sia, “Automatic Identification of Needle Insertion Site in Epidural Anesthesia with a Cascading Classifier,” *Ultrasound in Medicine and Biology*, vol. 40, no. 9, pp. 1980–1990, 2014.
- [72] M. Hall, *Correlation-based feature selection for machine learning*. PhD thesis, The University of Waikato, 1999.
- [73] Y. Liu and Y. F. Zheng, “FS_SFS: A novel feature selection method for support vector machines,” *Pattern Recognition*, vol. 39, pp. 1333–1345, July 2006.
- [74] N. Cristianini and J. Shawe-Taylor, *An Introduction to Support Vector Machines and Other Kernel-based Learning Methods*. Cambridge University Press, 2000.
- [75] D. M. Powers, “Evaluation: from Precision, Recall and F-measure to ROC, Informedness, Markedness and Correlation,” Dec. 2011.
- [76] J. Davis and M. Goadrich, “The relationship between Precision-Recall and ROC curves,” in *Proceedings of the 23rd international conference on Machine learning - ICML '06*, (New York, New York, USA), pp. 233–240, ACM Press, June 2006.
- [77] T. Oliphant, *A guide to NumPy*. USA: Trelgol Publishing, 2006.

- [78] G. Bradski and A. Kaehler, *Learning OpenCV: Computer vision with the OpenCV library*. 2008.
- [79] F. Pedregosa and G. Varoquaux, “Scikit-learn: Machine learning in Python,” *The Journal of Machine Learning Research*, vol. 12, pp. 2825–2830, 2011.
- [80] D. Tran, A. a. Kamani, E. Al-Attas, V. a. Lessoway, S. Massey, and R. N. Rohling, “Single-operator real-time ultrasound-guidance to aim and insert a lumbar epidural needle.,” *Canadian journal of anaesthesia = Journal canadien d’anesthesie*, pp. 313–321, Jan. 2010.
- [81] P. N. Brett, T. J. Parker, a. J. Harrison, T. a. Thomas, and a. Carr, “Simulation of resistance forces acting on surgical needles,” *Proceedings of the Institution of Mechanical Engineers, Part H: Journal of Engineering in Medicine*, vol. 211, pp. 335–347, Apr. 1997.

List of Publications

Journals Papers

1. **Shuang Yu**, Kok Kiong Tan, Ban Leong Sng, Shengjin Li, Alex Tiong Heng Sia, Automatic Identification of Needle Insertion Site in Epidural Anesthesia with a Cascading Classifier, *Ultrasound in Medicine & Biology*, 2014, 40(9), 1980-1990.
2. **Shuang Yu**, Kok Kiong Tan, Chengyao Shen, Alex TH Sia, Development of an ultrasound image processing approach to enable automated needle localization for epidural anesthesia, *International Journal of Mechatronics & Automation*, 2014, 4(2), 137-146.
3. **Shuang Yu**, Kok Kiong Tan, Ban Leong Sng, Shengjin Li, Alex Tiong Heng Sia, Lumbar Ultrasound Image Feature Extraction and Classification with Support Vector Machine, *Ultrasound in Medicine & Biology*, 2015, 41(5), 2677-2689.

Conference Papers

1. **Shuang Yu**, Kok Kiong Tan, Ban Leong Sng, Shengjin Li, Alex TH Sia, Feature Extraction and Classification for Ultrasound Images of Lumbar Spine with Support Vector Machine, Annual International Conference of the IEEE Engineering in Medicine and Biology Society (EMBC 2014), pp.4659-4662.

2. **Shuang Yu**, Kok Kiong Tan, Classification of Lumbar Ultrasound Images with Machine Learning, The 10th International Conference on Simulated Evolution and Learning (SEAL 2014), 287-298.
3. **Shuang Yu**, Kok Kiong Tan, Chengyao Shen, Alex TH Sia, Ultrasound Guided Automatic Localization of Needle Insertion Site for Epidural Anesthesia, Proceedings of 2013 IEEE International Conference on Mechatronics and Automation, 2013, 985-990.
4. **Shuang Yu**, Kok Kiong Tan, Ban Leong Sng, Shengjin Li, Alex Tiong Heng Sia, Real-time Automatic Spinal Level Identification with Ultrasound Image Processing, International Symposium on Biomedical Imaging 2015, 243-246

Appendices

Appendix A

Protocol for Real-time Volunteer Study

A.1 Computer Software Setup:

Install the necessary software package and driver on computer to ensure that the program can work properly.

- (1). PyCharm: Python integrated development environment

<https://www.jetbrains.com/pycharm/download/>

- (2). Anaconda: Python library package for data analysis and engineering

<http://continuum.io/downloads>

- (3). OpenCV for Python: image processing library

<http://www.lfd.uci.edu/~gohlke/pythonlibs/>

- (4). DVI2USB Video Capture Card Driver

<http://www.epiphan.com/products/dvi2usb-3-0/downloads/>

A.2 Hardware Preparation

- (1). Make sure that the ultrasound machine is equipped with the **2MHz curved probe**; otherwise, change the probe to curved probe. Connect the ultrasound machine to power supply and start the ultrasound machine. **Tune**

the scanning depth to 7.3cm (default) or 9.1cm.



(2). Connect one end of the video capture card to the VGA (or DVI) output port of the ultrasound machine, and then connect the other end to the computer USB port.

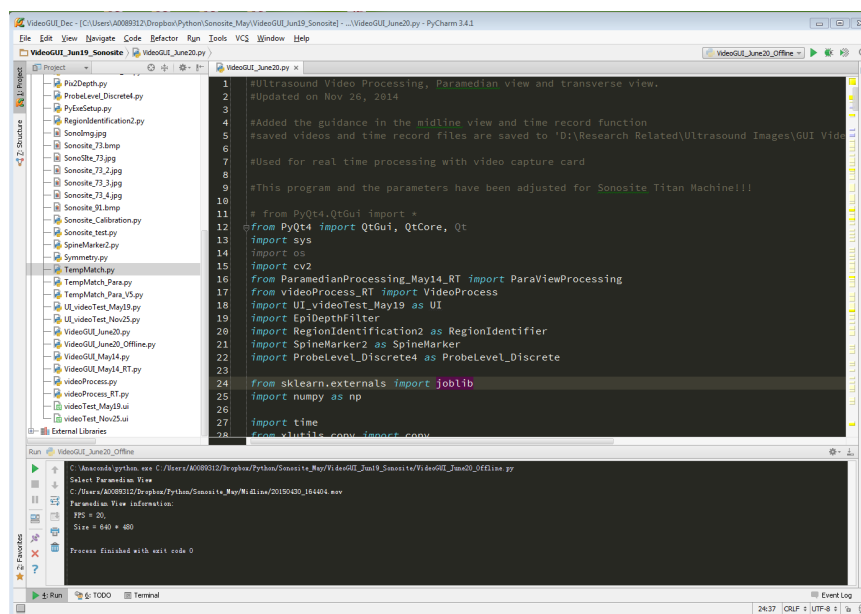


(3). Check whether the video capture card now flashes GREEN light. If it is RED light, then pull out the USB connector and reconnect again or repeat step (2). If GREEN light of the video capture card is on, then double click on the '**Epiphan Caputure Tool**' icon on the desktop to check whether the ultrasound image appears properly on the main window. If the

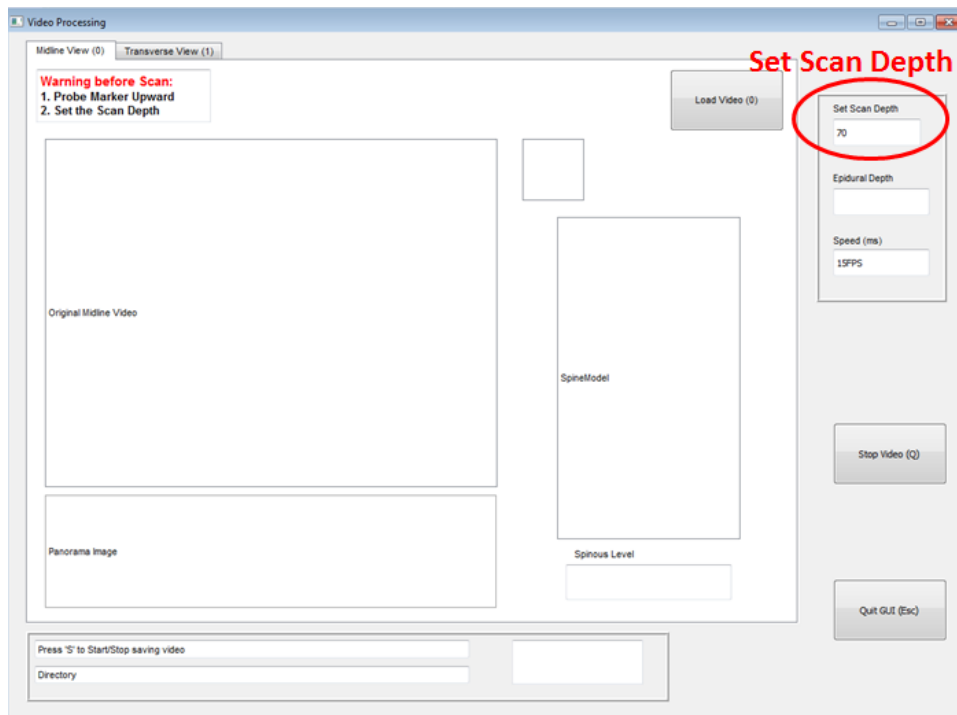
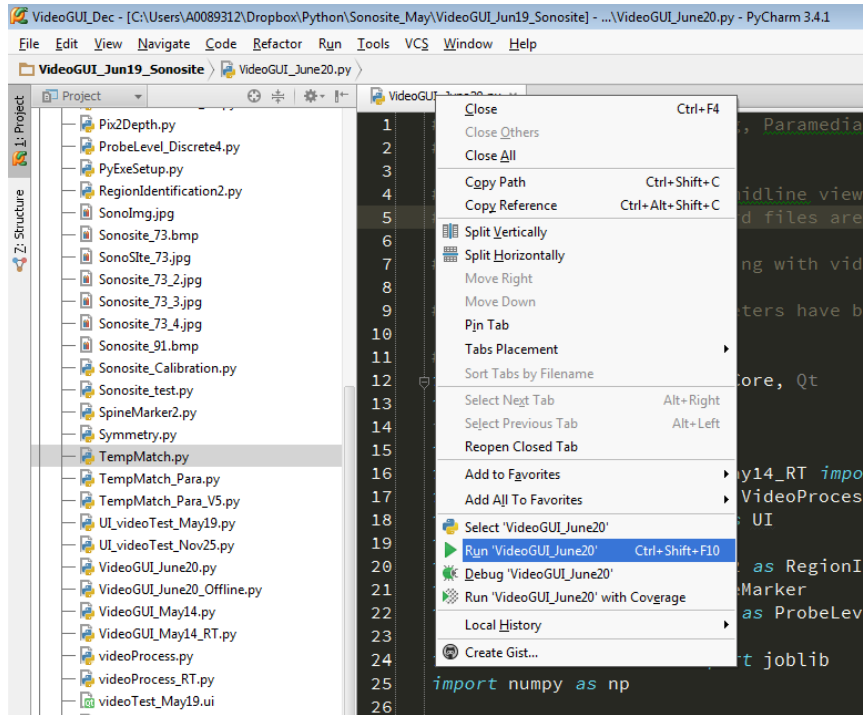
ultrasound video frames are captured properly, then close the window and continue with following steps. Otherwise, check if the video capture card is properly connected.



(4). Start the computer and load the PyCharm program by double clicking of the ‘PyCharm’ icon on the desktop.



(5). Open the VideoGUI project on the PyCharm program. Load the ‘VideoGUI.py’ (or ‘VideoGUIJune20.py’) file on the IDE. Then right click on the tab and choose ‘Run VideoGUI’. The user interface will then appear. Set the scanning depth the same as the depth set in ultrasound machine (eg: ultrasound machine set as 7.3 cm, fill 73 on the user interface. The default is 73).



A.3 Volunteer Preparation

- (1). Ask the volunteer to sit on the chair, **facing the computer screen**, so that operator can see the computer interface while scanning.

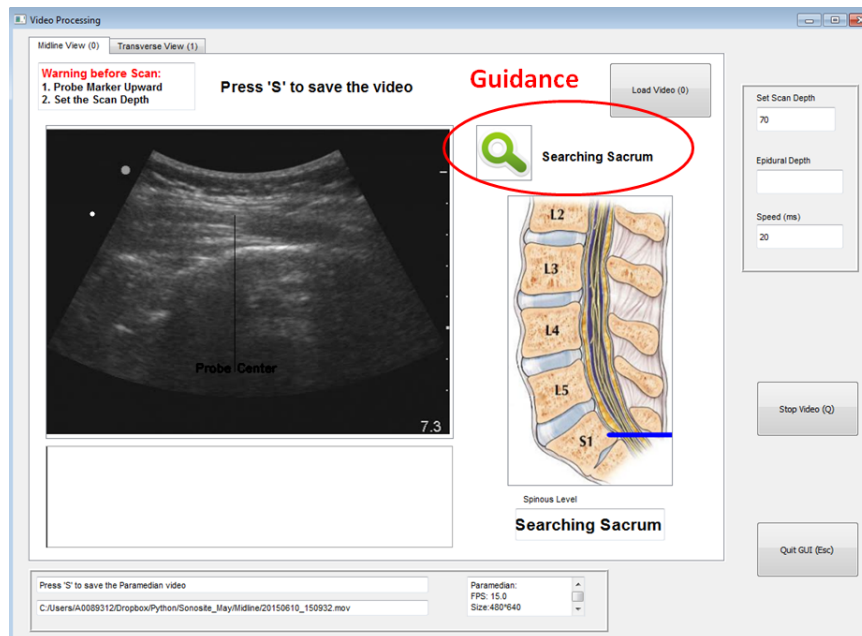
(2). Ask the volunteer to **bend forward**. However, if the volunteer is thin, ask them to keep their back straight.

A.4 Longitudinal View Scanning

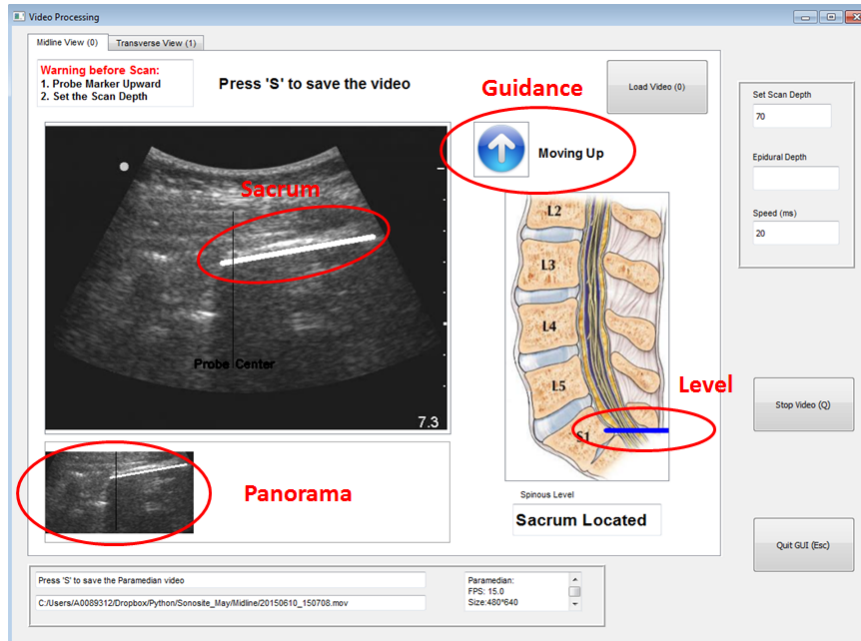
(1). Hold the probe in the midline view, with **marker facing upward**.

(2). **Press the keyboard '0' or click on the 'Load Video' button** on the 'Midline' tab, to start video processing in the midline view.

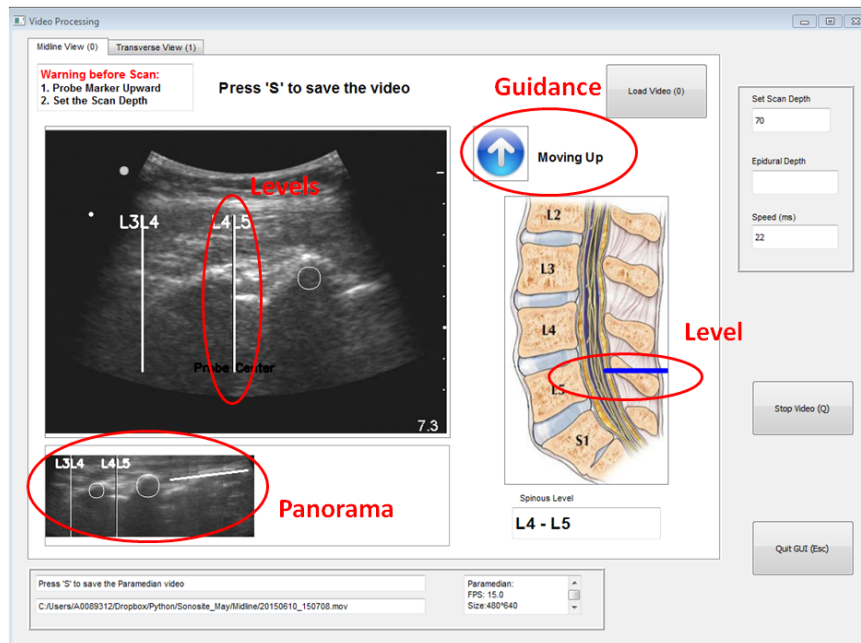
(3). **Place the probe near sacrum area** and checking on the computer interface to see whether the sacrum has been identified.



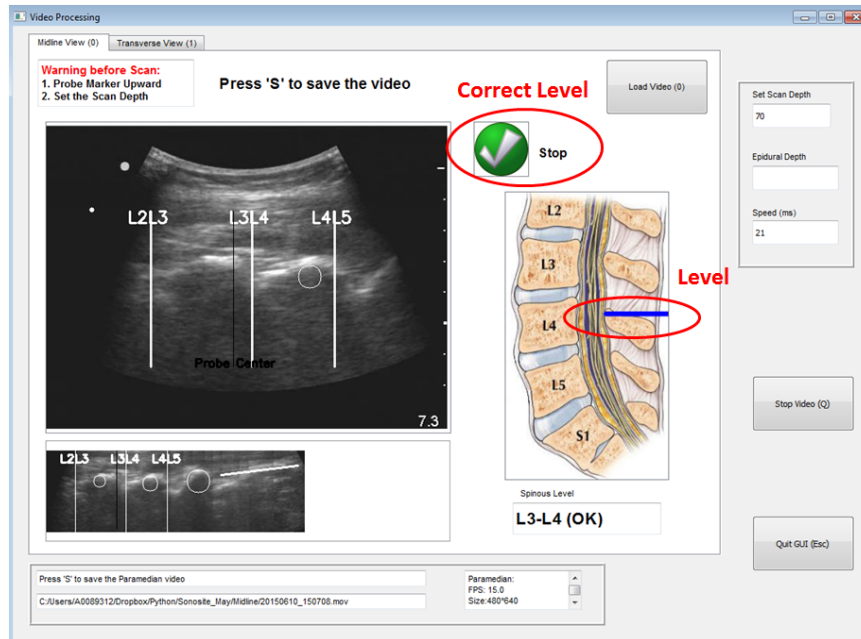
(4). If sacrum is identified by the algorithm continuously and the guidance sign has changed to 'moving up', then move the probe upward constantly along the midline. **NOTICE: CANNOT moving backward once the user interface shows the sign of 'moving up'**; If moving backward is required in case of improper scan position, please press '0' to start all over from sacrum again.



(5). Keep moving the probe upward constantly, the L4L5, L3L4 and L2L3 level will be shown on the screen. Move the L3L4 level to align with the probe center, the black reference line.

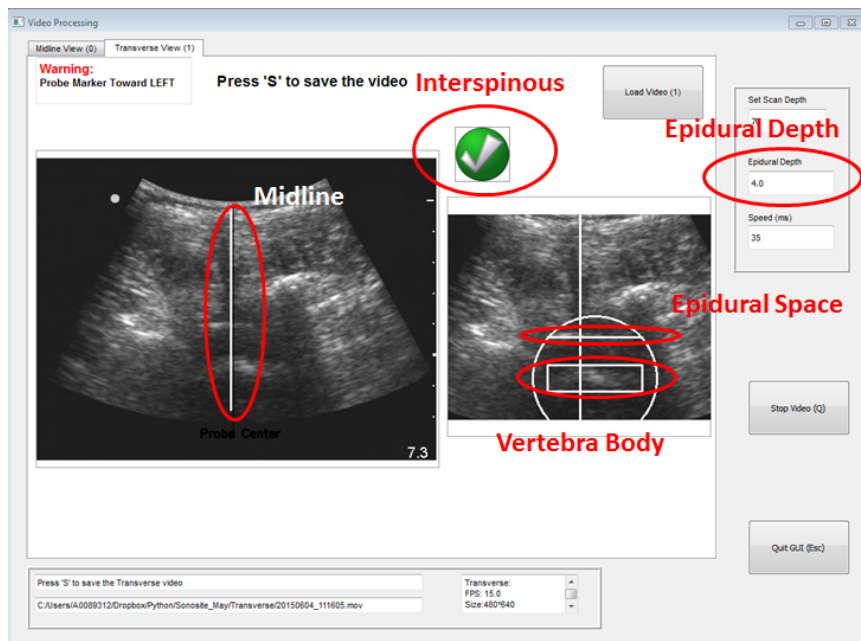
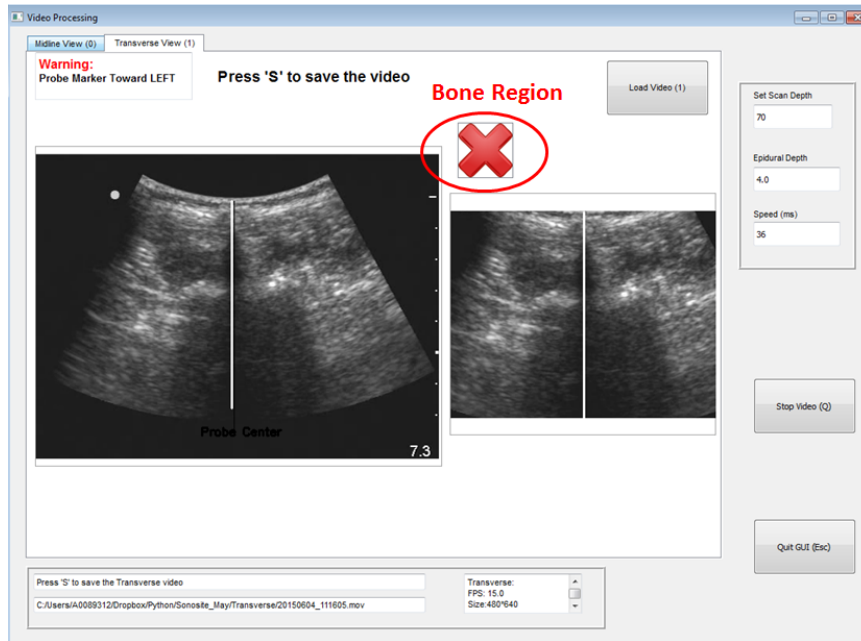


(6). If the 'Right' sign appears, stop scanning and turn the probe to the transverse view along the probe center.



A.5 Transverse View Scanning

- (1). Turn the probe in the transverse view, with **marker leftward**.
- (2). Press keyboard **'1'** or click on the **'Load Video'** button on the **'Transverse'** tab, to start video processing in the transverse view.
- (3). Slightly move the probe upward or downward to search for the interspinous region. The computer interface will show a red cross if the region is identified as bone region and a green checkmark if the region is identified as interspinous region.



(4). In the bone region, align the identified midline with the probe center, the black reference line (because the midline identification is more accurate in the bone region).

(5). Slightly tune the probe until the **green checkmark** appears **constantly without flashing**.

Appendix B

IRB Approval for Ultrasound Image Collection

CIRB Ref: **2013/318/D**

13 June 2013

Dr Sng Ban Leong
Department of Women's Anaesthesia
KK Women's and Children's Hospital

Dear Dr Sng

SINGHEALTH CENTRALISED INSTITUTIONAL REVIEW BOARD (CIRB) APPROVAL

Study Title: Ultrasound Imaging Guided Automatic Localization of Needle Insertion Site for Epidural Anaesthesia with Computer Programming System

We are pleased to inform you that the SingHealth CIRB D has approved the above research project to be conducted in KK Women's and Children's Hospital.

The documents reviewed are:

- a) CIRB / DSRB Application Form received on 31 May 2013
- b) Participant Information Sheet and Consent Form: Version 2 dated 31 May 2013
- c) Data Collection Form

The SingHealth CIRB operates in accordance with the ICH/ Singapore Guideline for Good Clinical Practices, and with the applicable regulatory requirement(s).

The approval period is from **13 June 2013 to 16 May 2014**. The reference number for this study is CIRB Ref: 2013/318/D. Please use this reference number for all future correspondence.

PATIENTS. AT THE HEART OF ALL WE DO.®

Members of the SingHealth Group
Singapore General Hospital • KK Women's and Children's Hospital
National Cancer Centre Singapore • National Dental Centre Singapore • National Heart Centre Singapore • National Neuroscience Institute • Singapore National Eye Centre
SingHealth Polyclinics • Bright Vision Hospital

The following are to be observed upon CIRB Approval:

1. No subject should be admitted to the trial before the Health Sciences Authority issues the Clinical Trial Certificate. (only applicable for drug-related studies).
2. The Principal Investigator should ensure that this study is conducted in compliance with the Singapore Guideline for Good Clinical Practice, the ethical guidelines of which are applicable to all studies to be carried out, and to ensure that the study is carried out in accordance to the guidelines and the submitted protocol. The Principal Investigator should meet with his collaborator(s) regularly to assess the progress of the study, and be familiar and comply with all applicable research policies in the Institution.
3. No deviation from, or changes of, the protocol should be initiated without prior written CIRB approval of an appropriate amendment, except when necessary to eliminate immediate hazards to the subjects or when the change(s) involve(s) only logistical or administrative aspects of the trial (e.g. change of monitor(s), telephone number(s)).
4. Only the approved Patient Information Sheet and Consent Form should be used. It must be signed by each subject prior to enrolling in the study and initiation of any protocol procedures. Two copies of the Informed Consent Form should be signed and dated. Each subject or the subject's legally accepted representative should be given a copy of the signed consent form. The remaining copy should be kept by the PI / medical record.
5. The Principal Investigator should report promptly to the SingHealth CIRB of:
 - i. Deviations from, or changes to the protocol including those made to eliminate immediate hazards to the trial subjects.
 - ii. Changes increasing the risk to subjects and/or affecting significantly the conduct of the trial.
 - iii. All serious adverse events (SAEs) and adverse drug reaction (ADRs) that are both serious and unexpected.
 - iv. New information that may affect adversely the safety of the subjects or the conduct of the trial.
 - v. Completion of the study.
6. Study Status Report should be submitted to the SingHealth CIRB for the following:
 - i. Annual review: Status of the study should be reported to the CIRB at least annually using the Study Status Report.
 - ii. Study renewal: the Study Status Report is to be submitted at least one month prior to the expiry of the approval period. A valid CIRB renewal is essential, as any research performed outside of an approved time frame is not legal, and thus not covered by the hospital's research insurance in case of unexpected adverse reactions.
 - iii. Study completion or termination: the Final Report is to be submitted within three months of study completion or termination.

Yours sincerely,



Dr Steve Yang
Chairman
SingHealth Centralised Institutional Review Board D

Enc.

Cc: Institution Representative, KKH
Head, Department of Women's Anaesthesia, KKH

Appendix C

Informed Consent Form for Ultrasound Data Collection

PARTICIPANT INFORMATION SHEET

Dear Mdm,

You are being invited to participate in a research study.

Before you take part in this research study, the study must be explained to you and you must be given the chance to ask questions. Please read carefully the information provided here. If you agree to participate, please sign the informed consent form. You will be given a copy of this document to take home with you.

STUDY INFORMATION

Protocol Title:

Ultrasound Imaging Guided Automatic Localization of Needle Insertion Site for Epidural Anaesthesia with Computer Programming System

Principal Investigator:

Dr Sng Ban Leong

Department of Women's Anaesthesia, KKH

Phone: 63941081 Fax: 62912661

Co-Investigators:

Dr Tan Kok Kiong, Department of Electrical and Computer Engineering, NUS

Ms Yu Shuang, Department of Electrical and Computer Engineering, NUS

Ms Li Shengjin, Duke-NUS GMS Singapore

PURPOSE OF THE RESEARCH STUDY

You are being invited to participate in this research study as you are undergoing a Caesarean section under spinal anaesthesia (local anaesthetics injected into your spinal area to numb the lower part of your body) containing routine spinal morphine (strong pain killer for pain relief after surgery).

This study is to test the effectiveness of using ultrasound to automatically identify a needle insertion site for spinal/ epidural anaesthesia before caesarean section. A computer image processing system is developed to automatically process the images when the ultrasound probe scans on the lumbar spine. Based on the processing result of ultrasound images, the system will provide guidance to the anaesthetists on which direction to move the probe, until best insertion site is reached. Therefore, the efficiency and success rate of spinal/ epidural anaesthesia will be improved by the proposed system.

This study will recruit 150 respondents from KK Hospital over a period of 2 years between June 2013 to May 2015.

STUDY PROCEDURES AND VISIT SCHEDULE

If you agree to take part in this study, you will be assessed on your eligibility for this study and some general medical information. The general medication information will include

demographic, surgical and obstetric information. This is performed in a comfortable environment in the privacy of the pre-anaesthesia clinic and general ward.

In addition to standardized regimen for spinal anaesthesia, anaesthetists will use ultrasound machine to scan your spine immediately before the spinal anaesthesia procedure. This scanning is to obtain images of the anatomical structure of the spinal bones for study purpose. The images will be used to search for a needle insertion site. The scanning process takes about 2 minutes. The image obtained will be stored in authorized computer for image processing. Only the Principal and Co-Investigators would have access to your image results. No tests other than those authorized in the signed consent will be performed on your image unless further consent is given. We will protect the confidentiality of the data by assigning them a specific code. Your ultrasound image will not be specifically identified but a code will link you to the sample. Decoding can only be performed by the Principal or Co-investigators. Image will be kept at KK Hospital for a period of 2 years after completion of the study. All the images will be destroyed at the end of 2 years.

Schedule of visits and procedures:

There are no additional visits or procedures for this study.

YOUR RESPONSIBILITIES IN THE STUDY

If you agree to take part in this study, a written consent will be obtained from you. If there are any queries, the investigators will be happy to answer any questions. There is no follow-up in the outpatient clinic.

WITHDRAWAL FROM STUDY

You are free to withdraw your consent and discontinue your participation at any time without prejudice to you or effect on your medical care. This ultrasound scanning has no impact on your surgery or ward management.

WHAT IS NOT STANDARD CARE OR EXPERIMENTAL IN THIS STUDY

This study is being conducted because there is a potential to increase the efficiency of spinal/epidural needle insertion by increasing the interpretability of ultrasound images with computer image processing algorithm. The system will alleviate the need for anaesthetists to interpret noisy ultrasound images in real time, meanwhile enabling them to perform other anaesthesia related tasks and procedures. We hope that your participation will help us to improve the computer image processing algorithm.

Although spinal anaesthesia is a commonly performed anaesthetic technique for caesarean section, this ultrasound scanning before needle insertion is undertaken for the purposes of research and not part of standard care.

POSSIBLE RISKS, DISCOMFORTS AND INCONVENIENCES

A scanning procedure is added to the standard regimen, which will take an additional 2 minutes. Other than this, there are no added risk and discomforts associated with this study. We appreciate your effort in participating in this study and we apologise for any inconvenience of your time.

POTENTIAL BENEFITS

There is no assurance you will benefit from this study. However, your participation may contribute to the improvement of ultrasound imaging interpretation and help with future real

time ultrasound imaging guidance system development.

ALTERNATIVES

The alternative will be to not take part in this study. If you are not participating in this study, spinal anaesthesia will be done under standard regimen and no additional time is taken for scanning. However, in case of difficult localization of needle insertion site, it might take more attempts if ultrasound machine is not used before attempts.

SUBJECT'S RIGHTS

Your participation in this study is entirely voluntary. Your questions will be answered clearly and to your satisfaction.

By signing and participating in the survey, you do not waive any of your legal rights to revoke your consent and withdraw from the survey at any time.

CONFIDENTIALITY OF STUDY AND MEDICAL RECORDS

Information collected for this study will be kept confidential. Your records, to the extent of the applicable laws and regulations, will not be made publicly available. Only your Investigators will have access to the confidential information being collected.

However, Regulatory Agencies, Institution Review Board and Ministry of Health will be granted direct access to your original medical records to check study procedures and data, without making any of your information public. By signing the Informed Consent Form attached, you or your legal representative is authorizing such access to your study and medical records.

Data collected and entered into the Data Collection Forms are the property of KK Hospital. In the event of any publication regarding this study, your identity will remain confidential.

COSTS OF PARTICIPATION

There will be no additional charges.

RESEARCH RELATED INJURY AND COMPENSATION

The Hospital does not make any provisions to compensate trial subjects for research related injury. However, compensation may be considered on a case-by-case basis for unexpected injuries due to non-negligent causes.

By signing this consent form, you will not waive any of your legal rights or release the parties involved in this study from liability for negligence.

WHO TO CONTACT IF YOU HAVE QUESTIONS

If you have questions about this research study and your rights or in the case of any injuries during the course of this study, you may contact the investigators Dr Sng Ban Leong of the Department of Women's Anaesthesia (office telephone 63941081 or after office hours 62934044) of KK Hospital or Prof Tan Kok Kiong or Yu Shuang (office telephone 65164460).

If you have questions about the study or your rights as a participant, you can call the SingHealth Centralised Institutional Review Board, which is the committee that reviewed and approved this study, the telephone number is 6323 7515 during office hours (8:30 am to 5:30pm).

CONSENT BY RESEARCH SUBJECT

Details of Research Study

Protocol Title:

Ultrasound Imaging Guided Automatic Localization of Needle Insertion Site for Epidural Anaesthesia with Computer Programming System

Principal Investigator:

Dr Sng Ban Leong

Department of Women's Anaesthesia, KK Women's and Children's Hospital

63941081, 62934044

Subject's Particulars

Name: _____

NRIC No.: _____

Address: _____

Sex: Female

Date of birth _____

dd/mm/yyyy

Race: Chinese/ Malay/ Indian /Others (please specify) _____

Part I

I, _____ (NRIC/Passport No. _____)
(Name of patient)

agree to participate in the research study as described and on the terms set out in the Patient Information Sheet. The nature of my participation in the proposed research study has been explained to me in

_____ by Dr/Mr/Ms _____
(Language / Dialect) (Name of healthcare worker)

I have fully discussed and understood the purpose and procedures of this study. I have been given the Participant Information Sheet and the opportunity to ask questions about this study and have received satisfactory answers and information.

I understand that my participation is voluntary and that I am free to withdraw at any time, without giving any reasons and without my medical care being affected.

I also give permission for information in my medical records to be used for research. In any event of publication, I understand that this information will not bear my name or other identifiers and that due care will be taken to preserve the confidentiality of this information.

[Signature/Thumbprint (Right / Left) of participant]

(Date of signing)

Part II – to be filled by parent / legal guardian / legal representative, where applicable

I, _____ hereby give consent for the above participant to participate in
(parent / legal guardian)
the proposed research study. The nature, risks and benefits of the study have been explained
clearly to me and I fully understand them.

[Signature/Thumbprint (Right / Left) of parent /legal guardian]

(Date of signing)

Part III – to be filled witness, where applicable

An impartial witness should be present during the entire informed consent discussion if a subject or the subject's legally acceptable representative is unable to read. After the written informed consent form and any written information to be provided to subjects, is read and explained to the subject or the subject's legally acceptable representative, and after the subject or the subject's legally representative has orally consented to the subject's participation in the study and, if capable of doing so, has signed and personally dated the consent form, the witness should sign and personally date the consent form.

Witnessed by: _____
(Name of witness)

(Designation of witness)

(Signature of witness)

(Date of signing)

Part IV– Investigator's Statement

I, the undersigned, certify to the best of my knowledge that the patient/patient's legally acceptable representative signing this informed consent form had the study fully explained and clearly understands the nature, risks and benefits of his/her / his ward's / her ward's participation in the study.

Name of Investigator

Signature

Date

Appendix D

IRB Approval for Real-time Volunteer Study

CIRB Ref: **2015/2513**

19 June 2015

Dr Sng Ban Leong
Department of Women's Anaesthesiology
KK Women's and Children's Hospital

Dear Dr Sng

SINGHEALTH CENTRALISED INSTITUTIONAL REVIEW BOARD (CIRB) APPROVAL

Protocol Title: Automatic Spinal Landmarks Identification with Real-time Ultrasound Image Processing System for Healthy Volunteers

We are pleased to inform you that the SingHealth CIRB D has approved the above research project to be conducted in KK Women's and Children's Hospital.

The documents reviewed are:

- a) CIRB Application Form dated 10 June 2015
- b) Participant Information Sheet and Consent Form: Version 2 dated 05 June 2015
- c) Data Collection Form: Version 1 dated 18 May 2015

The SingHealth CIRB operates in accordance with the ICH/ Singapore Guideline for Good Clinical Practices, and with the applicable regulatory requirement(s).

The approval period is from **19 June 2015 to 18 June 2016**. The reference number for this study is CIRB Ref: 2015/2513 Please use this reference number for all future correspondence.

The following are to be observed upon SingHealth CIRB Approval:

1. No subject should be admitted to the trial before the Health Sciences Authority issues the Clinical Trial Certificate. (only applicable for drug-related studies).
2. The Principal Investigator should ensure that this study is conducted in compliance with the Singapore Guideline for Good Clinical Practice, the ethical guidelines of which are applicable to all studies to be carried out, and to ensure that the study is carried out in accordance to the guidelines and the submitted protocol. The Principal Investigator should meet with his collaborator(s) regularly to assess the progress of the study, and be familiar and comply with all applicable research policies in the Institution.

PATIENTS. AT THE HEART OF ALL WE DO.®

SingHealth Duke-NUS Academic Medical Centre

Singapore General Hospital • KK Women's and Children's Hospital • Sengkang Health
National Cancer Centre Singapore • National Dental Centre Singapore • National Heart Centre Singapore
National Neuroscience Institute • Singapore National Eye Centre • SingHealth Polyclinics • Bright Vision Hospital

3. No deviation from, or changes of, the protocol should be initiated without prior written SingHealth CIRB approval of an appropriate amendment, except when necessary to eliminate immediate hazards to the subjects or when the change(s) involve(s) only logistical or administrative aspects of the trial (e.g. change of monitor(s), telephone number(s)).
4. Only the approved Participant Information Sheet and Consent Form should be used. It must be signed by each subject prior to enrolling in the study and initiation of any protocol procedures. Two copies of the Informed Consent Form should be signed and dated. Each subject or the subject's legally accepted representative should be given a copy of the signed consent form. The remaining copy should be kept by the PI / medical record.
5. The Principal Investigator should report promptly to the SingHealth CIRB of:
 - i. Deviations from, or changes to the protocol including those made to eliminate immediate hazards to the trial subjects.
 - ii. Changes increasing the risk to subjects and/or affecting significantly the conduct of the trial.
 - iii. All serious adverse events (SAEs) and adverse drug reaction (ADRs) that are both serious and unexpected.
 - iv. New information that may affect adversely the safety of the subjects or the conduct of the trial.
 - v. Completion of the study.
6. Study Status Report should be submitted to the SingHealth CIRB for the following:
 - i. Annual review: Status of the study should be reported to the SingHealth CIRB at least annually using the Study Status Report.
 - ii. Study renewal: the Study Status Report is to be submitted at least two months prior to the expiry of the approval period. A valid SingHealth CIRB renewal is essential, as any research performed outside of an approved time frame is not legal, and thus not covered by the hospital's research insurance in case of unexpected adverse reactions.
 - iii. Study completion or termination: the Final Report is to be submitted within three months of study completion or termination.

Yours sincerely,


Dr Steve Yang
Chairman
SingHealth Centralised Institutional Review Board D

cc: Institution Representative, KKH
Head, Department of Women's Anaesthesiology, KKH

Appendix E

Informed Consent Form for Real-time Volunteer Study

PARTICIPANT INFORMATION SHEET

You are being invited to participate in a research study.

Before you take part in this research study, the study must be explained to you and you must be given the chance to ask questions. Please read carefully the information provided here. If you agree to participate, please sign the informed consent form. You will be given a copy of this document to take home with you.

STUDY INFORMATION

Protocol Title:

Automatic Spinal Landmarks Identification with Real-time Ultrasound Image Processing System for Healthy Volunteers

Principal Investigator:

Dr Sng Ban Leong

Department of Women's Anaesthesia, KK Women's & Children's Hospital

100 Bukit Timah Road, Singapore 229899

Phone: 63941081 Fax: 62912661

PURPOSE OF THE RESEARCH STUDY

You are being invited to participate in a research study of automatic spinal landmarks identification with real-time ultrasound image processing system. We hope to learn the effectiveness of using a developed computer programming system to automatically identify the spinal landmarks. You were selected as a possible subject in this study because you are qualified for the selection criteria.

This study will recruit 30 subjects from KK Women's and Children's Hospital over a period of 1 year.

STUDY PROCEDURES AND VISIT SCHEDULE

If you agree to take part in this study, you will be asked to sit down on chair bending forward a little bit. The operator will then use ultrasound probe to scan your lumbar spine. The image processing system will process the ultrasound images and identify the spinal landmarks on the image automatically. The operator will evaluate the computer programming system based on whether correct spinal landmarks are detected and whether proper guidance is provided for moving the probe. The whole procedure is non-invasive.

Your participation in the study will last around 7 minutes. No follow up is required for this study.

Any ultrasound images and medical data obtained during the course of this study will be stored and analysed only for the purposes of this study for a period not exceeding 6 years, and will be destroyed after completion of the study.

Schedule of visits and procedures:

There are no additional visits or procedures for this study.

YOUR RESPONSIBILITIES IN THIS STUDY

If you agree to take part in this study, a written consent will be obtained from you. If there are any queries, the investigators will be happy to answer any questions.

WITHDRAWAL FROM STUDY

You are free to withdraw your consent and discontinue your participation at any time without prejudice to you or effect on your medical care. If you decide to stop taking part in this study, you should tell the Principal Investigator.

Your doctor, the Principal Investigator and/or the Sponsor of this study may stop your participation in the study at any time for one or more of the following reasons:

- Failure to follow the instructions of the Principal Investigator and/or study staff
- The study is cancelled

WHAT IS NOT STANDARD CARE OR EXPERIMENTAL IN THIS STUDY

The study is being conducted because there is a potential to identify the spinal landmarks and increase the interpretability of ultrasound images with computer image processing algorithm. The system will alleviate the need for doctors to interpret noisy ultrasound images in real time. We hope that your participation will help us to evaluate whether the developed image processing system is accurate in identifying the spinal landmarks revealed by ultrasound images.

Although scanning the lumbar spine area with ultrasound machine may be part of standard medical care, in this study this / these procedure(s) are being performed for the purposes of the research.

POSSIBLE RISKS, DISCOMFORTS AND INCONVENIENCES

There is a potential risk of having rash if you are allergic to ultrasound gel, but the possibility of allergy to ultrasound gel is rare.

POTENTIAL BENEFITS

There is no assurance you will benefit from this study. However, your participation may contribute to the improvement of ultrasound imaging interpretation and help with future real time ultrasound imaging guidance system development.

ALTERNATIVES

The alternative will be to not take part in this study.

SUBJECT'S RIGHTS

Your participation in this study is entirely voluntary. Your questions will be answered clearly and to your satisfaction.

In the event of any new information becoming available that may be relevant to your willingness to continue in this study, you or your legal representative will be informed in a timely manner by the Principal Investigator or his/her representative.

By signing and participating in the study, you do not waive any of your legal rights to revoke your consent and withdraw from the study at any time.

CONFIDENTIALITY OF STUDY AND MEDICAL RECORDS

Information collected for this study will be kept confidential. Your records, to the extent of the applicable laws and regulations, will not be made publicly available. Only your Investigator(s) will have access to the confidential information being collected.

However, the Regulatory Agencies, Institutional Review Board and Ministry of Health will be granted direct access to your original medical records to check study procedures and data, without making any of your information public.

By signing the Informed Consent Form attached, you or your legal representative are authorizing (i) collection, access to, use and storage of your "Personal Data, and (ii) disclosure to authorised service providers and relevant third parties.

"Personal Data" means data about you which makes you identifiable (i) from such data or (ii) from that data and other information which an organisation has or likely to have access. This includes medical conditions, medications, investigations and treatment history.

Research arising in the future, based on this Personal Data, will be subject to review by the relevant institutional review board.

By participating in this research study, you are confirming that you have read, understood and consent to the SingHealth Data Protection Policy- the full version is available at www.singhealth.com.sg/pdpa. Hard copies are also available on request.

Data collected and entered into the Data Collection Form are the property of KKH. In the event of any publication regarding this study, your identity will remain confidential.

COSTS OF PARTICIPATION

There will be no additional charges.

RESEARCH RELATED INJURY AND COMPENSATION

The Hospital does not make any provisions to compensate study subjects for research related injury. However, compensation may be considered on a case-by-case basis for unexpected injuries due to non-negligent causes.

By signing this consent form, you will not waive any of your legal rights or release the parties involved in this study from liability for negligence.

WHO TO CONTACT IF YOU HAVE QUESTIONS

If you have questions about this research study or in the case of any injuries during the course of this study, you may contact the Principal Investigator Dr Sng Ban Leong of the Department of Women's Anaesthesia (office telephone 63941081) of KK Women's and Children's Hospital. After office hours, in case of emergencies, you may also contact Dr Sng Ban Leong (mobile 98306621).

This study has been reviewed by the SingHealth Centralised Institutional Review Board for ethics approval.

If you have questions about your rights as a participant, you can call the SingHealth Centralised Institutional Review Board at 6323 7515 during office hours (8:30 am to 5:30pm).

If you have any complaints about this research study, you may contact the Principal Investigator or the SingHealth Centralised Institutional Review Board.

CONSENT BY RESEARCH SUBJECT

Details of Research Study

Protocol Title:

Automatic Spinal Landmarks Identification with Real-time Ultrasound Image Processing System for Healthy Volunteers

Principal Investigator:

Dr Sng Ban Leong

Department of Women's Anaesthesia, KK Women's and Children's Hospital

63941081, Fax 62912661

Subject's Particulars

Name:

NRIC No.:

Address:

Sex: Female/Male

Date of birth _____

dd/mm/yyyy

Race: Chinese/ Malay/ Indian /Others (please specify) _____

I, _____ (NRIC/Passport No. _____)
(Name of patient)

agree to participate in the research study as described and on the terms set out in the Patient Information Sheet.

I have fully discussed and understood the purpose and procedures of this study. I have been given the Participant Information Sheet and the opportunity to ask questions about this study and have received satisfactory answers and information.

I understand that my participation is voluntary and that I am free to withdraw at any time, without giving any reasons and without my medical care being affected.

By participating in this research study, I confirm that I have read, understood and consent to the SingHealth Data Protection Policy. I also consent to the use of my Personal Data for the purposes of engaging in related research arising in the future.

Signature/Thumbprint (Right / Left) of participant

Date of signing

To be filled by parent / legal guardian / legal representative, where applicable

I, _____ hereby give consent for the above participant to participate in
(parent / legal guardian)
the proposed research study. The nature, risks and benefits of the study have been explained clearly to me and I fully understand them.

Signature/Thumbprint (Right / Left) of parent /legal guardian

Date of signing

Translator Information (if required)

The study has been explained to the participant/ legal representative in

_____ by _____
Language Name of translator

To be filled witness, where applicable

An impartial witness should be present during the entire informed consent discussion if a subject or the subject's legal representative is unable to read. After the written informed consent form and any written information to be provided to subjects, is read and explained to the subject or the subject's legal representative, and after the subject or the subject's legal representative has orally consented to the subject's participation in the study and, if capable of doing so, has signed and personally dated the consent form, the witness should sign and personally date the consent form.

Witnessed by: _____
Name of witness Designation of witness

Signature of witness Date of signing

Investigator's Statement

I, the undersigned, certify to the best of my knowledge that the patient/patient's legal representative signing this informed consent form had the study fully explained and clearly understands the nature, risks and benefits of his/her / his ward's / her ward's participation in the study.

Name of Investigator Signature Date